Doctoral Dissertation (Shinshu University)

Fabrication of biodegradable PHBH-based composite nanofibers and monofilament for wound healing application

March 2020

RINA AFIANI REBIA

Department of Bioscience and Textile Technology

Interdisciplinary Graduate School of Science and Technology,

Shinshu University

Table of Contents

Chapter 1

General introduction

Chapter 1

1.1. General introduction

1.1.1. Biodegradable polymer

The most production of synthetic polymers is produced from petrochemicals or fossil-based and not biodegradable with pollutes impact on the environment. Nowadays, biodegradable polymers have been attracted much attention to break those problems such as disposal products and the possibility to change the material sourced from fossil to renewable feedstock. The biodegradable polymer can be classified into two categories as synthetic and natural polymer by their source. Poly(lactic acid) (PLA), poly(glycolic acid) (PGA), poly(ε-caprolactone) (PCL), and their copolymers are the synthetic biodegradable polymer by chemically synthesized from biomass-originated monomers [1,2]. The natural biodegradable polymer is divided into two groups as proteins (collagen, fibrin, silk, etc.) and polysaccharides (starch, alginate, chitin/chitosan, hyaluronic acid derivatives, etc.) [1]. Furthermore, there is biological origin synthesized by using microorganisms and plats such as bacterial cellulose, poly(glutamic acid), poly[(*R*)-3-hydroxybutyrate] (PHB) from polyhydroxyalkanoates (PHA), and its copolymers [2,3].

1.1.2. Polyhydroxyalkanoates (PHAs)

PHAs are one of biodegradable and biocompatible aliphatic polyester synthesized by a wide variety of microorganisms or bacteria through the fermentation of sugar, lipids, fatty acids, alkanes, alkenes, alkanoic acids [4-6]. PHB is the first discovered as a homopolymer that can be produced by a wide range of bacteria from the PHA family. Figure 1-1 exhibits the biosynthesis with a section of microbial cells containing the discrete granules of PHB.

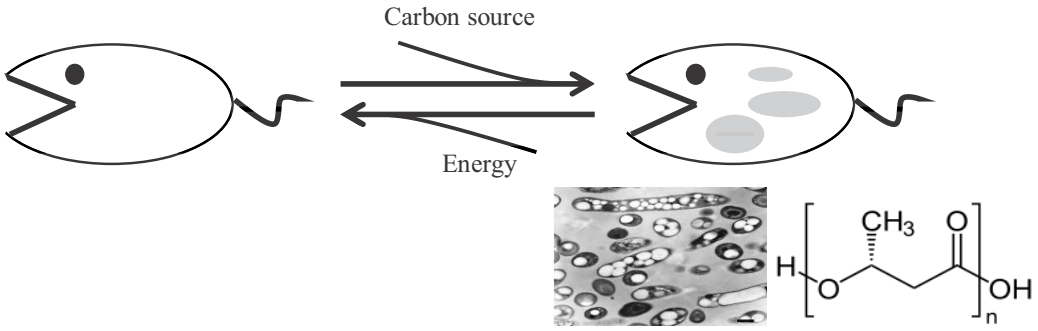

Figure 1-1. Biosynthesis of PHB polymer.
(TEM picture of microorganism accumulating 81% PHA and chemical structure of PHB) [4]

PHB is highly crystalline in the range of 55 – 80%, with melting temperature 180°C and has stiff, rigid, and brittle characteristics as well as poor mechanical properties became major drawbacks to the most standard application [4-6]. To improve the overall physical properties of PHB, PHAs containing more than 150 types of monomer have been synthesized in different microorganisms [10]. PHB copolymer with other second monomer units such as 3-hydroxyvalerate (3HV), poly(3-hydroxybutyrate-*co*-3-hydroxyvalerate) (PHBV) has been investigated to improve its properties. Thus, copolymerization with hydroxyalkanoic acid monomers such as 3-hydroxyhexanoates (3HHx), poly(3-hydroxybutyrate-*co*-3-hydroxyhexanoate) (PHBH) was attempted to reduce the obstacles of PHB homopolymer.

Figure 1-2 and Table 1-1 exhibit the chemical structure of PHAs family, mechanical, and thermal properties of PHB, its copolymer, and common plastics, respectively. Overall, the copolymers show a wide range of physical properties depending on the chemical structure of second monomer units and the composition of monomer units. Particularly, PHBH demonstrated softer and more flexible properties compared to PHB homopolymer and suitable for practical applications. PHBH was firstly trademarked as Nodax by P&G and manufactured by Kaneka Corporation (Japan) to raise its production capacity and increase the ratio of 3HHx in the

copolymer unit in developing bio-based and biodegradable polymer [4,5]. Furthermore, PHBH can be processed for film, packaging, foam, injection, fibers, and so on.

Recently, PHBH and other copolymers of PHB have been attracted much intention for using in medical applications. These polymers have been developing as implanted medical devices for dental, craniomaxillofacial, orthopedic, hernioplasty, skin surgery, drug delivery, and surgical suture [10]. The most advantage of these polymers is complete degradability by microorganisms under aerobic and anaerobic conditions without forming a toxic product [6,11]. Especially in the living systems including *in vivo* and *in vitro*, these polymers can be degraded by an enzyme present in blood and animal tissue as *in vivo* condition.

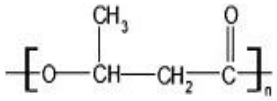

P(3HB) or PHB, Poly[(*R*)-3-hydroxybutyrate]

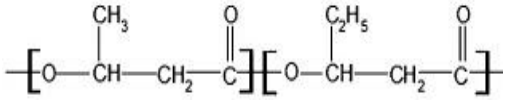

P(3HB-*co*-3HV) or PHBV, Poly[(*R*)-3-hydroxybutyrate-*co*-(*R*)-3-hydroxyvalerate]

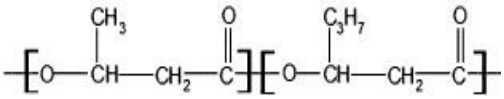

P(3HB-*co*-3HHx) or PHBH, Poly[(*R*)-3-hydroxybutyrate-*co*-(*R*)-3-hydroxyhexanoate]

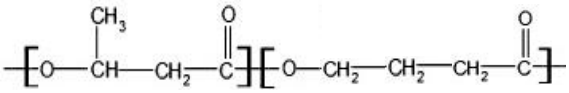

P(3HB-*co*-4HBx), Poly[(*R*)-3-hydroxybutyrate-*co*-4-hydroxybutyrate]

Figure 1-2. Chemical structures of PHB and its copolymers [4].

Table 1-1. Thermal and mechanical properties of PHB, its copolymer, and common plastics [4,11].

Polymer	Melting temp. (°C)	Glass-transition temp. (°C)	Young's modulus (GPa)	Tensile strength (MPa)	Elongation to break (%)
P(3HB)	175	4	3.5	45	5
P(3HB-*co*-3HV)					
3 mol% 3HV	170	-	2.9	38	-
8 mol% 3HV	165	1	-	19	35
9 mol% 3HV	162	-	1.9	37	-
14 mol% 3HV	150	-	1.5	35	-
20 mol% 3HV	145	-1	1.2	25	50
25 mol% 3HV	137	-	0.7	30	-
P(3HB-*co*-4HB)					
3 mol% 4HB	166	-	-	28	45
10 mol% 4HB	159	-	-	24	242
16 mol% 4HB	150	-7	-	26	444
64 mol% 4HB	50	-35	-	17	590
90 mol% 4HB	50	- 42	-	65	1080
P(3HB-*co*-3HHx)					
5 mol% 3HHx	160	-2	-	32	260
10 mol% 3HHx	127	-1	-	21	400
Polypropylene (PP)	175	-10	1.7	35	400
Polyethylene-terephthalate (PET)	262	-	2.2	56	3400
Polystyrene (PS)	110	-	3.1	50	21
Low density polyethylene (LDPE)	130	-36	-	10	620

1.1.3. Poly (vinyl alcohol) (PVA)

PVA is a nontoxic, biodegradable, biocompatible semi crystalline, highly hydrophilic polymer that received much attention from great properties such as good thermal stability, good physical properties, water solubility, gas permeability, flexible polymer and inexpensive [12-14]. PVA is produced through methanolysis process from different grades of polyvinyl acetate (PVAc), where final properties of polymer depend on the degree of hydrolysis (HD) [13,15]. DeMerlis et al. [13] reported that PVA is categorized as partially hydrolyzed and fully hydrolyzed, the chemical structure of PVA as shown in Figure 1-3. This polymer is largely used as fiber, film, in the paper industry, in textile sizing, etc. Since the PVA can control the fiber diameter from micro meter to nanometer and its characteristic can be modified by crosslinking reaction, interest in research of

this polymer has been increasing. The modification of PVA can be modified by chemical or physical treatment. The chemically modification by aldehydes, carboxylic acids, anhydrides [16] whereas physical treatment by heat treatment process can be carried out. In these reactivity, PVA has been preparing and fabricating by blending with other polymers to reduce its drawback.

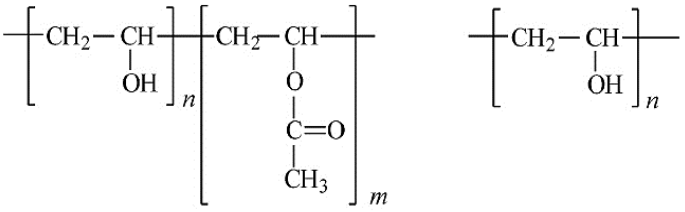

Figure 1-3. Chemical structures for PVA [13].

The interesting properties of PVA as ultra-fine fiber are suitable for important application including filtration, membrane, transdermal patches. The jelly preparation of PVA is useful when applied to the skin, sustained release tablet formulations, and so on [13]. In the case of PVA nanofibers electrospun preparation, water was used to dissolve PVA as solvent. Park et al. [16] reported that blending with poly(acrylic acid) (PAA) can improve the electrospinning stability and additional heat treatment condition at 100°C for 1 h can improve the water resistance of electrospun PVA fiber. Furthermore, PVA has the ability to soluble in water and be able to degrade by microorganisms in the landfill without any dangerous impact on the environment.

1.1.4. Natural antibacterial products

For a long time, plants have been a valuable source of natural products for maintaining human health as a traditional medicine. In developing countries, there are still a lot of people uses medicinal plants as traditional medicine, which has effective compounds derived from plants. In

the last decade, natural products have more intensive studies for alternative medicine. Understanding the pharmacology of medicinal herbs for natural therapies has also gained more attention in modern science. Research has proved that natural products can be as effective as conventional medicine. Thus, various natural compounds are now used as therapeutic agents such as antibacterial, anti-inflammatory, anti-cancer, etc. The plant extract, essential oils, aloe vera, and honey are the sample for natural antibacterial. Compared with iodine and silver as the synthetic antibacterial reagent, the use of natural antibacterial prevents wound infection as well as to diminish the risk of sensitization and development of resistance [17]. Furthermore, plant-derived antibacterial such as *Centella* and propolis have been intensively investigating in combination with polymer matrix. Recent studies demonstrated that these natural products are able to incorporate into nanofibers.

1.1.4.1. *Centella asiatica*

Figure 1-4. *Centella* powder.

Centella asiatica is a type of herb found in tropical swampy areas, such as Indonesia, Malaysia, Thailand, and India. It belongs to the family Umbelliferae, a common perennial herbaceous creeper flourishing abundantly in moist areas. It is made up of three main chemical constituents namely *asiaticoside*, pair of chemicals (called *brahmoside* and *brahminoside*) and *madecassoside* [18]. *Asiaticoside,* a triterpene glycoside as an antibiotic, plays a role in wound healing. *Brahmoside* and *brahminoside* are diuretic in nature, have a slightly sedative action, good

for wound treatment. Furthermore, *madecassoside* is a glycoside with strong anti-inflammatory agent. Hence, it is capable to promote better blood circulation to accelerate wound healing. The previous study reported that *centella* extract demonstrated a resistance to microbial contamination against *S. Aureus*, *E. Coli*, and *P. Aeruginosa*, *B. Cereus* and *M. Luteus* [19,20]. Overall, *Centella asiatica* with antibacterial, antiseptic, and anti-inflammatory properties could accelerate wound healing as well as treating damaged tissue and reduce the scar.

1.1.4.2.Propolis

Figure 1-5. Propolis powder.

Propolis is a sticky, natural resinous mixture produced by honeybees. In general, propolis is composed of 50% resin and vegetable balsam, 30% wax, 10% essential and aromatic oils, 5% pollen and 5% various other substances, including organic debris [21]. For biomedical applications, purification is necessary to remove inert components (wax, ash, bioactive compounds, and pollen) and get phenols and flavonoids as effective components. Several methods for extraction of the propolis are reported, such as maceration (MAC), ultrasound-assisted extraction in addition to Soxhlet extraction (SOX) [22]. Propolis was commonly extracted using 70-80% ethanol [23,24]. Table 1-2 shows the various solvents used for the extraction of propolis.

Raw propolis contained more than 300 compounds, among which polyphenols, terpenoids, steroids, sugars, and amino acids. Propolis has been using in medicine pharmaceuticals to protect against the entry of microorganisms, fungi, and bacteria [25]. Besides its antibacterial, antifungal,

and antiviral properties, propolis has many other beneficial biological activities such as antioxidant, antiinflammatory, antitumor, hepatoprotective, local anesthetic, immunostimulatory, and antimutagenic [26]. Several studies proved that propolis has excellent potential for wound healing application [21,22]. In this research, propolis was combined with the biodegradable polymer matrix through electrospinning process.

Table 1-2. The various solvents used for the extraction of propolis [27].

Water	Methanol	Ethanol	Chloroform	Dichloromethane	Ether	Acetone
Anthocyanins, starches, tannins, saponins, terpenoids, polypeptides, and lectins	Anthocyanins, terpenoids, saponins, tannins, xanthoxyline, totarol, quassinoids, lactones, flavones, phenones, polyphenols, polypeptides, and lectins	Tannins, polyphenol, polyacetylenes, terpenoids, sterols, and alkaloids	Terpenoids, flavonoids	Terpenoids, tannins, polyphenols, polyacetylenes, sterols, and alkaloids	Alkaloids, terpenoids, coumarins, and fatty acids	Flavonols

1.1.4.3. Hinokitiol

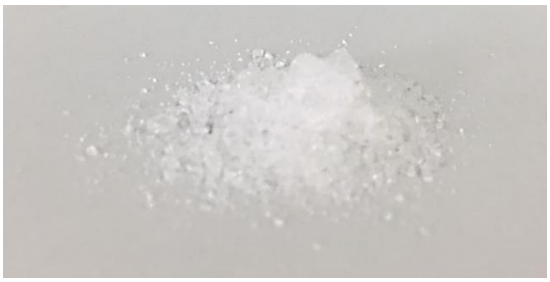

Figure 1-6. Hinokitiol powder.

Hinokitiol, also known as *β*-thujaplicin (*β*-TH), is a tropolone derivative found in the heartwood of cupressaceous plants. All isomers, in particular, *β*-TH are naturally occurring in several cupressaceous trees and shrubs such as western red cedar (*Thuja plicata* Donn), eastern white cedar (*Thuja occidentalis* L.), hinoki cypress (*Chamaecypraisobtusa*), and Hiba (*Thujopsis dolabrata*) [28]. *β*-TH is the most intensively studied isomer and is well-known for its inhibitory

effect on the growth of fungi, bacteria, insects, and plants [26]. Furthermore, hinokitiol β-TH has biological effects such as differentiation-inducing, anti-inflammatory, antibacterial, antifungal, antioxidant capacities, and antitumor activity [29,30]. Hinokitiol is widely used in hair tonics, toothpaste, cosmetics, skin lotion, body soap, and food as an antimicrobial agent [26,29-30]. However, the utilization of hinokitiol for wound healing incorporated with a polymer matrix is hardly available.

1.1.5. Wounds

1.1.5.1. Wound healing

In general terms, the wound is classified as an acute and chronic wound. The acute wound occurs as a result of surgery or trauma (burns, lacerations, and abrasions) and can repair themselves in the stages of healing within the predicted time-frame. A chronic wound defined as the wound that does not heal in an orderly set of stages and in a predictable time after treatment. In some cases, an acute wound has the possibility to be a chronic wound when it does not follow the healing stages. The healing stages started from inflammation for 1 – 5 days, proliferation (3 – 21 days), and tissue remodeling (14 – 2 years) as the last stage [17,31]. Bacterial infection plays a role in complications and delays in the wound healing process. The longer the wound opened and healed, the greater the injury will be colonized by microorganisms from skin and its surroundings. This condition will delay wound healing. Furthermore, inflammation not only causes discomfort or anxiety but also leads to a high risk of systematic illness or serious complication. Thus, advanced antimicrobial wound dressings are witnessing to allow the sustained release of the loaded antimicrobials, permitting the realization of their antibacterial activity while maintaining an excellent concentration to the healing tissues.

1.1.5.2.Wound closure

Wound closure defined as an aesthetic closure of a wound, whether traumatic or surgically induced. It can be also referred to as wound closure immediately following the injury and before the formation of granulation tissue. A suture as closure will facilitate closure by upholding tissue together for faster healing of the wound. In the wound closure technique, it has evolved from the earliest development of suture of suturing materials to comprise resources such as synthetic sutures, absorbable, staples, tapes, and adhesive compounds [32]. The process of healing stages is the same in the case of acute and chronic wounds. The infection during the tissue remodeling process due to not immediately close the wound and surrounding of open wound is not clean enough that can be the effect on the fast-growing microbial. Therefore, the suture material trend included antimicrobial suture, bio-active suture (drug-eluting and stem cells seeded suture), and smart suture (elastic and electronic suture) are developed.

1.1.6. Electrospinning

Antimicrobial nonwoven mat is also produced by the electrospinning technique. This technique is the most convenient and economical method. The advantage of a product made through this process is ultra-fine polymer fibers with large surface-to-volume ratio, and cost-effective. Nanofiber has opportunity to be an excellent candidate for many critical applications, such as separation membrane, wound dressing materials, and drug delivery as medical application, electric substrate, textile, etc. Furthermore, it is received a great deal of attention as a scaffold because of their structure is similar to the extracellular matrix (ECM) for skin regeneration and to facilitate cell attachment and proliferation due to the high porosity of the mat [35,36]

In the preparation of PHB and its copolymer electrospun solution, hexafluoro-2-propanol (HFIP) and chloroform are often used as a solvent. Previous research reported that the use of these polymers obtained an easy and feasible process [8,12]. These polymers also have an advantage as biodegradable and biocompatible polymers that can be good candidate for medical application (wound dressing and healing) [4,11].

In the electrospinning process, a strong electric force is used to travel the polymer solution through the atmosphere and lead to the collector. The opposite charge is applied to the nozzle and collector roll and increasing the voltage magnitude to gain the fiber with nano dimensions. During the process, the evaporation of solvent in liquid polymers is allowed when the jet move toward the collector, the electric force is utilized lengthen to form a Taylor cone, and the electrostatic force overcomes the surface tension of liquid polymer [33, 34]. Figure 1-7 shows a schematic representation of the basic setup for the electrospinning process.

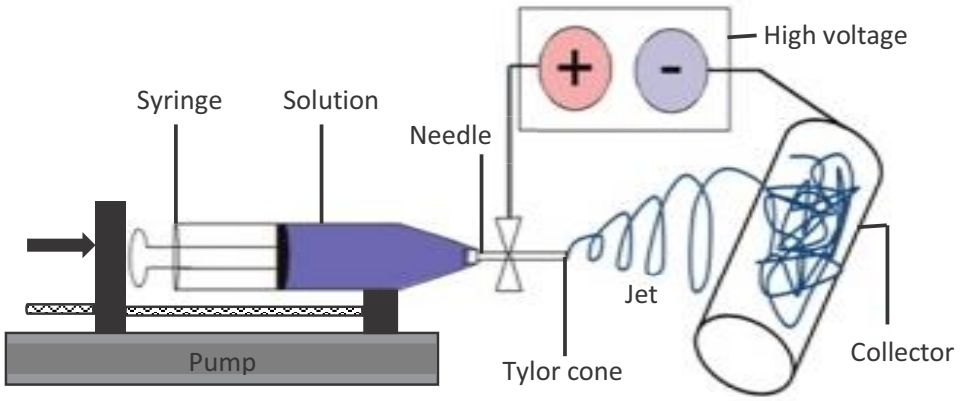

Figure 1-7. A schematic representation of the basic setup for the electrospinning process.

In spite of the apparent simplicity, the electrospinning system is complicated due to many parameters such as:

1. Solution properties including viscosity, conductivity, and surface tension.
2. Solvent and polymer concentration.

3. Controlled parameter including hydrostatic pressure in the capillary (solution feeding rate), electric potential at the tip, and distance between the tip and collector screen.
4. Ambient parameter including temperature, humidity, and air velocity in the electrospinning chamber.

These variation parameters influence on the final product [34].

1.1.7. Melt spinning

Melt spinning as a method is also used to product antibacterial suture. Melt spinning is the most convenient and economical method for polymer fiber manufacturing due to the absence of solvents and the simplicity of the process. In the melt spinning process, the fiber-forming substance is melted for extrusion through the spinneret and then directly solidified by cooling. The different types of spinneret based on the number of holes, of which one to thousands. Some processing parameters such as temperature, dimensions, the number of spinneret holes, mass throughput, length of the spinning path, take-up velocity, and cooling conditions affect spinnability [37]. Hence, melt spinning is generally followed by the mechanical drawing of filament to orient molecular chains. Melt spinning can produce various filaments structure with high production speed for many critical applications such as textiles, fishing lines, and suture.

In the melt spinning process by extrusion, the fiber-forming substance is melted through the spinneret and directly solidified by cooling to get the monofilaments. The melt spinning of PHB and its copolymer are slightly complicated because of a glass transition below room temperature and quite low crystalline rate [8]. When these polymers are cooled down, monofilament becomes hard and brittle due to the growth of spherulites crystal at room temperature [38]. It has been shown that processing parameters affect the spinnability of PHB and its copolymer fiber. The one and

two-step annealing method after melt spinning resulted in increasing the mechanical properties [39]. Cold-drawing and two-step-drawing methods increased the mechanical properties of PHB and its copolymer. In addition, a combination of direct rapid cooling in ice water and isothermal crystallization near T_g, followed by one-step drawing and annealing, improved PHB and Poly(3-hydroxybutyrate-*co*-3-hydroxyvalerate) (PHBV) fiber properties [40]. The resulted filament followed by the drawn and heat-treatment showed fully oriented of PHB and its copolymer monofilament. Such a one-step technology is required to improve high tensile strength. Figure 1-8 shows a schematic melt spinning of PHB and its compolymer monofilament.

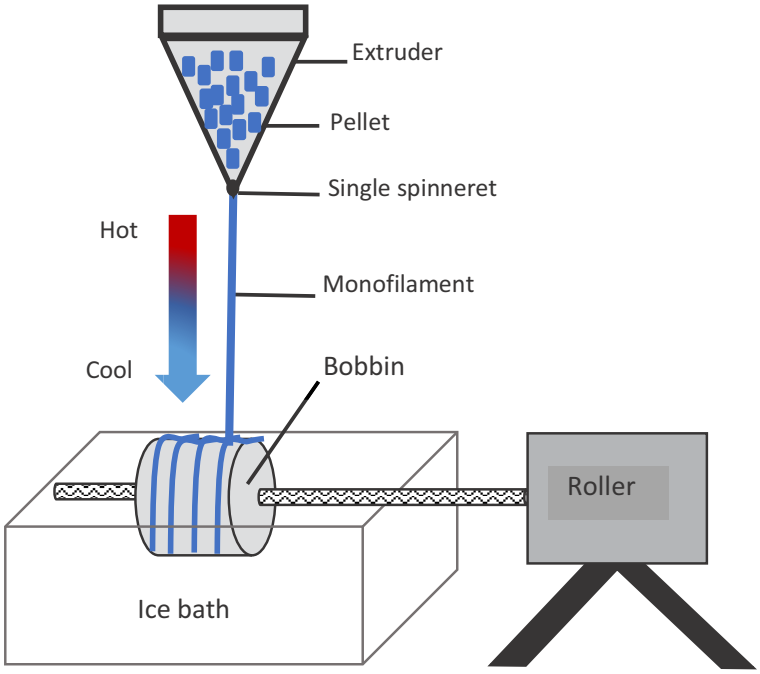

Figure 1-8. A schematic melt spinning of PHB and its copolymer monofilament followed by rapid cooling in ice water.

1.2. Purpose of research

The project research covered the fabrication of biodegradable PHBH nanofibers and monofilament. The research aimed to use PHBH fibers for medical applications such as wound healing and closure. For this purpose, the physical improvement of the polymer matrix was indispensable to accelerate the wound healing process. In general, the use of PHBH polymer has been desirable from the advantage of biodegradable, biocompatibility, and a non-toxic polymer for the human body. The blend system in PHBH nanofiber with another polymer or natural product with evaluation the characteristic of its polymer that might have good potential for wound healing application. In order to develop its antibacterial property, PHBH monofilament was loaded with the natural antibacterial solution (*centella*, propolis, hinokitiol).

The healing process of the wounded skin involves inflammation, proliferation, and tissue remodeling stages. During the 1-5 days of inflammation, the healing is hindered by the antibacterial activity around the open wound. For this purpose, PHBH composite nanofibers with natural products and PHBH monofilament loaded with the natural product were performed using electrospinning and melt spinning (followed by dip-coating method), respectively.

In chapter 1, the general introduction was described how the idea for my Ph.D project evolved.

In chapter 2, PVA was chosen as blending polymer to improve the drawback of PHBH polymer. The PHBH/PVA nanofiber was analyzed in surface properties, characteristics, degradation, and biocompatibility.

In chapter 3, fabrication of PHBH composite with various natural antibacterial reagents such as *centella*, propolis, and hinokitiol was reported. The characteristics and effects of PHBH composited nanofibers were discussed.

In chapter 4, the physical changes of PHBH monofilament by heat treatment in various solvents were investigated. The physical change of fibers in length, diameter, and cross-section after heat treatment method in several organic solvents was evaluated.

In Chapter 5, dip-coating as a method to evaluate the penetration of propolis solution into PHBH monofilament was investigated. The characteristics of monofilaments were analyzed regarding the morphology, mechanical properties, physical change, inner structure, and antibacterial activity.

In Chapter 6, the experimental evidence obtained from this dissertation work is summarized.

1.3. References

[1] Song, R.; Murphy, M.; Li, C.; Ting, K.; S, C.; Zheng, Z.; Current development of biodegradable polymeric materials for biomedical applications. *Drug. Des. Devel. Ther*. **2018**, *11*, 3117-3145.

[2] Tian, H.; Tang, Z.; Zhuang, X.; Chen, X.; Jing, X. Biodegradable synthetic polymers: Preparation, functionalization and biomedical application. *Prog. Polym. Sci.* **2012**, *37*, 237–280.

[3] Kawashima, Y.; Orita, I.; Nakamura, S.; Fukui, T. Compositional regulation of poly(3-hydroxybutyrate-*co*-3-hydroxyhexanoate) by replacement of granule-associated protein in *Ralstonia eutropha. Microb. Cell. Fact.* **2015**, *14*, 187.

[4] Iwata, T.; Tsuge, T.; Taguchi, S.; Abe, H.; Tanaka, T. Bio-polyesters. In *Bio-based polymers*, 1st ed.; Kimura, Y.; CMC Publishing Co., Ltd.: Tokyo, Japan, 2013, pp. 71-85. ISBN978-4-7813-0271-3.

[5] Philip, S.; Keshavarz, T.; Roy, I. Polyhydroxyalkanoates: biodegradable polymers with a range of applications. *J. Chem. Technol. Biotechnol.* **2007**, *82*, 233-247.

[6] Bugnicourt, E.; Cinelli, P.; Lazzeri, A.; Alvare, V. Polyhydroxyalkanoate (PHA): review of synthesis, characteristics, processing and potential applications in packaging, *eXPRESS Polym. Lett.* **2014**, *8*, 791-808.

[7] Nolan-ITU, Pty, Ltd. Biodegradable Plastic – developments and environmental impacts. *Environment Australia*. **2002**, 3111-01/EA rpt1-3doc.

http://www.europeanplasticfilms.eu/docs/AustralianReportonBiodegradablePlastics.pdf

[8] L. Gong, L.; Chase, D.B.; Noda, I.; Liu, J.; Martin, D.C.; Ni, C.; Rabolt, J.F. Discovery of β-form crystal structure in electrospun poly[(*R*)-3-hydroxybutyrate-*co*-(*R*)-3 hydroxyhexanoate] (PHBHx) nanofibers: from fiber mats to single fibers, *Macromolecules* **2015**, *48*, 6197-6205.

[9] Kwon, M.C.; Choi, W.Y.; Seo, Y.C.; Kim, J.S.; Yoon, C.S.; Lim, H.W.; Kim, H.S.; Ahn, Jh.; Lee, H.Y. Enhancement of the skin-protective activities of *Centella asiatica* L. Urban by a nano-encapsulation process. *J. Biotechnol.* **2012**, *157*, 100-106.

[10] Bonartsev, A.P.; Myshkina, V.L.; Nikolaeva, D.A.; Kirpichnikov, M.P. Poly(3-hydroxybutyrate) and poly(3-hydroxybutyrate)-based biopolymer systems. *Biochemistry (Moscow) Suppl. Ser. B: Biomed. Chem.* **2011**, *5*, 10–21.

[11] Lee, S.Y. Bacterial polyhydroxyalkanoates. *Biotechnol. Bioeng*. **1996**, 49, 1-14.

[12] Asran, A.Sh.; Razghandi, K.; Aggarwal, N.; Michler, G.H.; Groth, T. Nanofibers from blends of polyvinyl alcohol and polyhydroxy butyrate as potential scaffold material for tissue engineering of skin. *Biomacromolecules* **2011**, *11*, 3413-3421.

[13] DeMerlis, C.C.; Schoneker, D.R. Review of the oral toxicity of polyvinyl alcohol (PVA). *Food Chem. Toxicol.* **2002**, *4*, 319-326.

[14] Park, J-C.; Ito, T.; Kim, K-O.; Kim, K-W.; Kim, B-S.; Khil, M-S.; Kim, H-Y.; Kim, I-S. Electrospun poly(vinyl alcohol) nanofibers: effects of degree of hydrolysis and enhanced water stability. *Polym. J.* **2010**, *42*, 273-276.

[15] Chiellini, E.; Corti, E.; D'Antone, A.S.; Solaro, R. Biodegradation of poly (vinyl alcohol) based materials. *Prog. Polym. Sci.* **2003**, *28*, 963-1014.

[16] Park, J.S.; Park, J.W.; Ruckenstein, E. Thermal and dynamic mechanical analysis of PVA/MC blend hydrogels. *Polymer* **2001**, *42*, 4271-4280.

[17] Andreau, V.; Mendoza, G.; Arruebo, M.; Irusta, S. Review: Smart dressings based on nanostructured fibers containing natural original antimicrobial, anti-inflammatory, and regenerative compounds. *Material* **2015**, *8*, 5154-5193.

[18] Dash, B.K.; Faruquee, H.M.; Biswas, S.K.; Alam, M.K.; Sisir, S.M., Prodhan, U.K. Antibacterial and antifungal activities of several extracts of *Centella asiatica L.* against some human pathogenic microbes. *Life Science and Medical Research* **2011**, LSMR-35.

[19] Yao, C.H.; Yeh, J.Y.; Chen, Y.S.; Li, M.H.; Huang, C.H. Wound-healing effect of electrospun gelatin nanofibres containing *Centella asiatica* extract in a rat model. *J. Tissue. Eng. Regen. Med.* **2017**, *11*, 905–915.

[20] Manotham, S.; Pengpat, K.; Eitssayeam, S.; Rujijanagul, G.; Sweatmam, D.R.; Tunkasiri, T. Fabrication of Polycaprolactone/*Centella asiatica* Extract Biopolymer Nanofiber by Electrospinning. *Appl. Mech. Mater.* **2015**, *804*, 151-154.

[21] Burdock, G.A. Review of the biological properties and toxicity of bee propolis (propolis). *Food. Chem. Toxicol.* **1998**, *36*, 347-363.

[22] Lima, G.G.; Souza, R.O.; Bozzi, A.D.; Poplawska, M.A.; Devine, D.M.; Nugent, M.J.D. Extraction Method Plays Critical Role in Antibacterial Activity of Propolis-Loaded Hydrogels. *J. Pharm. Sci.* **2016**, *105*, 1-10.

[23] Cunha, I.B.S.; Sawaya, A.C.H.F.; Caetano F.M.; Shimizu, M.T.; Marcucci, M.C.; Drezza, F.T.; Povia, G.S.; Carvalho, P.O. Factors that influence the yield and composition of Brazilian propolis extracts. *J. Braz. Chem. Soc.* **2004**, *15*, 964-970.

[24] Park, Y.K.; Ikegaki, M. Preparation of water and ethanolic extracts of propolis and evaluation of the preparations. *Biosci. Biotechnol. Biochem.* **1998**, *62*, 2230-2232.

[25] Wagh, V.D. Propolis: a wonder bees product and its pharmacological potentials. *Adv. Pharmacol. Sci.* 2013, Article ID 308249.

[26] Dyrskov, L.; Strobel, B.W.; Svensmark, B.; Hansen, H.C.B. *β*-Thujaplicin: New Quantitative CZE Method and Adsorption to Goethite. *J. Agric. Food Chem.* **2004**, *52*, 1452−1457.

[27] Fokt, H.; Pereira, A.; Ferreira, A.M.; Cunha, A. and C. Aguiar, "How do bees prevent hive infections? The antimicrobial properties of propolis. *Current research technology and education topics in applied microbiology and microbial biotechnology* **2010,** *1*, 481–493.

[28] Higashi, Y.; Tohda, S. Simple HPLC Analysis of Hinokitiol in Skin Lotion with Visible Light Detection after Pre-Column Dabsylation. *Am. J. Anal. Chem.* **2017**, *8*, 345-353.

[29] Shih, Y-H.; Lin, D-J.; Chang, K-W.; Hsia, S-M.; Ko, S-Y.; Lee, S-Y.; Hsue, S-S.; Wang, T-H.; Chen, Y-L.; Shieh, T-M. Evaluation physical characteristics and comparison antimicrobial and anti-inflammation potentials of dental root canal sealers containing hinokitiol *in vitro*. *PloS One* **2014**, *9*, e94941. doi:10.1371/journal.pone.0094941.

[30] Jayakumar, T.; Hsu, W-H.; Yen, T-L.; Luo, J-Y.; Kuo, Y-C.; Fong, T-H.; Sheul, J-R. Hinokitiol, a natural tropolone derivative, offers neuroprotection from thromboembolic stroke *in vivo*. *Evid. Based. Complement. Alternat. Med.* **2013**, Article ID 840487.

[31] Robson, M.C.; Barbul, A. Guidelines for the best care of chronic wounds. *Wound Rep. Reg.* **2006**, *14*, 647–648.

[32] Dennis, C.; Sethu, S.; Nayak, S.; Mohan, L.; Morsi, Y.Y.; Manizasagam, G.; Suture material – current and emerging trends. *J. Biomed. Mater. Res. Part A* **2016**, 104A, 1544-1559.

[33] Zeytuncu, B.; Akman, S.; Yucel, O.; Kahraman MV. Preparation and characterization of UV-cured hybrid polyvinyl alcohol nanofiber membranes by electrospinning. *Mat. Res.* **2014**, *17*, 565-569.

[34] Azuma, Y.; Yoshie, N.; Sakurai, M.; Inoue, Y.; Chujo, R. Thermal behaviour and miscibility of poly(3-hydroxybutyrate)/poly(vinyl alcohol) blends, *Polymer* **1992**, *33*,4763-4767.

[35] Ignatova, M. G.; Manolova, N. E.; Rashkov, L. B.; Markova, N.D.; Toshkova, R.A.; Georgieva, A.K.; Nikolova, E.B. Poly(3-hydroxybutyrate)/caffeic acid electrospun fibrous material coated with polyelectrolyte complex and their antibacterial activity and *in vitro* antitumor effect against HeLa cells. *Mat. Sci. Eng. C-Mater.* **2016**, *65*, 379-392.

[36] Bulman, S.EL.; Goswami, P.; Tronci, G.; Russell, S.J.; Carr, C. Investigation into the potential use of poly(vinyl alcohol)/methylglyoxal fibres as antibacterial wound dressing components. *J. Biomater. Appl.* **2015**, *8*, 1198-1200.

[37] Myllari, V.; Skrifvars, M.; Syrajala, S.; Jarvela, P. The Effect of Melt Spinning Process Parameters on the Spinnability of Polyetheretherketone. *J. Appl. Polym. Sci.* **2012**, *126*, 1564-1571.

[38] Lee, J-C.; Yasui, Jeong, Y.; Sakurai, S.; Yamane, H. Higher-order structural analysis of bacterial poly[(*R*)-3-hydroxybutyrate-*co*-(*R*)-3-hydroxyhexanoates] highly oriented films. *Polymer* **2008**, *49*, 2362-2367.

[39] Schmack, G.; Jehnichen, D.; Vogel, R.; Tandler, B. Biodegradable Fibers of Poly(3-hydroxybutyrate) Produced by High-Speed Melt Spinning and Spin Drawing. *J. Polym. Sci. Part B: Polym. Phy.,* **2000**, *38*, 2841.

[40] Tanaka, T.; Fujita, M.; Takeuchi, A.; Suzuki, Y.; Uesugi, K.; Ito, K.; Fujisawa, T.; Doi, Y.; Iwata, T. Formation of highly order structure in poly[(*R*)-3-hydroxybutyrate-*co*-(*R*)-3-hydroxyvalerate] high-strength fibers. *Macromolecules* **2006**, *39*, 2940 – 2946.

Chapter 2

Biodegradable PHBH/PVA blend nanofibers: Fabrication, characterization, *in vitro* degradation, and *in vitro* biocompatibility

Chapter 2

2.1. Introduction

Nanofiber is an excellent candidate for many important applications, such as water and air filtrations [1], drug delivery [2], and tissue engineering [3-6]. Furthermore, nanofibers received a great deal of attention as scaffold because of their structure being similar with the extracellular matrix (ECM) for skin regeneration and to facilitate the cell attachment and proliferation [7,8]. Recently, there has been an increase of interest in the development of the nanofiber scaffold from biodegradable polymers.

Polyhydroxyalkanoates (PHAs) are one of biodegradable and biocompatible aliphatic polyesters synthesized by a wide variety of bacteria through the fermentation of sugars, lipids, fatty acids, alkanes, alkenes, and alkanoic acids [9-11]. In the biomedical field, PHAs have been demonstrated to be certified fully biodegradable and a good biological material with biocompatibility of the polyester family. The most advantage of PHAs polymer is their ability to be able to be completely degraded by microorganisms under aerobic and anaerobic conditions without forming toxic product [10,12]. More than 150 kinds of PHAs consisting of various co-monomers have been reported, however, only few of them have been considered for commercial production, such as poly [(*R*)-3-hydroxybutyrate] (PHB), poly [(*R*)-3-hydroxybutyrate-*co*-(*R*)-3-hydroxyhexanoate] (PHBHx) and poly [(*R*)-3-hydroxybutyrate-*co*-(*R*)-3-hydroxyvalerate)] (PHBV) [13]. PHB has high crystallinity in the range of 55 – 80%, with a melting point at 180°C and has stiff, rigid and brittle characteristics as well as poor mechanical properties that became major drawbacks to most standard applications [14]. Nevertheless, copolymerization with other monomer units such as 3-hydroxyvalerate (3HV), 3-hydroxyhexanoate (3HH) and 4-

hydroxybutyrate (4HB) into this main chains greatly improves homopolymer property [6,15,16]. Specifically, characteristics of PHB copolymers are relatively depending on the amount of secondary monomer units. The use of higher secondary monomer unit is able to present a lower melting point, highly ductile properties, and result to be more flexible than PHB homopolymer. Poly[(*R*)-3-hydroxybutyrate-*co*-(*R*)-3-hydroxyhexanoate] (PHBH) is a copolymer which is developed by addition of randomly arranged 3-hydroxybutyrate (3HB) and 3-hydroxyhexanoate (3HH) units [16]. Cheng *et al.* [17] reported in cast membranes that the addition of more 3-hydroxyhexanoate components into a PHBH copolymer reduced the Young's modulus and tensile strength but increased the elongation at break due to a lower crystallinity. The low Young's modulus means that the material has a high elasticity. However, the production cost of PHAs polymer is higher than general purpose polymer and depends on the efficiency of the bacterial fermentation. Therefore, these have attracted attention for obtaining materials through low production cost, innovation by blending with other flexible polymers, or developing biodegradable polymer for other potentials which have high value such as medical applications.

Blending polymer is one method to combine characteristics in each polymer material to improve properties and advantage in material performance. Over the years there have been efforts to reduce cost and overcome the drawbacks of PHAs by blending with natural fibers and various flexible polymers. In addition, various studies has been carried out on the effect of the morphology, the miscibility, the thermal stability, the crystallization, the mechanical properties, the gas barrier properties, and disintegration, degradation behavior, the cell attachment and cell proliferation [3,6,15,16,18-21]. A report showed that blending PHB/cellulose acetate (CA) nanofiber affected the crystallization of PHB and increased the glass transition temperature [22]. PHBH/poly(D,L-lactic acid) (PDLLA) blend exhibited that the higher the PDLLA content, the higher the

elongation, toughness, and tensile strength [15]. Zang *et al.* [23] also reported that PHB/polylactic acid (PLA) showed stable melting temperature which indicates an improvement in thermal stability. Blend of PHB/poly (ε-caprolactone) (PCL) showed that the higher PCL content, the higher the flexibility and hydrophilicity as well as the better the cell proliferation [24]. In addition, blend of PHBH with cellulose [16], collagen [3], poly(butylene adipate-*co*-terephthalate) (PBAT) [18], PDLLA [15] has been done.

Poly(vinyl alcohol) (PVA) is used in a wide range of industrial and medical applications. PVA which is a nontoxic, biodegradable, biocompatible semi crystalline, highly hydrophilic polymer was received much attention due to its great properties such as good thermal stability, good physical properties, water solubility, gas permeability, flexible polymer, and inexpensive cost [6,25,26]. PVA is produced through hydrolysis (methanolysis) process from different grades of polyvinyl acetate (PVAc) which final properties of polymer depend on the degree of hydrolysis (HD) [25,27]. In the case of a preparation of electrospun PVA nanofibers, water was used as solvent to dissolve PVA. Reviewed in PHB/PVA blend system, hexafluoroisopropanol (HFIP) [6,19,28] and chloroform [21] have been used as solvent to dissolve both of polymers.

In this chapter, PHBH/PVA with different ratio of polymer and mixed solvent are used to prepare and fabricate the electrospun nanofibers. To the best of my knowledge, the fabrication of blend PHBH copolymer/PVA by electrospinning for new biodegradable composite material have not been reported yet to compare the different copolymers and cells behavior. I attempted to investigate the effect of 3-hydroxyhexanoate (3HH) units in the polymer of PHBH by blending with PVA polymer. Then, the effect of different ratios between PHBH and PVA polymer in the blend nanofibers was investigated by the characterization such as surface characteristics against

water and proliferation of fibroblast cells. The advantage of this research is to provide the potential of biodegradable PHBH/PVA blend for wound dressing.

2.2. Materials and methods

2.2.1. Materials

PHBH containing 5.5 mol% of 3HH (M_w = 5.37x10^5 g/mol%) and PVA (degree of polymerization 1730) containing 99.5 mol% (HD) were provided from Kaneka Corp. and Unitika, Ltd., respectively. The solvent was 1,1,1,3,3,3-hexafluoro-2-propanol (HFIP) which was purchased from Wako Pure Chemical Industries, Ltd.

2.2.2. Preparation of electrospun PHBH/PVA nanofibers

The different compositions comprised of PHBH/PVA electrospun nanofibers are 100/0, 90/10, 70/30, 50/50, 30/70, 10/90, and 0/100. PHBH and the PHBH/PVA electrospun solutions were prepared in 1 wt% of the polymer concentration. PHBH/PVA electrospun solution of 100/0, 90/10, 70/30, and 50/50 were dissolved in HFIP. PHBH/PVA blend solution of 30/70 and 10/90 were dissolved in mixed solvents of HFIP/water with ratios of 90/10 and 70/30. Furthermore, PVA was dissolved in water to prepare 8 wt% of the polymer concentration. The blend solutions was stirred at room temperature for 24 h. Electrospun of blend nanofiber was fabricated using electrospinning apparatus with a high voltage power supply (Kato Tech, Japan).

2.2.3. Characterizations

2.2.3.1. Scanning electron microscopy (SEM)

The morphology of the blend PHBH/PVA nanofibers was investigated by scanning electron microscopy (SEM - JSM-6010LA, JEOL) at an accelerating voltage of 10-15 kV at various

magnifications with surface coated by platinum (Pt) in a sputtering device for 60 sec at 30 mA. Fiber diameters were calculated by using Image J by measuring 100 fibers per different ratio of blend nanofiber.

2.2.3.2. Fourier transform infrared (FT-IR) spectroscopy

The functional groups present in pure PHBH, pure PVA, and their blend were analyzed by Attenuated Total Reflectance (ATR) FT-IR spectroscope (Perkin Elmer Spectrum GX). The spectra of each sample were obtained in the range of 4000 - 500 cm^{-1} with a resolution of 4 cm^{-1}. The infrared beam enters the ATR crystal at an angle of typically 45° and is reflected at the crystal to sample interface with the low signal of noise ratio.

2.2.3.3. Differential scanning calorimetry (DSC)

The thermal behavior of each sample was measured by using Thermo Plus (DSC 8230). An amount of 2.0 ± 0.2 mg sample were placed in an aluminum pan. Each sample was measured by comparing with 2 mg aluminum oxide (Al_2O_3) as a standard sample under a nitrogen atmosphere. These nanofibers were heated from 30 - 250^oC with a heating rate of 10 K/min. The melting temperature and melting enthalpy of blend nanofibers were determined from the change of thermal curves.

2.2.3.4. X-ray (XRD)

Wide-angle X-ray diffraction (WAXD) was used for the crystalline structure analysis of nanofibers. The two-dimensional (2D) patterns of nanofibers were recorded by X-ray diffraction equipment (SPring-8, Japan) with a wavelength of 0.1 nm at 2θ scanning angle between 5 – 30^o. The detector distance from the sample to the detector (PILATUS 3X2M) was 290.6 mm and the

exposure time was 2.0 sec. The X-ray diffraction of nanofibers was investigated by the FIT-2D application.

2.2.3.5. Water contact angle (WCA)

The surface wettability of nanofibers was analyzed by water contact angle (WCA) (Contact angle meter CA-150 type) at 2 sec after dripped 2 µl of purified water at the surface of nanofibers samples randomly.

2.2.3.6. Water absorption

Samples were cut into 1 cm x 1 cm pieces. The samples were divided into without applying heat treatment and subjected to heat treatment at 100°C for 3 h. The nanofibers were immersed in distilled water at room temperature without agitation. After 24 h, the samples were removed, dried by the filter paper, and weighed. The water absorption value was calculated by using the following equation:

$$\text{Water absorption } (\%) = \frac{(W1 - W0)}{W0} \times 100 \qquad (1)$$

where W1 and W0 are the weight of samples after immersion and the initial weight before immersion, respectively. The surface of nanofiber after immersing in water was analyzed by SEM measurement.

2.2.4. *In vitro* degradation

Nanofibers were cut into 1 x 1 cm² with a weight of ± 2.5 mg and immersed in 1 ml phosphate buffer saline (PBS) at pH 7.4 containing 0.04 g/L lipase (Sigma-Aldrich, type XIII, ≥ 15 units/mg solid) with enzyme activity approximately 100 U/mg, 3U/ml. The samples were agitated and

incubated *in vitro* at 37°C and 100 rpm. The enzymatic degradation solution was changed every 3 days. These samples were removed from enzymatic solution after 1, 2, 3, and 4 weeks, and washed by distilled water for 2-3 times, and dried with filter paper followed by vacuum for 3 days. The weight loss of samples by the enzymatic degradation was calculated by using the following equation:

$$\text{Weight loss } (\%) = \frac{(W0 - W1)}{W0} \times 100$$

where W1 and W0 are the weight of samples after degradation and the initial weight before degradation, respectively. The surface of nanofiber after degradation by enzyme was analyzed by SEM measurement.

2.2.5. *In vitro* biocompatibility

The nanofiber was cut into a round shape with a diameter of 10 mm with three replicates per sample. The sterilization of nanofibers was performed by deeply soaking the sampleas in 70% aqueous ethanol solution in a multi-well TCPS dish and washed by PBS 3 times. After sterilization, the samples in a multi-well TCPS dish were fixed by put a glass tube to prevent from floating during further incubation in the fibroblast cell solution.

The concentration of cells was calibrated using the solution of 50,000 cells/mL which was poured into various 5 microtubes of the various volumes of 100, 200, 300, 400, and 500 μL. Then, added PBS solution to 1,000 μL in total to get a concentration of cells of 5,000 cells/mL, 10,000 cells/mL, 15,000 cells/mL, 20,000 cells/mL, and 25,000 cells/mL, respectively. The calibration curve was obtained by measuring absorbance value from five calibration solutions to calculate the number of cells.

To investigate the attachement between cells reaction and surface of nanofibers, the shape of the cell was observed by SEM. When the incubation was terminated, paraformaldehyde (PFA) served as a cross-linking fixation agent to stop the proliferation of cells and preserve their shape. The samples were dehydrated with ethanol, freeze-drying and analyzed by SEM.

2.3. Results and discussions

2.3.1. Morphology and fiber diameters

Homogeneous blend nanofibers without beads were obtained from pure PHBH (A) and blend from composition of PHBH/PVA of 90/10 (B), 70/30 (C), and 50/50 (D). The morphology and the fiber distribution of pure PHBH and blend nanofibers with over 50% of PHBH content exhibited a smooth surface, uniform diameter, and without beads along their length. The average diameter of pure PHBH (A) is ~538 nm and blend PHBH/PVA (50/50) nanofiber is ~408 nm (D), Table 2-1 and Figure 2-1. The majority of the fiber diameters were in the range from 240 – 820 nm. The fiber diameter of nanofiber was decreased with the increase of the PVA content. The diameter of the nanofibers and their distribution could be easily controlled by blending with PVA polymer. This condition indicated that the addition of PVA polymer might affect the viscosity of the electrospun solution and resulted in a smaller diameter and a narrow distribution. On the other hand, pure PVA and blend PHBH/PVA in composition of 30/70, 10/90 by using HFIP resulted in nonhomogeneous fibers with many small beads due to low solubility of PVA for HFIP (data not shown). Ashraf *et al.* [6] also reported that increasing in PVA content of more than 50% in PHB/PVA blend nanofibers showed nonhomogeneous fibers with a ribbon-like structure. Furthermore, a mixed solvent between HFIP and water was used to prepare PHBH/PVA with PVA-rich content.

The morphology of nanofibers observed by SEM and the fiber distribution of PHBH/PVA ratio of 30/70 (E1&E2) and 10/90 (F1&F2) were shown in Figure 2-2. These morphologies show that the use of HFIP/water mixed solvent is a useful method to fabricate PHBH/PVA blend nanofiber with PVA-rich content. The average diameter of PHBH/PVA (30/70) with HFIP/water mixed solvent (70/30) was ~143 nm, with the majority fiber being in the range from 89-266 nm (E2). These nanofibers exhibited single fiber with slightly visible beads along the length, depending on the ratio water in mixed solvent and humidity during fabrication. The addition of water would increase the conductivity of the polymer solution and decrease the fiber diameter. Thinner fibers indicated that the morphology and diameter of nanofibers was greatly influenced by the weight ratios of PHBH/PVA, different ratios of mixed solvent under the same processing condition such as concentration solution at 1wt%, the voltage at 20 kV, and temperature at 23ºC. The outcomes of PHBH/PVA blend nanofiber with PVA-rich content depended on the variable of mixed solvent ratio in the preparation of the solution and different humidity levels during the electrospun process. In the mixed solvent ratio of HFIP/water (70/30), lower humidity was accelerated required for the evaporation of the solvent. At the higher humidity, the presence of water in the solvent does not allow us to have a complete drying of the solution during the flight process of the polymer solution jet into the collector [29]. Furthermore, the decrease of humidity or increase of water content during the electrospinning process generated thinner nanofibers due to the surface tension.

In the case of pure PVA nanofiber, HFIP or mixed solvent as the solvents obtained nonhomogeneous nanofiber due to the difficulty of the feeding of solution through the needle. In this study, 8 wt% pure PVA spinning solution was prepared by dissolution in water and fabricated at the same electrospinning condition with pure PHBH. The average diameter of pure PVA

nanofiber was ~381nm (G). Table 2-1 shows the condition of electrospun nanofibers with the variable of polymer ratio and solvent ratio.

Table 2-1. Preparation of PHBH/PVA solutions, fabrication condition of electrospun nanofibers and average diameters of the resulting fibers.

Code	wt %	PHBH (%)	PVA (%)	Solvent	Hum. (%RH)	High voltage (kV)	Temp. (°C)	Ave. diameter (nm)	SD
A	1	100	0	HFIP	20	20	23	538	131
B	1	90	10	HFIP	20	20	23	468	79
C	1	70	30	HFIP	30	20	23	432	48
D	1	50	50	HFIP	30	20	25	408	66
E1	1	30	70	HFIP/water (90/10)	40	20	23	279	78
E2	1	30	70	HFIP/water (70/30)	20	20	23	143	33
F1	1	10	90	HFIP/water (90/10)	40	20	23	335	90
F2	1	10	90	HFIP/water (70/30)	20	20	23	137	26
G	8	0	100	Water	20	20	23	381	65

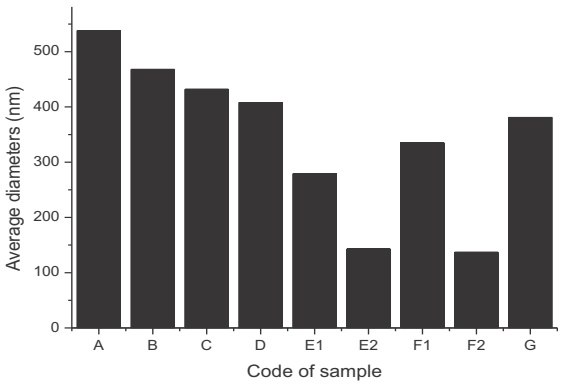

Figure 2-1. Fiber diameters of electrospun PHBH/PVA nanofibers.

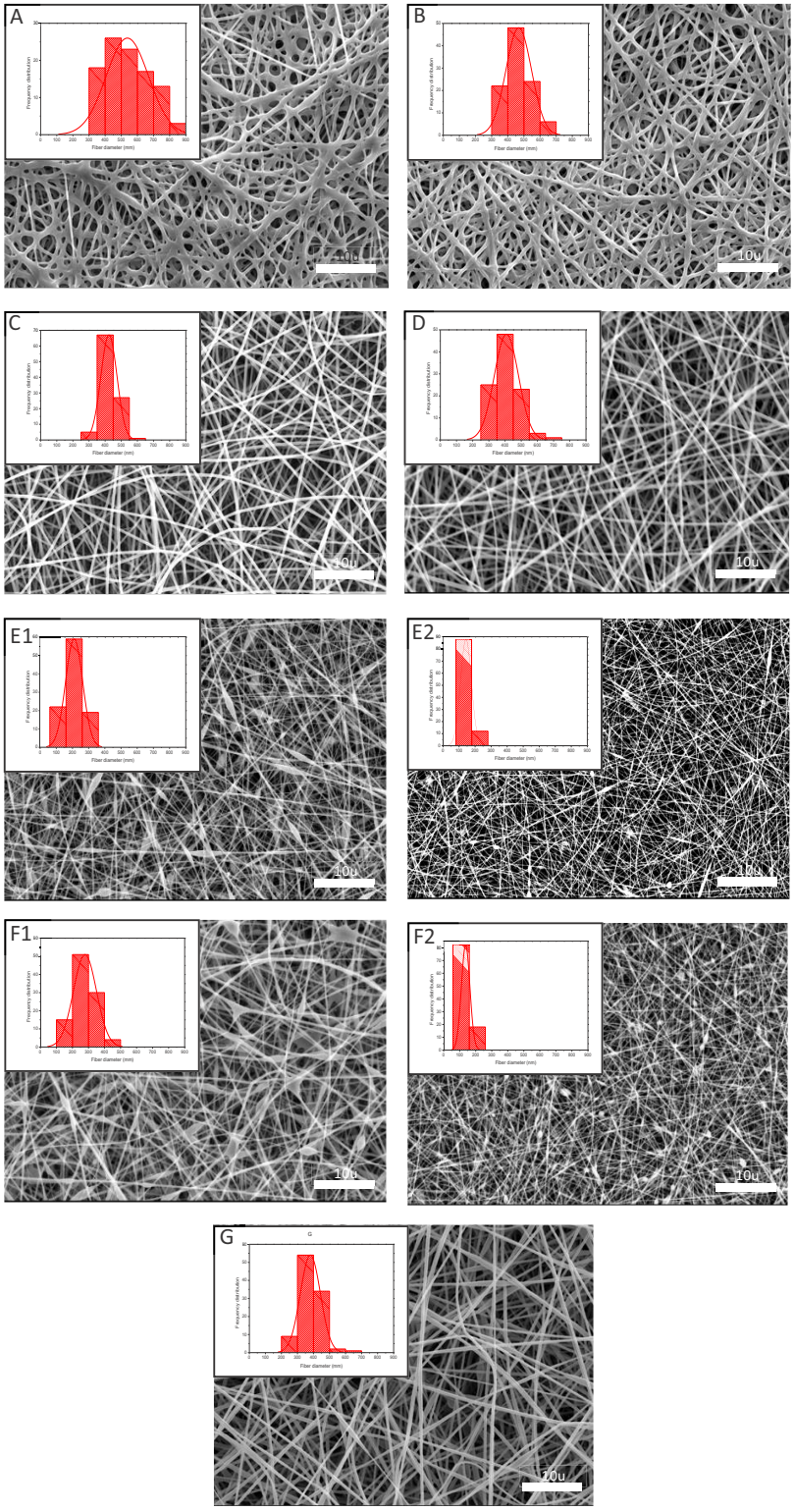

Figure 2-2. SEM micrographs with magnification x2000 and fiber distribution of the electrospun nanofiber 1wt% of pure PHBH (A), blend PHBH/PVA: (B) 90/10, (C) 70/30, (D) 50/50 using HFIP as a solvent, and PHBH/PVA: (E1) 30/70 and (F1) 10/90 by using the mixed solvent of HFIP/water 90/10, PHBH/PVA (E2) 30/70 and (F2) 10/90 by using the mixed solvent of HFIP/water 70/30, and pure PVA (G) by using water.

2.3.2. Fourier transform infrared spectroscopy (FT-IR)

Figure 2-3 shows infrared spectra of pure PHBH, pure PVA, and their blend nanofibers. Some peaks of PHBH and PVA were found to be overlapping. The most evidence absorbance bands for interaction between PHBH and PVA molecules were carbonyl and hydroxyl group bands. Figure 2-3c shows an enlarged view of FT-IR spectra of the pure PHBH (A), pure PVA (G), and their blend at a wavenumber of 1780 – 1660 cm^{-1}. In the spectrum of pure PHBH (A), a strong sharp and steep band was observed at 1719 cm^{-1} being the C=O stretching vibration. It was assigned to the highly ordered crystalline structure. Moreover, the band at 1740 cm^{-1} was very weak which is attributed to amorphous carbonyl vibration of PHBH [30,31]. Moreover, some peaks appeared at 2850, 2874, 2937, and 2970 cm^{-1} are CH stretching, CH stretching, asymmetric stretching of CH_2, and C-CH_3, respectively. Other characteristic bands for PHB appeared at ~1278, ~1180, and ~1052 cm^{-1}, those are assigned to ester of polymer structure while peaks at 980, 1228, 1260, and 1722 cm^{-1} were exhibited to attribute to the crystalline phase of PHBH [6].

These bands at 3265 cm^{-1} and 2912 cm^{-1} were attributed to OH and CH_2 stretching of pure PVA, respectively. Other characteristic bands for PVA appeared at 1420, 1325, 1088 cm^{-1}, and 920 cm^{-1}, those are attributed to O-H, C-H bending; C-O-H bending; C-O, and rocking CH_2, respectively. Figure 2-3b and 2-3c, for blend nanofiber at a ratio of 50/50 (D) showed that the peak shifted to 2932 cm^{-1}, 1721 cm^{-1}, and 3311 cm^{-1} which is the representative of the asymmetric stretching of CH_2, C=O and O-H, respectively. The resume of assignments of FT-IR was shown in Table 2-2. These shifted peaks indicate the intermolecular interaction between the two polymers. The intermolecular interaction has an important role in the amorphous phase inside of blend polymer due to be considered to be an evidence of the compatibility in the blend polymer [6,32].

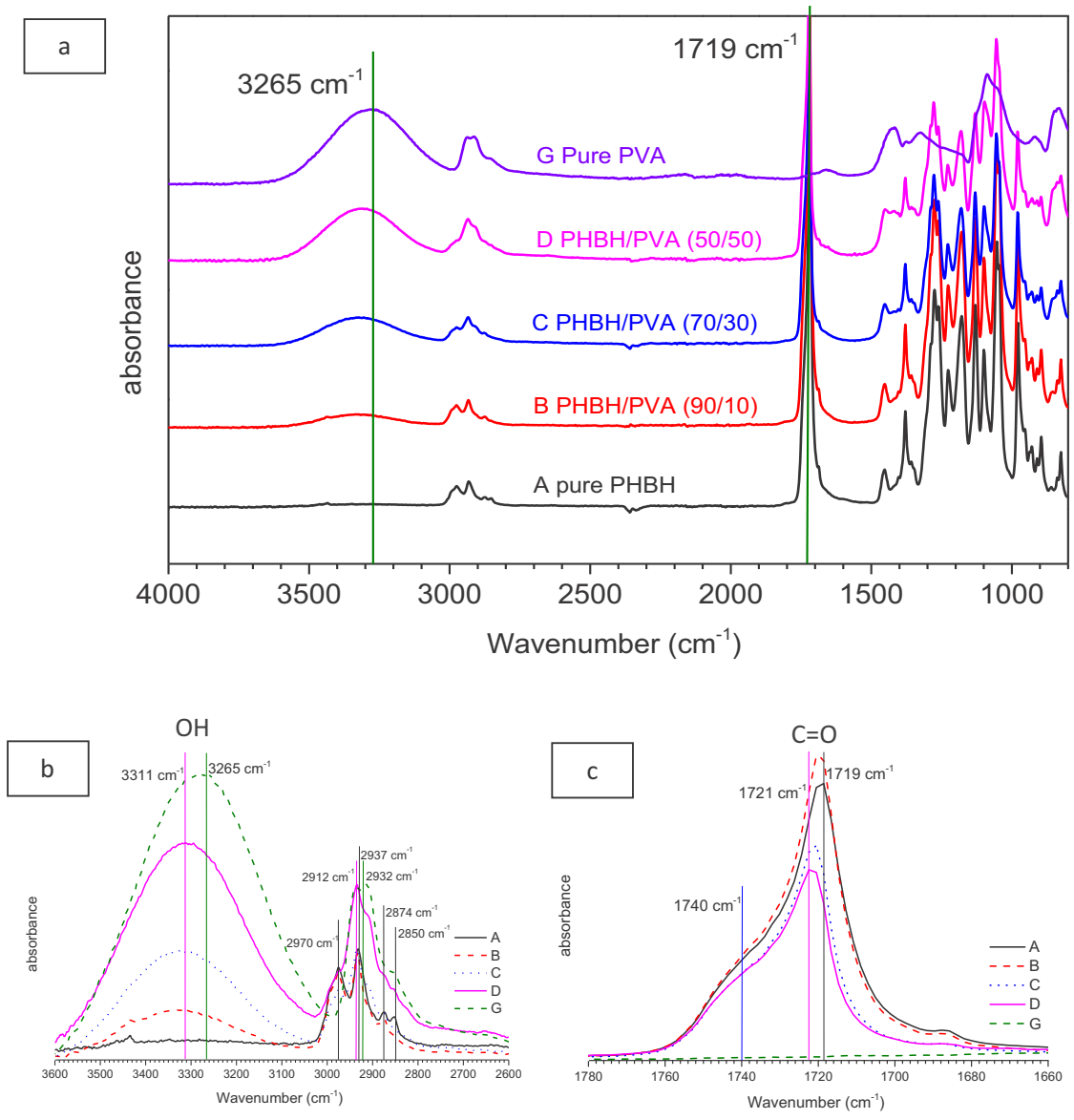

Figure 2-3. a. FT-IR spectra of pure PHBH (A), different ratio nanofibers of PHBH/PVA (B) 90/10, (C) 70/30, (D) 50/50, and pure PVA (G) (1000 – 4000 cm^{-1}). b. and c. show intensity in the OH stretching in the 2600-3600 cm^{-1} and C=O stretching in the 1660-1780 cm^{-1} vibration.

Table 2-2. Assignments of FT-IR absorption bands for electrospun pure PHBH, pure PVA, and ratio of 50/50 blend nanofiber.

Peaks for electrospun nanofibers (cm^{-1})			**Assignment**
PHBH	PVA	PHBH/PVA (50/50)	
	3265	3311	Stretching of OH
2970			C-CH_3
2937	2912	2932	Asymmetric stretching of CH_2
2874			CH stretching
2850			CH stretching
1740	1740		C=O carbonyl group stretching Vibration of the crystalline carbonyl group
1719	1721		Stretching of C=O (Acetate group) (Crystalline)
1455		1454	Asymmetric deformation of CH_3
	1420		O-H, C-H bending, $\gamma(CH_2)$, $\delta(OH)$
1380		1381	Symmetric wagging of CH_3
	1325		C-O-H bending
1276		1278	Symmetric C-O-C stretching
1180		1181	Asymmetric C-O-C stretching
1130		1130	Symmetric stretching vibration of C–O–C group
1100		1098	Symmetric C-O-C stretching
	1088		Stretching of C-O and bending of OH(amorphous sequence of PVA)
1053		1055	C-O stretching and CH_2 rocking
1098		Shoulder	C-C stretching (Crystalline)
	920		Bending of CH_2

2.3.3. Differential scanning calorimetry (DSC)

DSC curves of pure PHBH, pure PVA, and their blends are shown in Figure 2-4. The thermal curve of pure PHBH and pure PVA showed a single peak, representing their melting point (T_m). These melting points (T_m) of pure PHBH and pure PVA were 141 and 229°C, respectively. Thermal curves at a different blend ratio of PHBH/PVA are characterized by two distinct peaks, describing their melting peak of PHBH and PVA. The positions of these peaks and melting point values were the same as those before blending. In the previous study of PHB and P(VAc-*co*-VA*)* blend film, the melting point (T_m) of PHB in the blends are almost the same with pure PHB, indicated that the blends are immiscible [21]. Yoshie et al. [28] have investigated in the *a*-

PVA/PHB blend film that both of them have occurred phase separation, it means no indication of interaction between them, and it is expected that the crystalline PHB and PVA are separate.

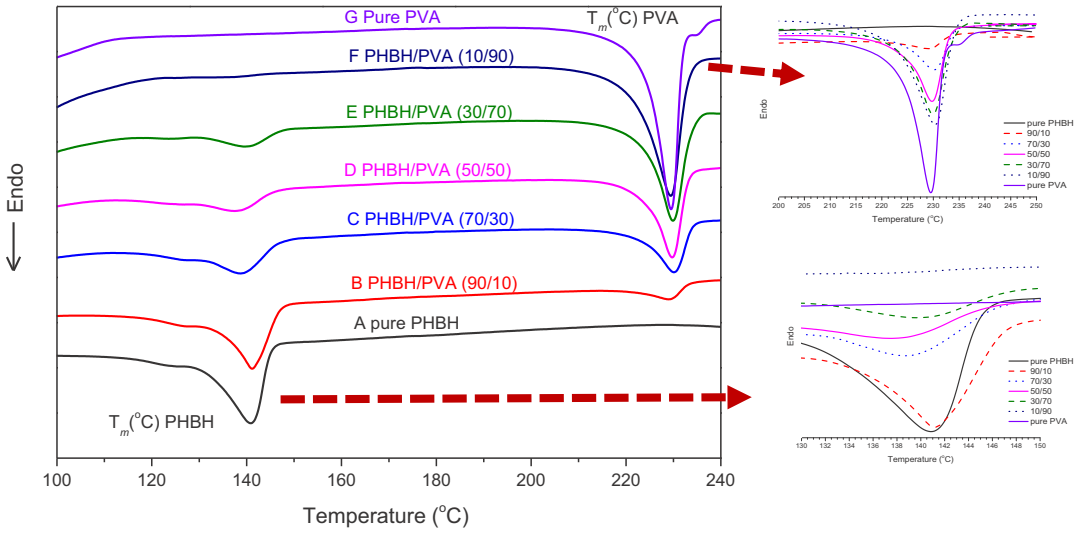

Figure 2-4. DSC curves of PHBH/PVA nanofibers

The values of heat fusion or melting enthalpy (ΔH_m) of pure PHBH, pure PVA, and the blends were given in Table 2-3. These heat fusions of pure PHBH and pure PVA were 43.8 and 70.5 J/g, respectively. The ΔH_m of PHBH decreased with the increase of PVA. Moreover, the melting peak of PHBH could not observed at 90% content of PVA in blend nanofibers. The ΔH_m of PVA decreased as well with the increase of PHBH. However, the melting peak of PVA still existed at 90% content of PHBH. The decrease of ΔH_m indicates the decrease of crystalline phase (crystallinity) of those polymers [22].

Figure 2-5 shows the comparison of values of ΔH_m of PHBH/PVA nanofibers to elucidate the interaction between PHBH and PVA. The experiment value of ΔH_m of PHBH was not in accordance with calculation value. The experiment value of ΔH_m of PHBH in blend nanofibers was lower than the calculation value from 70% into 30% of PHBH content. It is indicated that the crystallization of PHBH will be affected and inhibited by the increase of PVA. The ΔH_m of PVA

between the experiment and calculation showed almost the same in blend nanofibers. It supposed that the crystallization of PVA would not be affected by the increase of PHBH. From DSC results, it can be presumed that PHBH/PVA nanofibers might be partially mixed in the amorphous state. The compatibility in the amorphous state could be proved by the existence of the hydrogen bonding interaction between PHBH and PVA polymer, as discussed in FT-IR results.

Table 2-3. The melting point (T_m) and heat fusion (ΔH) of pure PHBH, pure PVA, and PHBH/PVA nanofibers obtained from Figure 2-4.

Ratio	T_m PHBH (℃)	ΔH PHBH (J/g)	T_m PVA (℃)	ΔH PVA(J/g)
Pure PHBH	141.0	43.8	-	-
90/10	140.0	42.5	227.9	6.9
70/30	138.1	24.5	229.4	24.6
50/50	136.8	15.2	230.1	36.0
30/70	138.9	7.3	229.0	47.3
10/90	-	-	230.0	66.1
Pure PVA	-	-	229.3	70.5

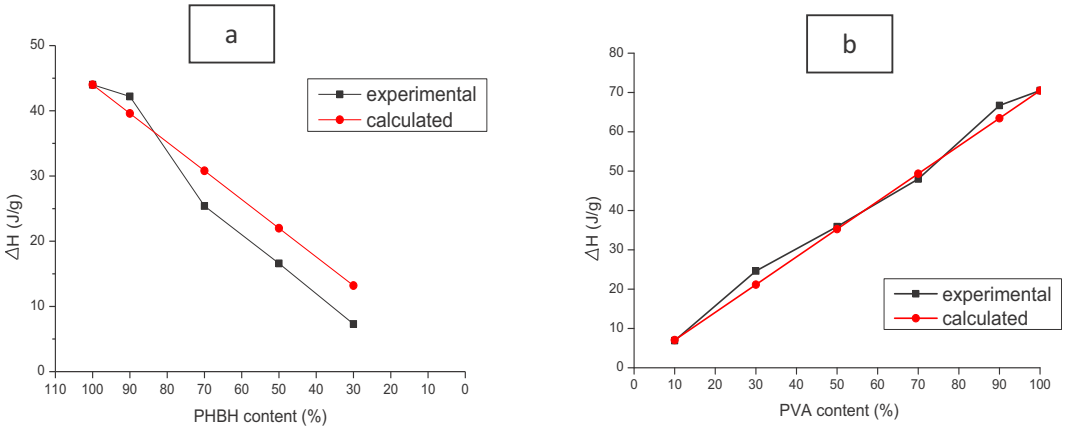

Figure 2-5. Comparison between experimental and calculated values against polymer content for PHBH heat fusion (ΔH) (a) and PVA heat fusion (ΔH) (b).

2.3.4. Crystalline structure by wide-angle X-ray diffraction (WAXD)

The reflection patterns of pure PHBH, pure PVA, and their blend without and with heat treatment are displayed by WAXD, as shown in Figure 2-6. There is no definitive new diffraction by the formation of a cocrystallize-crystal structure in PHBH/PVA nanofibers (D). From this figure, it clearly describes that every refraction pattern of nanofibers has mainly characteristic diffraction of the PHBH component. By comparing with heat treatment condition, each diffraction of pure PHBH, pure PVA, and their blend showed more clearly than that without heat treatment, especially in the ratio of more than 70% PVA due to crystallization of PVA.

Figure 2-7 represents the WAXD patterns of pure PHBH, pure PVA, and their blends without and with heat treatment. The WAXD pattern of pure PHBH exhibited distinct crystalline peaks at 8.8°, 11°, 13.1°, 14.3°, 16.8°, 17.4°, and 19.6°. These crystalline peaks are attributed α-form structure of PHB, which assigned to (020), (110), (021), (101), (121), (040), and (002) of the orthorhombic unit cell, respectively [8]. The WAXD pattern of pure PVA displayed a single diffraction peak at 12.8°, assigned to (101).

These reflection patters and peaks positions in PHBH-rich blend of PHBH/PVA are similar to those of pure PHBH, which indicated that PHB unit cell was no change by blending with PVA. Moreover, the crystalline intensity of their blends decreased with the increase of PVA. Furthermore, the intensity of peak for PVA crystalline in the sample with heat treatment was higher than without heat treatment, as shown in Figure 2-7 (b). Blend nanofibers with PVA more than 70% displayed an increase in the intensity of crystalline peak by heat treatment as well as similar to pure PVA. It means the amount of PVA crystalline structure increased by the heat treatment condition. The increase of PVA crystallinity on a blend ratio of more than 70% PVA intended to

maintain the morphology of nanofiber when soaked in PBS as a medium for cell attachment experiment.

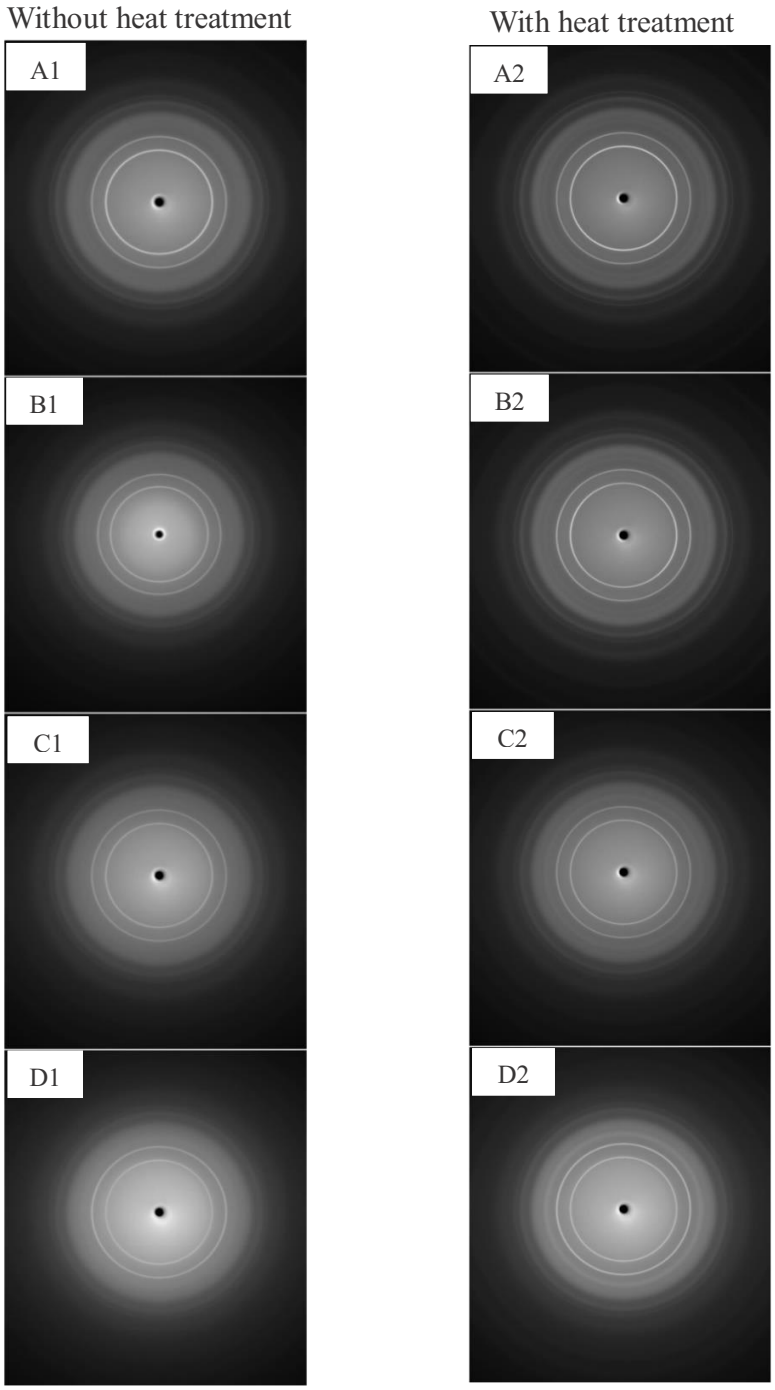

Figure 2-6. WAXD patterns of pure PHBH (A), PHBH/PVA of 90/10 (B), 70/30 (C), and 50/50 (D) without (1) and with heat treatment (2) by Laue camera.

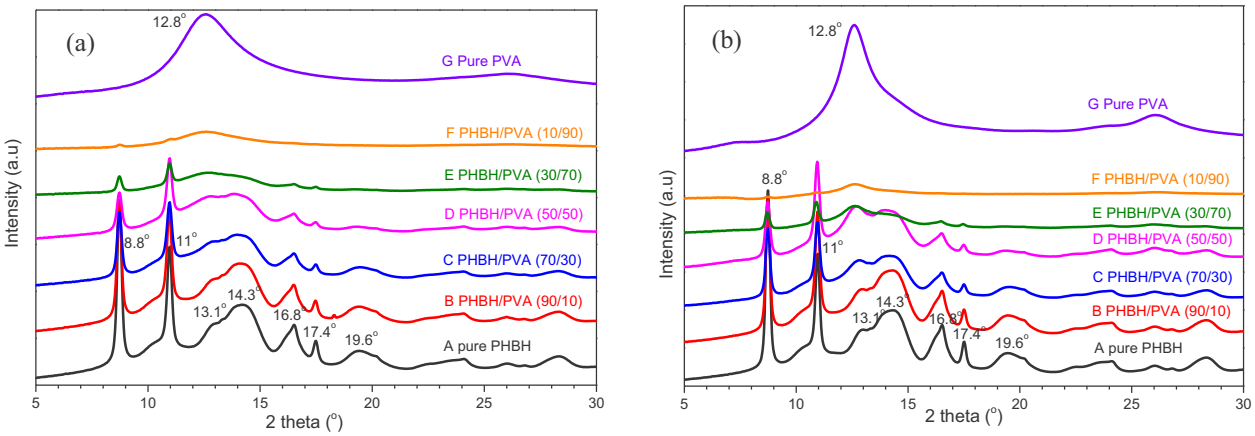

Figure 2-7. WAXD patterns of nanofiber without heat treatment (a) and with heat treatment (b).

2.3.5. Water contact angle (WCA)

In this study, samples are divided into two groups: without and with heat treatment. The heat treatment was used for stabilization of PVA in the blend PHBH/PVA nanofibers against water because the sample without heat treatment was easy to be deformed by water. However, it seemed to be challenging to measure the WCA for a blend ratio of more than 90% PVA because the sample wrinkled easily in contact with the drop of water. As seen in Figure 2-8, WCA values of pure PHBH, PHBH/PVA (90/10), (70/30), and (50/50) without heat treatment were 88°, 105°, 128°, and 130°, respectively. It should be highlighted that PHBH/PVA nanofibers showed the hydrophobic surface character since the WCA of the sample was higher than 90° [33].

The WCA of nanofiber with PVA more than 10% showed more hydrophobic than pure PHBH. These results exhibited that the WCA of nanofibers without or with heat treatment increased with the increase of PVA. From the report by Asran et al. [6] WCA values in the PHB/PVA films decreased with the increase of PVA. Therefore, the surface became more hydrophilic by the addition of PVA. However, in this study, WCA of PHBH/PVA nanofibers showed the opposite results against WCA values of PHB/PVA film. This result suggested that

WCA values may not only be affected by PVA content but also by the morphology of the nanofiber.

Figure 2-9 exhibits the relation between the WCA values and the fiber diameter of the nanofibers. It shows that the WCA value increased due to the change of morphology in nanofiber, which is the decrease of fiber diameter. Interestingly, some samples showed that water drop from WCA measurement on nanofibers was absorbed to nanofibers with PVA-rich content. Furthermore, water absorption analysis was conducted to the understanding of stability water in the blend nanofibers.

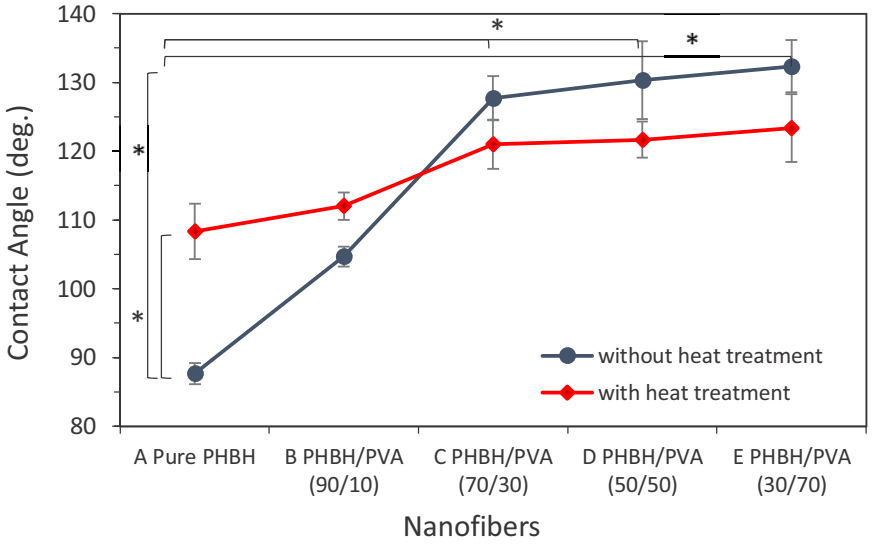

Figure 2-8. Water contact angle of pure PHBH and blend nanofibers without and with heat treatment. "*" was statistically significant ($p<0.05$) between (A) pure PHBH without and with heat treatment. Furthermore, "*" was statistically significant ($p<0.05$) between (A) pure PHBH with (C), (D), (E) PHBH/PVA nanofibers.

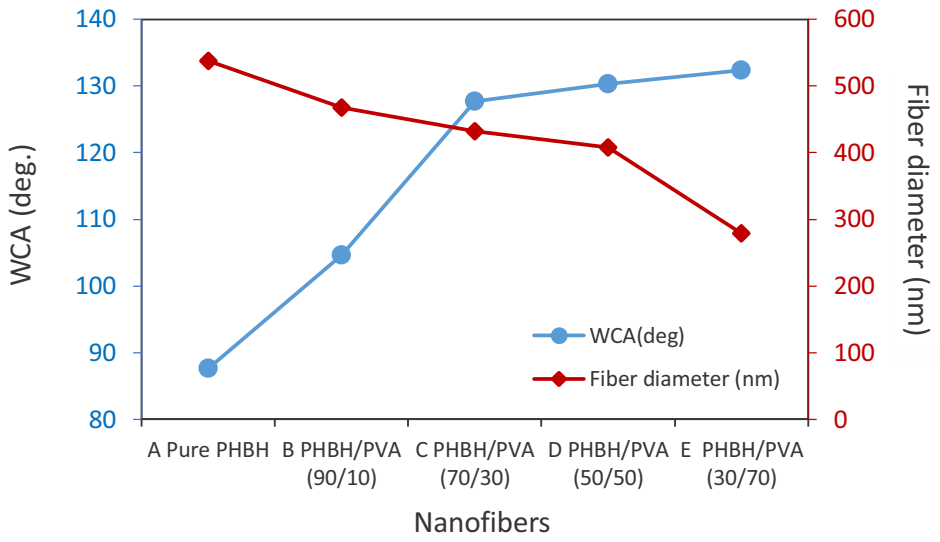

Figure 2-9. Relation between WCA values and fiber diameter of the nanofibers.

2.3.6. Water absorption

The water absorption was measured to evaluate the amount of water that can be absorbed into the blend nanofibers. The water absorption for samples without and with heat treatment is shown in Figure 2-10. Pure PHBH and PHBH/PVA (90/10) nanofibers showed a low water absorption. Pure PHBH and 90% PHBH showed low water absorption. Interestingly, after immersion in water, the nanofibers with PVA more than 30% and higher WCA, showed higher water absorption than pure PHBH. The water absorption of PHBH/PVA (70/30) nanofibers exhibited more than 350%. Li et al. [34] reported that the silk fibroin/PVA freeze-dried blend scaffolds were able to uptake water about 7.3 times the weight of the sample. It means the characteristic of PVA (hydrophilicity) affected the water absorption of nanofiber.

To analyze the cell attachment of nanofibers with PVA-rich content, heat treatment at 100°C for 3 h was applied to keep the surface of nanofiber stable. Park et al. [35] reported that heat treatment at 100°C for 1 h in the blend nanofibers of PVA/ poly(acrylic acid) was able to improve the water-resistance of electrospun PVA fiber. Their result showed that the trend between

nanofiber without and with heat treatment was almost similar. However, this result showed a slight decrease in water absorption in the sample with heat treatment than without heat treatment. It suspected due to the increase of PVA crystallinity by heat treatment, as discussed in WAXD results.

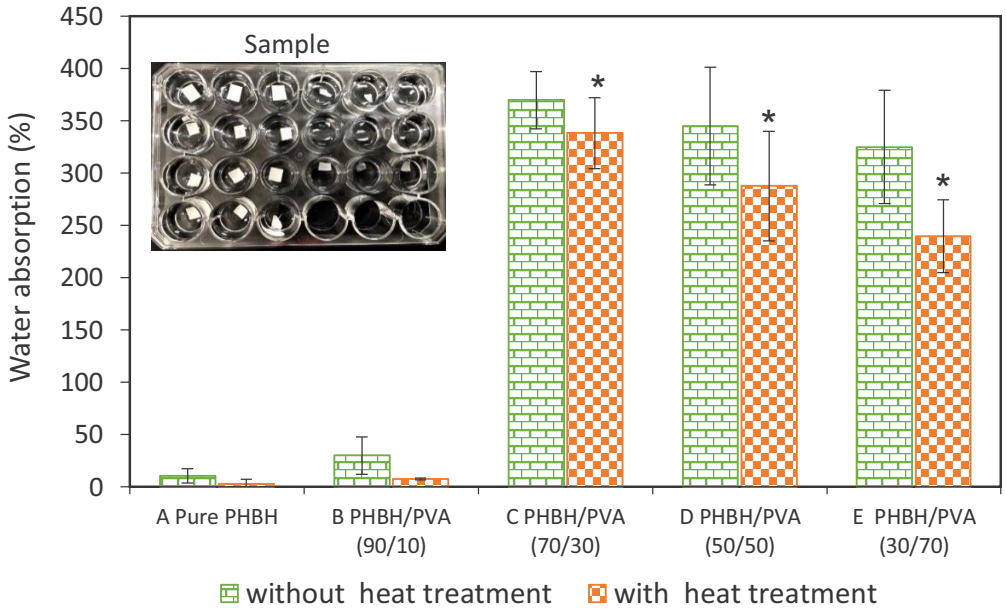

Figure 2-10. Water absorption of pure PHBH and its blend without and with heat treatment after immersion in water for 1 day. "*" was statistically significant ($p<0.05$) between (A) pure PHBH and blend nanofibers PHBH/PVA (B) 90/10 with blend nanofibers PHBH/PVA (C) 70/30, (D) 50/50, and (E) 30/70 of without and with heat treatment.

SEM images confirmed that the surface and structure of pure PHBH and PHBH/PVA nanofibers of 90/10, 70/30, and 50/50 were not changed (data not shown). Figure 2-11 shows the SEM-photographs of PHBH/PVA nanofibers of 30/70 and 10/90 after immersion in water for 1 day. The nanofiber of 30/70 (E) showed the swollen effect of the fiber and morphological change by immersion. The nanofibers with heat treatment exhibited lower swollen compared to without heat treatment. However, PHBH/PVA nanofiber of 10/90 (F) with heat treatment showed low

stability against water and gradually dissolved. It cannot be keep any nanofibers structure. Therefore, samples of 30/70 (E) and 10/90 (F) were not used for biocompatibility analysis.

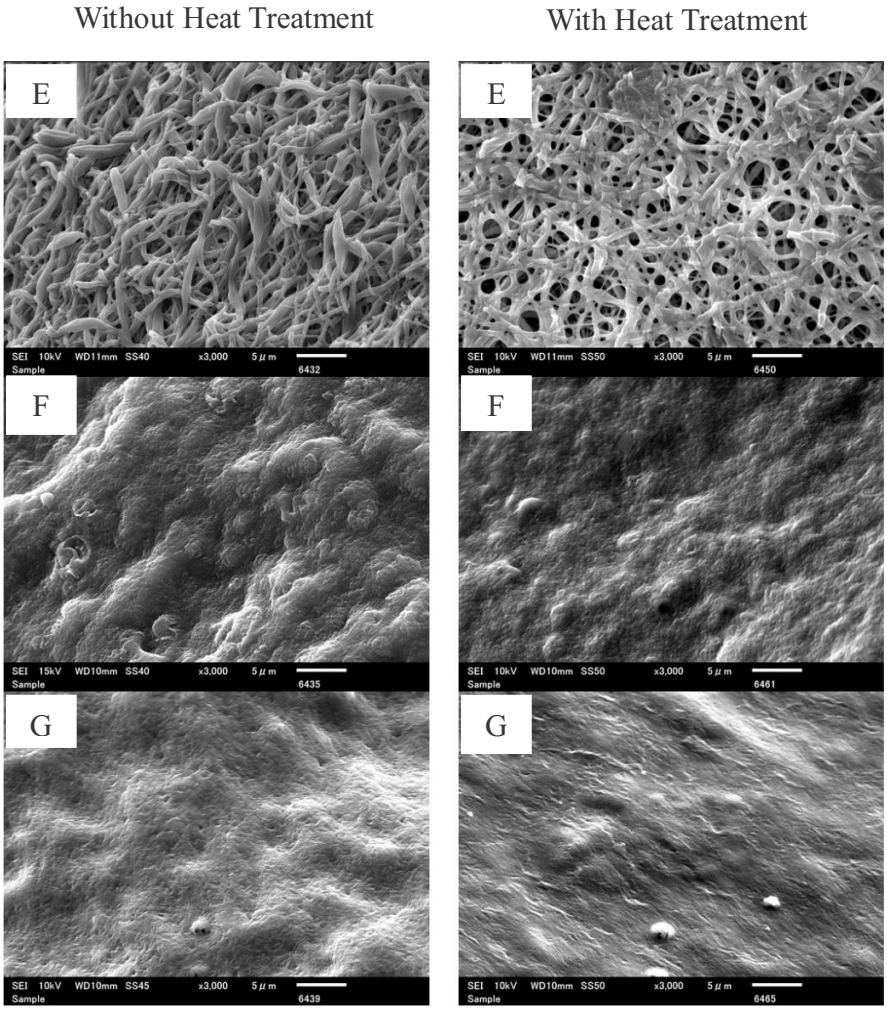

Figure 2-11. SEM with magnification x5000 of nanofiber with PHBH/PVA (30/70) (E), (10/90) (F), and pure PVA (G) without and with heat treatment after immersion in water for 1 day.

2.3.7. *In vitro* biodegradation

It has been reported that PBS containing lipase enzyme can accelerate the degradation of PHBHx film with different HHx content [36] and P3/4HB monofilament suture [37]. The degradation of PHBH/PVA nanofibers was performed in the lipase solution at 37°C for 4 weeks. Figure 2-12 shows the weight loss of pure PHBH and PHBH/PVA nanofibers by enzymatic

degradation. The degradation rate of nanofibers by enzyme depended on PHBH/PVA ratio. The degradation of nanofibers of pure PHBH and PHBH/PVA (90/10) displayed a low degradation rate and no change in 1 week. However, after 4 weeks, the weight loss nanofibers of pure PHBH and PHBH/PVA (90/10) were 5.1 and 11.9%, respectively. It was reported by Zhijiang et al. [22] that the weight loss of pure PHB nanofiber by buffer solution was ~3% after 30 days. Furthermore, pure P(HB-*co*-5.5%-HHx) nanofiber in this research showed a faster degradation rate than pure P(HB-*co*-5%-HHx) and P(HB-*co*-20%-HHx) film with a weight loss ~3% by lipase enzyme degradation for 50 days [36]. This may be due to the high surface area and low crystallinity of PHBH in PHBH nanofiber compared with PHBH film.

The weight loss of nanofiber with 30 and 50% of PVA was 18.3 and 20.5% after 4 weeks, respectively. The degradation rate for nanofibers of PHBH/PVA 50/50 is three times as high as pure PHBH after 4 weeks. During the degradation, the lipase attacks on nanofibers and the degradation firstly occurs in the amorphous region. This amorphous region degrades faster than the crystalline region due to the hydrolysis of the polymer chains [15,37]. The presence of PVA (hydrophilic polymer) affected the degradation rate of blend nanofibers. The high degradation in blend nanofiber with PVA-rich content was due to low crystallinity of PHBH by the addition of PVA and the hydrolytic degradation of PVA in PBS and enzyme solution. Table 2-4 shows the weight loss of blend nanofibers in PBS and lipase enzyme. The degradation rate of samples in PBS and lipase enzyme solution showed the faster than that in only PBS solution. It means that the addition of lipase in solution affects the degradation rate of nanofibers.

Figure 2-13 shows the physical appearance for nanofibers after degradation of which their shape declined and corrugated. SEM micrographs also confirmed the surface change after degradation for 4 weeks (Figure 2-14). Morphology for nanofibers of the pure PHBH (A) and

PHBH/PVA of 90/10 (B) showed that some nanofibers have broken in small cleavage. By the addition of PVA, they showed damage and winding of nanofibers. In the case of ratio 50/50 (D), these nanofibers showed the coalescence of fibers, which indicates the start of dissolution. These results show that the degradation rate can be easily controlled by the presence of the PVA component for PHBH/PVA nanofibers.

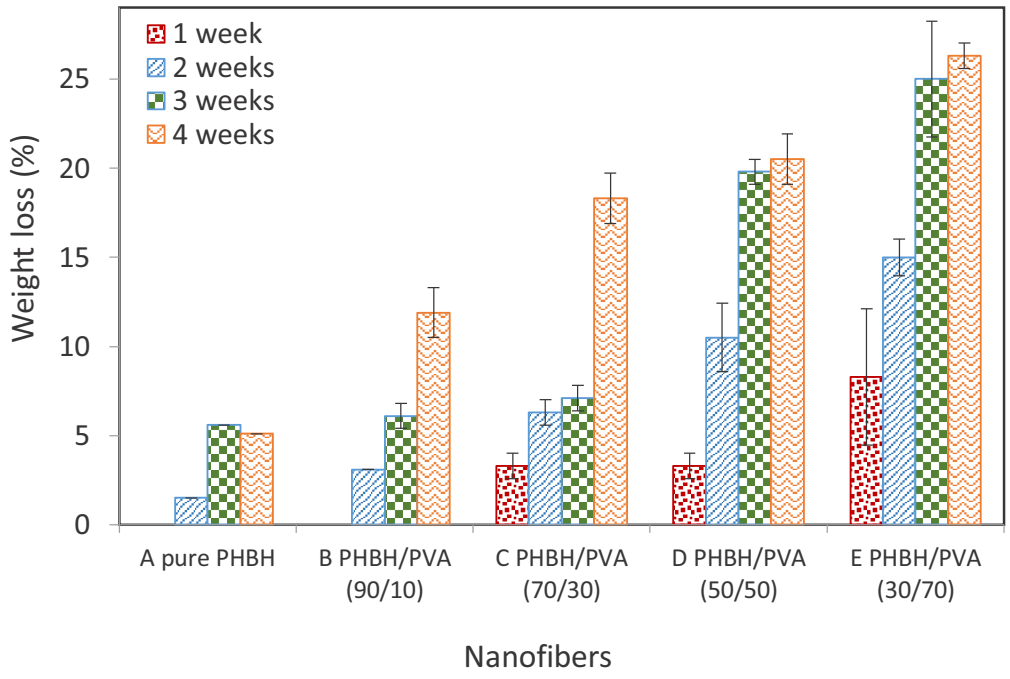

Figure 2-12. *In vitro* degradation for nanofiber samples of (A) pure PHBH, PHBH/PVA nanofibers of (B) 90/10, (C) 70/30, (D) 50/50, (E) and 30/70 in PBS containing lipase enzyme.

Table 2-4. Weight loss (%) of blend nanofibers after incubation in PBS and lipase enzyme solution.

Nanofibers	Weight loss (%)					
	PBS (pH 7.4)		Lipase enzyme solution (pH 7.4)			
	1 week	2 weeks	1 week	2 weeks	3 weeks	4 weeks
Pure PHBH	0.0	0.4	0.0	1.5	5.6	5.1
PHBH/PVA (90/10)	0.2	1.1	0.0	3.1	6.1	11.9
PHBH/PVA (70/30)	3.5	4.2	3.3	6.3	7.1	18.3
PHBH/PVA (50/50)	4.9	5.5	3.3	10.5	19.8	20.5
PHBH/PVA (30/70)			8.3	15.0	25.0	26.3

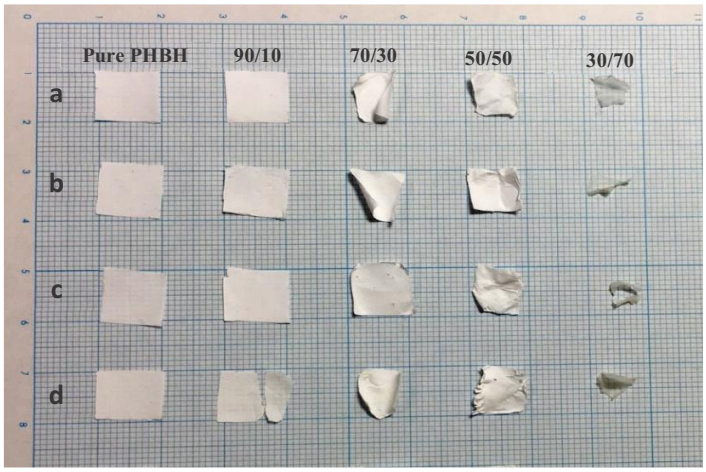

Figure 2-13. Physical appearance for nanofiber samples of pure PHBH, ratio PHBH/PVA of 90/10, 70/30, 50/50, and 30/70 after degradation in enzymatic solution for 1 week (a), 2 weeks (b), 3 weeks (c), and 4 weeks (d).

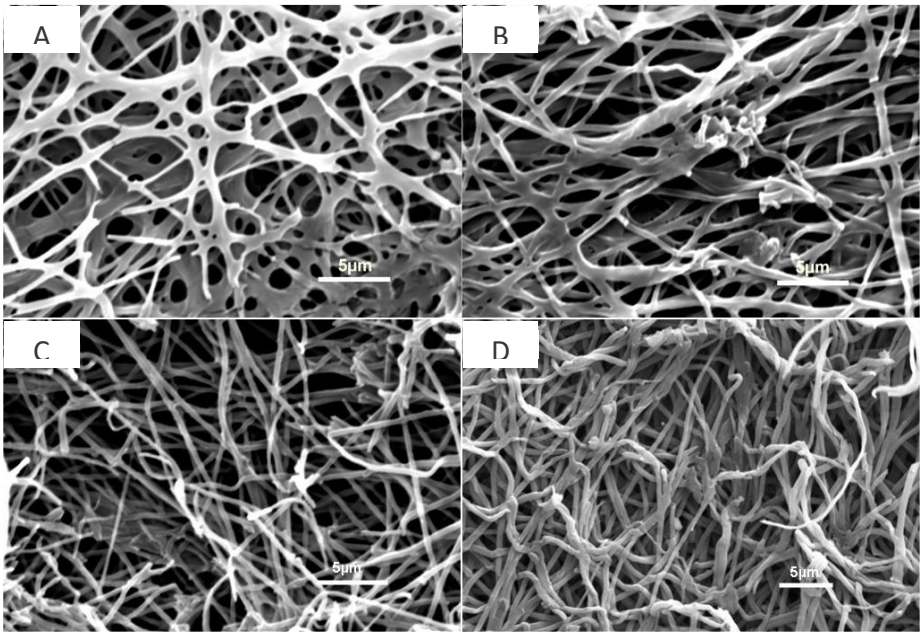

Figure 2-14. SEM micrographs with magnification x2000 of pure PHBH (A) and ratio PHBH/PVA of 90/10 (B), 70/30 (C), and 50/50 (D) after enzymatic degradation for 4 weeks.

2.3.8. *In vitro* biocompatibility

NIH3T3 cells were cultivated on the pure PHBH and PHBH/PVA nanofiber of 90/10, 70/30, and 50/50 to investigate its *in vitro* biocompatibility. The number of attached and grown cells on nanofibers was calculated after incubation at 36°C for 1, 3, 5, and 7 days as shown in Figure 2-15.

As a result, the number of adhered and grown cells on the pure PHBH nanofiber was higher than the control surface (TCP) and those other PHBH/PVA nanofibers. In the previous study, pure PHB nanofiber showed that it could promote the attachment of dermal fibroblast, however not as high as the control [6]. In this study, NIH3T3 cells growth on pure PHBH nanofibers increased in 5 days compared with 1 day, then decreased in the 7 days. The decrease of cell number grown on the surface nanofibers was considered due to the cells growing available surface area on nanofibers [38]. In contrast, low mouse fibroblast growth ability was showed by the addition of more than 30% PVA for blend nanofibers. Asran et al. [6] reported that the ability of fibroblast cells to attach and proliferate on nanofibers declined by increasing the PVA content in PHB/PVA nanofibers. It supposed that the mouse fibroblasts and human fibroblasts have similar trend growth cells line. Jeong et al. [39] also confirmed that the relative amount of living cells of human dermal fibroblasts, NIH3T3 fibroblasts, and mouse skeletal muscle cells (C2C12) on polyaniline-camphorsulfonic acid/poly(L-lactide-*co*-Ɛ-caprolactone) (CPSA-PAni/PLCL) nanofiber scaffolds showed the same behavior.

The reason for the decline of fibroblast cells on the blend nanofiber might be due to NIH3T3 cells being challenging to grow on the surface, which has higher water absorption and hydrophilic surface characteristics. The higher water absorption was found in the nanofibers PHBH/PVA of more than 30% PVA content (Figure 2-10). The study by Ngiah *et al.* [40] about gelatin nanofiber coated PHB exhibited that increasing the water uptake caused a decrease in the adhesion and the proliferation capacity of the fibroblast cells but did not affect the keratinocytes. Moreover, previous studies by Asran *et al.* [6] reported that hydrophilicity surface of PHB/PVA nanofibers decreased dermal fibroblasts proliferation. Hydrophilic substrates were found to have a negative effect on dermal fibroblasts proliferation and were found to be better on the intermediate wettable

surface obtained through blending [41]. The study by Hsieh *et al.* [42] reported that the number of mouse NIH3T3 fibroblasts was increased due to a chemical cross-linked PVA-g-starch 3D scaffold. It seems that the middle value of wettability substrates provided better cells growth. Subsequently, fibroblasts were found to have maximum adhesion when contact angles were between 60 and 80°[43]. However, this study showed the opposite result with Asran et al. [6], of which the WCA value of nanofibers PHBH/PVA with more than 30% of PVA content was over 120°. The higher hydrophobic surface nanofiber might be suppressed the growth of fibroblasts cells as well. Even though the cells proliferation in the pure PHBH better than blend nanofiber, however, PHBH/PVA nanofibers might have the potential for cell proliferation by using other types of cells.

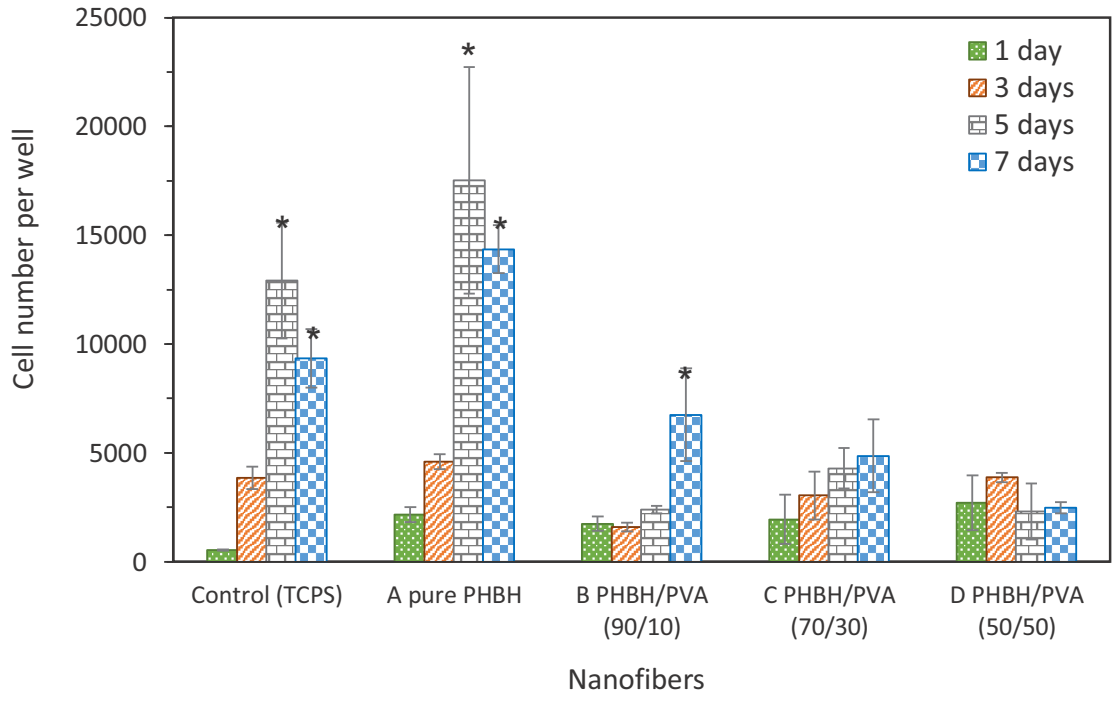

Figure 2-15. The proliferation of NIH3T3 cells on control (TCPS), (A) pure PHBH, and PHBH/PVA nanofibers of (B) 90/10, (C) 70/30, and (D) 50/50 after cells cultured for 1, 3, 5, 7 days, respectively. "*" was statistically significant ($p<0.05$) for each sample between 1 day to 3, 5, and 7 days.

Figure 2-16 represents the SEM images of NIH3T3 fibroblast cells cultured for 3 days on different PHBH/PVA nanofibers. The shape of fibroblasts attached to pure PHBH nanofiber (A), PHBH/PVA blend nanofiber of 90/10 (B), and 70/30 (C) changed from their original shape on the TCP (F) to round spindle-like shape. The reason might be that nanofibers with fiber diameters of 80 – 500 nm mimic the extracellular matrix (ECM). Moreover, cells on pure PHBH and PHBH-rich nanofibers were spread and migrated along the fiber direction and on its surface. However, the cell morphology of PHBH/PVA 50/50 (D) nanofiber was still round with little activity.

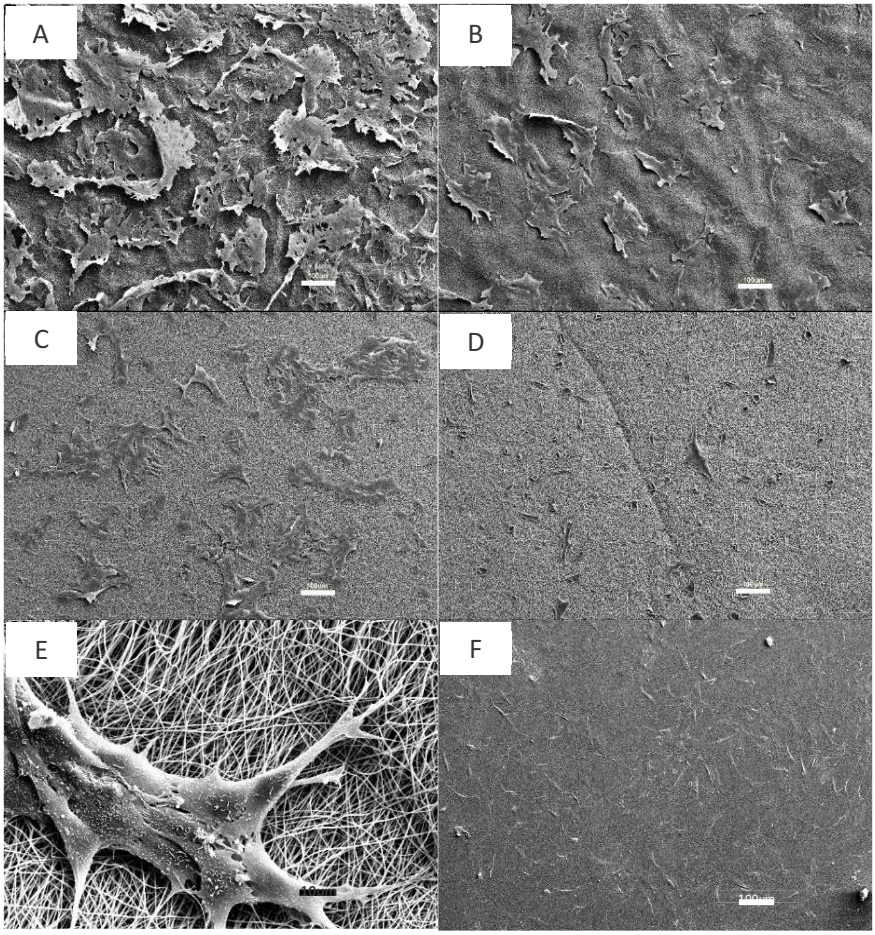

Figure 2-16. SEM images with magnification x100 of NIH3T3 cells where cultured for 3 days on pure PHBH nanofiber (A) and PHBH/PVA nanofibers of 90/10 (B), 70/30 (C), 50/50 (D) and TCPS (F). (E) High magnification with magnification x1000 of cells shape on the PHBH/PVA nanofiber of 70/30 (C).

2.4. Conclusions

Poly(3-hydroxybutyrate-*co*-3-hydroxyhexanoate) (PHBH)/poly(vinyl alcohol) (PVA) nanofibers was successfully prepared and fabricated by electrospinning in the 1 wt% of HFIP solution and the mixture of HFIP/water. The addition of water into blend solution of PVA-rich content turned a more stable solution during the electrospinning process. As the PVA in PHBH/PVA blend increased, the diameter of nanofibers decreased. It was observed that the fiber diameter and its distribution could be controlled by the increase of PVA at various ratios of HFIP/water solvent and humidity. PHBH/PVA nanofiber was immiscible in the crystalline state but compatible in the amorphous state. The blend system of PHBH with PVA affected in the stability of nanofibers against water. Interestingly, the surface of PHBH/PVA nanofiber of 70/30 and 50/50 was stable as the fibers did not swell. Moreover, the degradation rate for nanofibers PHBH/PVA of 50/50 (D) was higher than the pure PHBH (A) after 4 weeks. In contrast, pure PHBH (A) nanofiber promoted the NIH3T3 cell attachment and proliferation compared to blend nanofiber PHBH/PVA of 50/50 (D). It supposed that NIH3T3 fibroblast cells were difficult to grow up and adhere to the surface nanofiber. The surface characteristics against for blend nanofiber was influencing on degradation rate and cell attachment and proliferation. However, it may be necessary to use other cells for evaluating biocompatibility, such as keratinocytes.

2.5. References

[1] S. Sundarrajan., K.L. Tan., S.H. Lim., S. Ramakrishna., Electrospun nanofibers for air filtration applications, *Procedia Engineering* 75 (2014) 159-163.

[2] R. Goyal., L.K. Macri., H.M. Kaplan., J. Kohn., Nanoparticles and nanofibers for topical drug delivery, *Journal of Controlled Release* 240 (2016) 77–92.

[3] S. Vigneswari., H.P.S. Abdul Khalil., A.A. Amirul., Designing of collagen based poly(3-hydroxybutyrate-*co*-4-hydroxybutyrate) scaffolds for tissue engineering, *Journal of Polymer Science* (2015) Article ID 731690, 10 pages.

[4] H. Itoh., Y. Li., K. H. K. Chan., M. Kotaki., Morphology and mechanical properties of PVA nanofibers spun by free surface electrospinning, *Polym. Bull.* 73 (2016) 2761-2777.

[5] E. Maseili., M. Morshed., M. H. Nasr-Esfahani., S. Sadri., J. Hilderink., Av. Hilderink., C. Blitterswijk., L.Va. Moroni., Fabrication, characterization and cellular compatibility of poly(hydroxyl alkanoate) composite nanofibrous scaffolds for nerve tisue engineering, *Plos One* Vol. 8 issue 2 (2013) E57157.

[6] A.Sh. Asran., K. Razghandi., N. Aggarwal., G.H. Michler., T. Groth., Nanofibers from blends of polyvinyl alcohol and polyhydroxy butyrate as potential scaffold material for tissue engineering of skin, *Biomacromolecules* 11 (2011) 3413-3421.

[7] A.A. Olkhov., S.V. Vlasov., A.L. Iordanskii., G.E. Zaikov., V.M.M. Lobo., Water transport, structure features and mechanical behavior of biodegradable PHB/PVA blends*, Journal of Applied Polymer Science* 90 (2003) 1471-1476.

[8] T.H. Ying., D. Ishii., A. Mahara., S. Murakami., T. Yamaoka., K. Sudesh., R. Samian., M. Fujita., M. Maeda., T. Iwata., Scaffolds from electrospun polyhydroxyalkanoate copolymers: fabrication, characterization, bioabsorption and tissue response, *Biomaterials* 29 (2008) 1307-1317.

[9] S. Philip., T. Keshavarz., I. Roy., Polyhydroxyalkanoates: biodegradable polymers with a range of applications, *Journal of Chemical Technology and Biotechnology* 82 (2007) 233-247.

[10] E. Bugnicourt., P. Cinelli., A. Lazzeri., V. Alvare., Polyhydroxyalkanoate (PHA): Review of synthesis, characteristics, processing and potential applications in packaging, *eXPRESS Polymer Letters* Vol. 8*,* 82 (2014) 791-808.

[11] T. Iwata., T. Tsuge., S. Taguchi., H. Abe., T. Tanaka., Handbook of R&D information in Japan, bio-based polymers (2013) ISBN978-4-7813-0271-3.

[12] S.Y. Lee., Bacterial polyhydroxyalkanoates, *Biotechnology and bioengineering* 49 (1996) 1-14.

[13] X. Lu., L. Wang., Z. Yang., H. Lu., Strategies of polyhydroxyalkanoates modification for the medical application in neural regeneration/nerve tissue engineering, *Advances in Bioscience and Biotechnology* 4 (2013) 731-740.

[14] L. Gong., D.B. Chase., I. Noda., J. Liu., D.C. Martin., C. Ni., J.F. Rabolt., Discovery of β-form crystal structure in electrospun poly[(*R*)-3-hydroxybutyrate-*co*-(*R*)-3-hydroxyhexanoate](PHBHx) nanofibers: from fiber mats to single fibers, *Macromolecules* 48 (2015) 6197–6205.

[15] M.-L. Cheng., P.Y. Chen., C.H. Lan., Y.M. Sun., Structure, mechanical properties and degradation behaviors of the electrospun fibrous blends of PHBHx/PDLLA, *Polymer* 52 (2011) 1391-1401.

[16] N. Hosoda., T. Tsujimoto., H. Uyama., Green composite of poly (3-hydroxybutyrate-*co*-3-hydroxyhexanoate) reinforced with porous cellulose, *ACS Sustainable Chem. Eng.* 2 (2014) 248−253.

[17] M-L. Cheng., C-C. Lin., H-L. Su., P-Y Chen., Y-M. Sun., Processing and characterization of electrospun poly(3-hydroxybutyrate-*co*-3-hydroxyhexanoate) nanofibrous membranes, *Polymer* 49 (2008) 546-553.

[18] M. Zhang., X. Diao., Y. Jin., Y. Weng., Preparation and characterization of biodegradable blends of poly (3-hydroxybutyrate-*co*-3-hydroxyhexanoate) and poly (butylene adipate-*co*-terephthalate), *Journal of Polymer Engineering* 36(5) (2016) 473-480.

[19] Y. Azuma., N. Yoshie., M. Sakurai., Y. Inoue., R. Chujo., Thermal behaviour and miscibility of poly(3-hydroxybutyrate)/poly(vinyl alcohol) blends, *Polymer* 33 (1992) 4763-4767.

[20] M.P. Arrieta., E. Fortunati., F. Dominici., E. Rayon., E. Jopez., J.M. Kenny., PLA-PHB/cellulose based films: Processing, structural and thermal properties, *Carbohydrate Polymers* 107 (2014) 16-24.

[21] P. Xing., X. Ai., L. Dong., Z. Feng., Miscibility and crystallization of poly (β-hydroxybutyrate)/poly(vinyl acetate-*co*-vinyl alcohol) blends, *Macromolecules* 31 (1998) 6898-6907.

[22] C. Zhijiang., X. Yi., Y. Haizheng., J. Jia., Y. Liu., Poly(hydroxybutyrate)/cellulose acetate blend nanofiber scaffolds: Preparation, characterization and cytocompatibility, *Materials Science and Engineering* C 58 (2016) 757-767.

[23] M. Zhang., N.L. Thomas., Blending polylactic acid with polyhydroxybutyrate: the effect on thermal, mechanical, and biodegradation properties, *Advances in Polymer Technology* vol. 30, No. 2 (2011) 67-79.

[24] B.O. Kim., and S.I. Woo., Compatibilizing capability of poly(β-hydroxybutyrate-,*co*-ε-caprolactone) in the blend of poly (β-hydroxybutyrate) and poly (ε-caprolactone), *Polymer Bulletin* 41 (1998) 707–712.

[25] C.C. DeMerlis., D. R. Schoneker., Review of the oral toxicity of polyvinyl alcohol (PVA), *Food and Chemical Toxicolog*, 41 (2002) 319-326.

[26] J.-C. Park., T. Ito., K.-O. Kim., K.-W. Kim., B.-S. Kim., M.-S. Khil., H.-Y. Kim., I.-S. Kim., Electrospun poly(vinyl alcohol) nanofibers: effects of degree of hydrolysis and enhanced water stability, *Polymer Journal* 42 (2010) 273-276.

[27] E. Chiellini., A. Corti., S. D'Antone., R. Solaro., Biodegradation of poly (vinyl alcohol) based materials, *Prog. Polym. Sci.* 28 (2003) 963-1014.

[28] N. Yoshie., Y. Azuma., M. Sakurai., Y. Inoue., Crystallization and compatibility of poly(vinyl alcohol)/poly(3-hydroxybutyrate) blends: Influence of blend composition and tacticity of poly(vinyl alcohol), *Applied Polymer Science* 56 (1995) 17-24.

[29] S. De Vrieze., T. Van Camp., A. Nelvig., B. Hagström., P. Westbroek., K. De Clerck., The effect of temperature and humidity on electrospinning, *J. Mater. Sci.* 44 (2009) 1357.

[30] A. Padermshoke., Y. Katsumoto., H. Sato., S. Ekgasit., I. Noda., Y. Ozaki., Surface melting and crystallization behavior of polyhydroxyalkanoates studied by attenuated total reflection infrared spectroscopy, *Polymer* 45 (2004) 6547–6554.

[31] T. Ikejima., N. Yoshie., Y. Inoue., Infrared analysis on blends of poly(3-hydroxybutyric acid) and stereoregular poly(vinyl alcohol): influence of tacticity of poly(vinyl alcohol) on crystallization of poly(3-hydroxybutyric acid), *Macromol. Chem. Phys.* 197 (1996) 869-880.

[32] Y.M. Lee., S.H, Kim., S.J. Kim., Preparation and characteristics of β-chitin and poly(vinyl alcohol) blend, *Polymer* 37 (1996) 5987-5905.

[33] M.P. Arrieta., J. Lopez., D. Lopez., J.M. Kenny., L. Peponi., Development of flexible materials based on plasticized electrospun PLA-PHB blends: Structural, thermal, mechanical, and disintegration properties, *European Polymer Journal* 73 (2015) 433-446.

[34] X. Li., J. Qin., J. Ma., Silk fibroin/poly(vinyl alcohol) blend scaffolds for controlled delivery curcumin, *Regenerative Biomaterials* (2015) 97-105.

[35] J.S. Park., J.W. Park., E. Ruckenstein., Thermal and dynamic mechanical analysis of PVA/MC blend hydrogels, *Polymer* 42 (2001) 4271–4280.

[36] Y.W. Wang., W. Mo., H. Yao., Q. Wu., J. Chen., G.-Q. Chen., Biodegradation studies of poly(3-hydroxybutyrate-*co*-3-hydroxyhexanoate), *Polymer Degradation and Stability* 85 (2004) 815-821.

[37] X. Chen., X. Yang., J. Pan., L. Wang., K. Xu., Degradation behaviors of bioabsorbable P3/4HB monofilament suture *in vitro* and *in vivo*, *Journal of Biomedical Materials Research Part B: Applied Biomaterial* (2009), DOI: 10.1002/jbm.b.31534.

[38] B. Duan., X. Yuan., Y. Zhu., Y. Zhang., X. Li., Y. Zhang., K. Yao., A nanofibrous composite membrane of PLGA-chitosan/PVA prepared by electrospinning, *European Polymer Journal* 42 (2006) 2013-2011.

[39] S. I. Jeong., I. D. Jun., M. J. Choi., Y. C. Nho.,Y. M. Lee., H. Shin., Development of electroactive and elastic nanofibers that contain polyaniline and Poly(L-lactide-*co*-Ɛ-caprolactone) for the control of cell adhesion, *Macromolecular bioscience* 8 (2008) 627-637.

[40] N. Ngiah., L. Madhavi., R. Anitha., C. Anandan., N.T. Srinivasa., U.T. Sivagnanam., Development and characterisation of coaxially electrospun gelatin coated poly (3-hydroxybutyric acid) thin films as potential scaffolds, *Material Science and Engineering C* 33 (2013) 4444-4452.

[41] N. Nagiah., L. Madhavi., R. Anitha., N.T. Srinivasa., U.T. Sivagnanam., Electrospinning of poly (3-hydroxybutyric acid) and gelatin blended thin films: fabrication, characterization, and application in skin regeneration, *Polym. Bull.* 70 (2013) 2337-2358.

[42] W.-C. Hsieh., J.-J. Liau., Cell culture and characterization of cross-linked poly(vinyl alcohol)-g-starch 3D scaffold for tissue engineering, *Carbonhydrate polymers* 98 (2013) 574-580.

[43] Y. Tamada., Y. Ikada., Effect of preadsorbed proteins on cell adhesion to polymer surface, *Journal of colloid and interface science* 155 (1993) 334-339.

[44] G. Fotakis., J.A. Timbrell., *In vitro* cytotoxicity assays: Comparison of LDH, neutral red, MTT and protein assay in hepatoma cell lines following exposure to cadmium chloride, *Toxicology Letters* 160 (2016) 171-177.

[45] Y. Tamada., E. A. Kulik., Y. Ikada., Simple method for platelet counting, *Biomaterials* 16 (1995) 259-261.

Chapter 3

Natural antibacterial reagents (*Centella*, Propolis, and Hinokitiol) loaded into PHBH composite nanofibers

Chapter 3

3.1. Introduction

Nowadays, nanofibers produced by electrospinning have received the considerably high attention to be an excellent candidate for many important applications in medical field such as drug delivery [1], oral cavity [2], tissue engineering [3–6], wound dressing and healing [7,8] due to the ultra-fine diameter, high surface area to volume ratio, and cost-effectiveness. A large number of studies devoted to utilizing nanofibers that could mimic the extracellular matrix (ECM) of the body and cellular activity [9], as well as sustained drug action such as in skin regeneration or healing [1,10,11] have been published over the last few years.

Open wounds were reported to be healed in a much faster-recovering pace by covering from infection using antimicrobials. Without covering, the healing process could be hindered by bacterial interference with cell-matrix interactions, followed by the delay of cell proliferation and tissue regeneration [12]. Recent studies have endeavored to incorporate novel drugs, antibacterial reagents, and other healing enhancers into nanofiber membranes for the sake of facilitating the wound healing process [7,10,11].

Natural antibiotics as one of herb, plant extracts, or pure compounds have been used in pharmaceutical products for centuries. With the advancement of nanotechnology, it provides unlimited opportunities for employing natural antibiotics as additives for engineering novel intriguing materials for wound treatments and healing. One of the advantages of using natural products such as plant extracts, essential oils, aloe vera, honey, and so on instead of synthetic reagents (iodine and silver) is to diminish the risk of sensitization and development of resistance [12]. *Centella asiatica,* a traditional medicine derived from plants, has been used widely in Southeast Asia, India, and other regions for skin treatments. The major biologically active

compounds in *centella* are triterpenoids, which include asiaticoside, madecassoside, asiatic acid, and madecassic acid [13–15]. The previous study of gelatin/*centella asiatica* [14] reported that *centella* extract demonstrated a strong inhibition against microbial pathogens such as *Staphylococcus aureus*, *Escherichia coli*, and *Pseudomonas aeruginosa,* which are most commonly implicated in wound infection. Polycaprolactone/*centella* biopolymer nanofibers also showed the antibacterial activity against *B. cereus* and *M. luteus* with the improvement of mechanical properties owing to the decrease of the fiber diameters after adding *centella* [5]. *In vitro* test using human dermal fibroblast and human dermal keratinocyte (HaCaT) cells and *in vivo* circular wound excision of rabbits, *centella* extract proved to accelerate wound healing process and the cell migration rates [16]. Furthermore, electrospun gelatin membrane containing *centella* improved cell proliferation *in vitro* for fibroblasts (L-929) and wound recovery *in vivo,* using male Sprague Dawley (SD) rats [14].

Propolis, a resinous substance with dark brown color, was produced via mixing collected from buds and bark of trees with beeswax and saliva by honeybees. The main chemical compounds in propolis are aromatic acids and phenolic compounds, especially flavonoid and phenolic acid [17–19]. Several of studies have demonstrated that propolis exhibited great potential for wound healing. In the study of polyurethane/propolis nanofibers [20], the authors concluded that nanofiber mats containing 30% (w/w) propolis had strong inhibitory effects against *E. coli*. In addition, PVA/hydroalcoholic extract propolis nanofiber [21] exhibited the antibacterial activity almost equal to the vancomycin, an effective commercial antibiotic. Propolis was also confirmed to possess antibacterial, antifungal, antiviral, antioxidant, anti-inflammatory, and antitumor characteristics [22].

Hinokitiol is one of the natural components isolated from Japanese cypress and western red cedar. It belongs to the class of tropolones that contain an unsaturated seven-membered carbon ring with *β*-Thujaplicin and is well-known for its inhibitory effects against the growth of fungi, bacteria, and insects [23]. Research on hinokitiol as a potential medication for the treatment of the dental root canal demonstrated strong antibacterial effects against *S. aureus* and anti-inflammation [24]. These natural products (*centella*, propolis, and hinokitiol) show the capability to be used as alternative antibacterial reagents to replace conventional synthetic antiseptics.

Poly(3-hydroxybutyrate-*co*-3-hydroxyhexanoate) (PHBH) is a copolymer, developed from poly[(*R*)-3-hydroxybutyrate] (PHB), the basic homopolymer in polyhydroxyalkanoates (PHA), which are a family of polyesters produced by bacteria through the fermentation of sugars, lipids, fatty acids, alkanes, alkenes, and alkanoic acids [1,6,25–27]. PHBH, one of the copolymers in more than 150 kinds of PHAs, which in turn consist of various co-monomers, has been considered for commercial production [28]. In the biomedical field, PHB and its copolymers have been demonstrated to be fully biodegradable and an excellent biological material with biocompatibility properties. The prominent advantage of these polymers is their ability to be completely degraded by microorganisms under aerobic and anaerobic conditions without forming toxic by-products [26,29]. Recently, these materials have been developed for medical applications such as suture, skin scaffold, tissue engineering, and so on. Moreover, biodegradable nanofibers as a material matrix for wound dressing and healing have received considerable attention because they have been found to be an effective strategy for delivering antibacterial agents or anti-inflammatory substances. Previous studies demonstrated that PHB/caffeic acid electrospun nanofibers coated with polyelectrolyte exerted the antibacterial activity and antitumor [7]. Poly(3-hydroxybutyrate-*co*-3-hydroxyvalerate) (PHBV)/Curcumin nanofibers showed positive effects on wound healing,

cell adhesion, and non-toxicity to L929 mouse fibroblast cell line [11]. Besides, PHBH nanofibers promoted the NIH3T3 fibroblast cell attachment and proliferation [4]. This polymer can be regarded as one of the most promising polymers obtained from renewable resources, suitable for drug or antibacterial products carrying.

In this study, *centella*, propolis, and hinokitiol with inherent biological activity were selected as representatives for natural antibacterial products and were integrated into PHBH biodegradable polymer. This study focused on developing nanofibrous membranes with antibacterial properties, comprised of natural antibacterial reagents and biodegradable PHBH polymer for combined effects on wound healing. The electrospinning technique was chosen as the mean of fabrication. To my knowledge, the fabrication and characterizations of *centella*, propolis, and hinokitiol loaded in biodegradable PHBH polymer have not been reported hitherto. I attempted to investigate the effects of the addition of *centella*, propolis, and hinokitiol to PHB copolymer with 3-hydroxyhexanoate (3HH) unit as the polymer matrix regarding crystallinity of the PHBH composite nanofibers, antibacterial activities, and sustained release behaviors. The advantages of this research are to promote the use of natural products over conventional synthetic antiseptics by studying three variants of natural antibacterial products, namely *centella*, propolis, and hinokitiol. It is also important to present harmlessness for products made of PHBH and natural antibacterial reagents if they are to be used in medical applications.

3.2. Materials and methods

3.2.1. Materials

PHBH containing 5.5 mol% of 3HH (M_w = 5.37x10^5 g/mol%) was provided from Kaneka Corp. The natural antibacterial reagent, such as *centella asiatica* powder, propolis powder,

hinokitiol powder were purchased from Dins Natural, Ltd., Stakich, Inc., and Wako Pure Chemical Industries, Ltd., respectively. Solvent to prepare PHBH solution for electrospinning was used 1,1,1,3,3,3-hexafluoro-2-propanol (HFIP) from Wako Pure Chemical Industries, Ltd. Acetone, ethanol 99.5%, and methanol to prepare the *centella* extract solution, propolis extract solution, and hinokitiol solution in order to incorporate with PHBH nanofibers mat were purchased from Wako Pure Chemical Industries, Ltd.

Staphylococcus aureus (NBRC 12732) and *Escherichia coli* (NBRC 3972) for antibacterial activity tests were purchased from the National Institute of Technology and Evaluation, Biological Resource Center (NBRC), Japan.

3.2.2. Preparation of natural antibacterial reagent solutions

Centella solutions were prepared using either ethanol or methanol, the concentrations of *centella* to solutions were 15 or 30% (w/v), respectively. The propolis solutions were prepared by dissolving propolis in acetone at 10% (w/v) and ethanol with the concentrations of 10% or 30% (w/v), respectively. Each prepared solution was mixed using a magnetic stirrer for 24 h at room temperature. Afterward, all solutions were filtered to remove insoluble substances. The hinokitiol solution was prepared by dissolving hinokitiol powder in 99.5% ethanol with a concentration of 30% (w/v), also stirred at room temperature for 24 h without filtration.

The concentrations of natural products in ethanol–*centella* (15EC and 30EC), methanol–*centella* (15MC and 30MC), acetone–propolis (10AP), and ethanol–propolis (10EP and 30EP) were determined from the dry weight of each natural product by evaporating solutions under vacuum. The concentration of hinokitiol in ethanol–hinokitiol (30EH) was 30% due to no insoluble substances in the ethanol solution.

These percentage concentrations of *centella*, propolis, hinokitiol are displayed in Table 3-1. These solutions were added to PHBH HFIP solutions with different ratios before the electrospinning process.

Table 3-1. The concentrations of natural products (NP) in each solution after vacuum dried and ratios of natural product solutions to total weight of PHBH spinning solutions.

Concentration(w/v)_Solution _Natural Product (NP)	**Percentage Concentration of NP Inside Solution (w/w)**	**Ratios NP Solutions over Total Weight of Spinning PHBH Solutions (v/v) (Code)**			
		1%	**5%**	**7%**	**10%**
15% Ethanol–*Centella*	2.16	15EC	15EC	-	15EC
30% Ethanol–*Centella*	4.14	30EC	30EC	-	30EC
15% Methanol–*Centella*	3.17	15MC	15MC	-	15MC
30% Methanol–*Centella*	7.21	30MC	30MC	-	30MC
10% Acetone–Propolis	8.95	10AP	10AP	10AP	-
10% Ethanol–Propolis	5.43	10EP	10EP	10EP	-
30% Ethanol–Propolis	12.25	30EP	30EP	30EP	-
30% Ethanol–Hinokitiol	30	30EH	30EH	30EH	-

3.2.3. Preparation and fabrication of PHBH composite nanofibers

PHBH was dissolved in HFIP at room temperature for 4 h to make solution 2 wt%. The natural antibacterial solutions were added into PHBH HFIP solutions and stirred continuously for 16–20 h to get homogeneous solutions. The ratios of ethanol–*centella* (15EC and 30EC) or methanol–*centella* (15MC and 30MC) were 1, 5, and 10% over the total weight of spinning PHBH solutions. Furthermore, ratios of acetone-propolis (10AP), ethanol–propolis (10EP and 30EP), and ethanol–hinokitiol (EH) to the total weight of spinning PHBH solutions were 1, 5, and 7%, (Table 3-1). These prepared blend solutions were filled into a glass syringe (10 mL) with a 0.6 mm diameter of stainless steel needle. The electrospinning process was carried out using a high voltage power supply by Kato Tech, Japan (Figure 3-1). The solution feeding rate was 0.1–0.3 mm/min,

15–20 kV voltage, and 15 cm tip-to-collector distance. The environmental conditions of the electrospinning chamber were at a humidity level of 20–30 RH% and temperature ranged between 23–26 °C. The electrospun fibers were collected on the surface of the collector, followed by drying at room temperature for 24 h to evaporate the solvents.

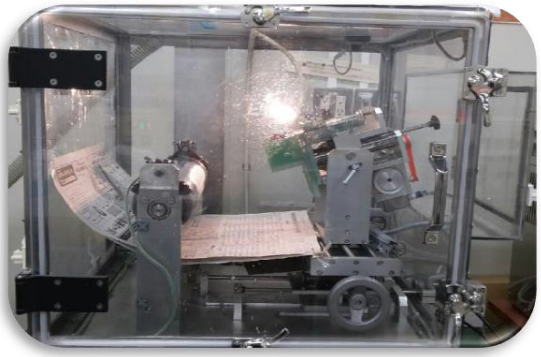

Figure 3-1. Electrospinning apparatus (Kato Tech, Japan).

3.2.4. Characterization of PHBH composite nanofibers

3.2.4.1.Scanning electron microscopy (SEM)

The morphology of neat PHBH and PHBH with natural products electrospun nanofibers was investigated by scanning electron microscopy (SEM, JSM-6010LA, JEOL, Tokyo, Japan) at an accelerating voltage of 10 kV with various magnifications, Figure 3-2. The samples were coated with platinum (Pt) in a sputtering device for 60 sec at 30 mA. Image J software was used to measure 50 fibers diameters from each SEM photograph.

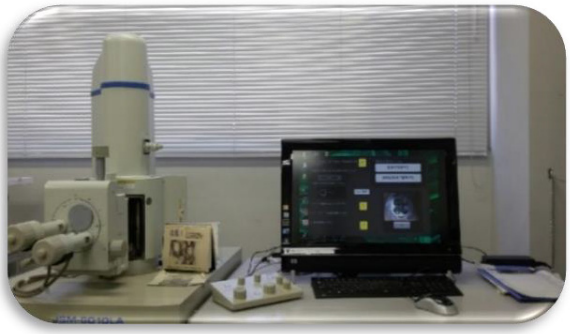

Figure 3-2. SEM, JSM-6010LA, JEOL, Tokyo, Japan.

3.2.4.2. Fourier transform infrared (FT-IR) spectroscopy

The presence of *centella*, propolis, and hinokitiol incorporated in electrospun nanofibers was analyzed using attenuated total reflectance (ATR) FT-IR spectroscopy (IR Prestige-21, Shimadzu Corp., Kyoto, Japan), Figure 3-3. The infrared spectra were recorded from 4000–600 cm^{-1}, with a resolution of 4 cm^{-1}. The infrared beam enters the ATR crystal at an angle of typically 45° and is reflected at the crystal to sample interface with a low signal of noise ratio.

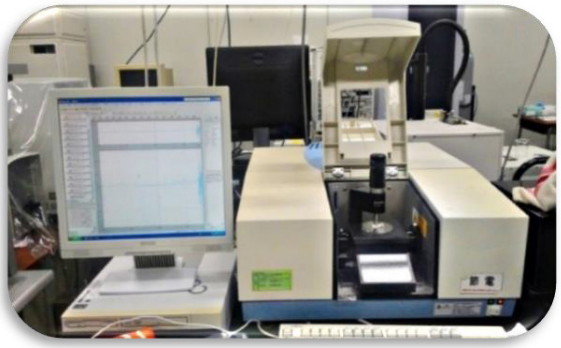

Figure 3-3. IR Prestige-21, Shimadzu Corp., Kyoto, Japan.

3.2.4.3. X-ray (XRD)

Wide-angle X-ray diffraction (WAXD) was used for crystalline structure analysis of PHBH nanofibers with or without *centella*, propolis, or hinokitiol. The two-dimensional (2D) patterns of nanofibers were recorded by X-ray diffraction equipment (SPring-8 synchrotron radiation facility in Japan) with a wavelength of 0.07085 nm at a 2θ scanning angle between 5–30°. The distance from the sample to the detector (PILATUS 3 × 2 M) was 326.5 mm and the exposure time was 2.0 sec. The X-ray diffraction of composite nanofibers was investigated by the MDIP application.

3.2.4.4. Mechanical properties

The mechanical properties of neat PHBH, PHBH/*centella*, PHBH/propolis, PHBH/hinokitiol nanofibers were investigated by using a tensile testing machine (EZTest/EZ-S, Shimadzu Corp., Kyoto, Japan) with 50-N load cell at room temperature, Figure 3-4.a. Ten

specimens were prepared from each composite nanofiber sheet (Figure 3-4.b). The specimens with thickness ranging from 0.05 to 0.14 mm were cut into a rectangular shape of 30 mm x 5 mm. Two grips stapled the ends of each sample with an initial distance of 10 mm and a crosshead speed of 10 mm/min. Tensile strength, Young's modulus, and elongation at break were calculated based on the stress-strain curves.

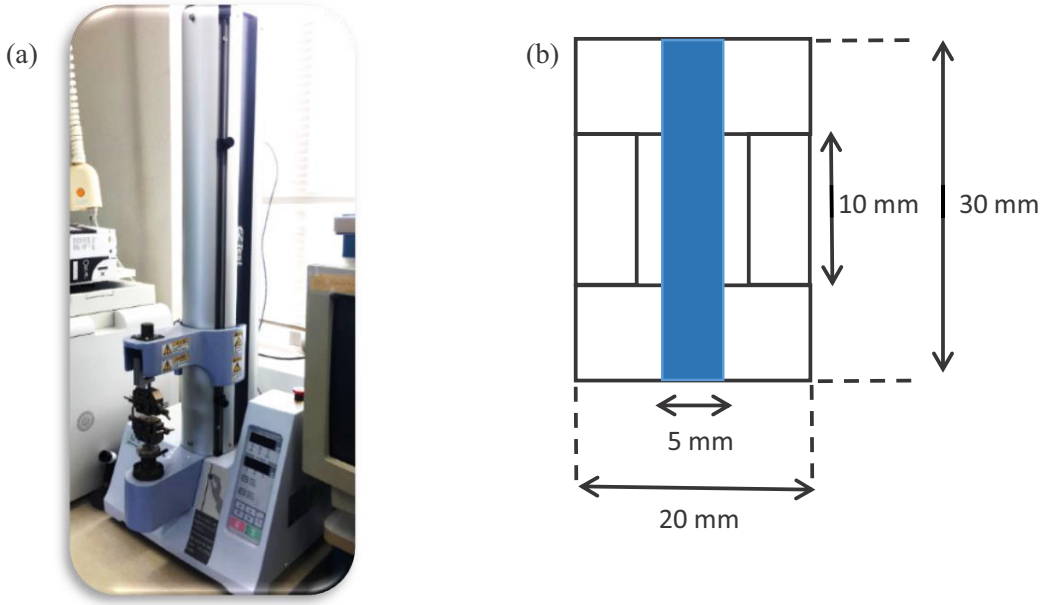

Figure 3-4. (a) A compact table top universal tensile tester. (b) A paper template used to prepare tensile specimens of the composite nanofibers.

3.2.5. Antibacterial activity test

To examine the antibacterial activity of natural antibacterial reagents, *S. aureus* and *E. coli* were chosen as representatives for gram-positive and gram-negative bacteria. The test method was the disk diffusion test, which has been well established by previous reports [2,20,30–33]. The bacterial culture was spread on the Luria Bertani (LB) agar surface by using a sterile cotton bat. The PHBH/*centella,* PHBH/propolis, and PHBH/hinokitiol composite nanofibers were placed on the surface of the Petri dishes then they were incubated at 30 °C (*E. coli*) and 37 °C (*S. aureus*) for

24 h. The diameters of inhibition zone (mm) were measured for 3 specimens each sample and the results were expressed as mean diameters with standard deviations (in millimeters).

3.2.6. Sustained release behavior of natural products from PHBH composite nanofibers

The release of *centella*, propolis, and hinokitiol was analyzed by a UV-visible spectrophotometer (UV2550, Shimadzu Corp., Kyoto, Japan), Figure 3-5. For release experiments, PHBH composite nanofibers with *centella*, propolis, or hinokitiol were cut into 2 × 2 cm and measured specimen weight. For each sample, 2 specimens were placed in a test tube filled with 50 mL of phosphate-buffered saline (PBS) (pH 7.4) incubated at 37 °C and stirred at 150 rpm. During the release, 4 mL of the supernatant was retrieved from the release medium at the time points of 5, 10, 20, 30, 40, 50, 60, 120, 240, 360, 480, 600, 720, 1440, 2880, 4320, and 5760 min and the same amount of fresh PBS was added immediately to maintain the medium volume.

Figure 3-5. UV-visible spectrophotometer (SHIMADZU UV2550).

The solutions in various concentrations were used to make a standard calibration curve at wavelength 200–700 nm. In detail, certain weight of extract *centella*, extract propolis, hinokitiol (0.8 mg) was dissolved in 100 mL ethanol/PBS or methanol/PBS (1:99, v/v) and then diluted to 400, 200, 100, 50, 25, 12.5, 6.25, 3.125, and 1.56 μg/mL. UV-vis spectrophotometer at a wavelength of 270 nm, 273 nm, 224 nm was used to measure the amount of released *centella*, propolis, and hinokitiol from PHBH composite nanofibers, respectively. The total amounts of

centella, propolis, and hinokitiol from the nanofiber mats were determined as the average value of the three tests. These results were presented in the form of a cumulative amount of release [30]:

$$\text{Cumulative amount of release (\%)} = M_t/M_\infty \times 100,$$

where M_t is the amount of *centella*, propolis, or hinokitiol released at the time t, M_∞ is the total amount of *centella*, propolis, and hinokitiol loaded in PHBH composite nanofibers.

3.2.7. Statistical analysis

All experiments were conducted in triplicate and the data are presented as mean ± standard deviation (SD). The significant differences were statistically analyzed by one-way analysis of variance (ANOVA) using R free software. Statistical significance was set at $p < 0.05$ to identify which groups were significantly different from other groups.

3.3. Results and discussions

3.3.1. Morphology of PHBH composite nanofibers with natural antibacterial products

The surface morphology of PHBH nanofibers containing different natural antibacterial products was investigated using SEM. Representative SEM images and the fiber diameter distributions of neat PHBH and PHBH nanofibers loaded with different amounts of *centella* solutions (1, 5, and 10%), propolis solutions (1, 5, and 7%), and hinokitiol solutions (1, 5, and 7%) are exhibited in Figure 3-6. In general, the different natural product solutions had effects on the surface morphology of composite nanofibers.

Table 3-2 shows the percentage of each natural product solution, the conditions of the electrospinning process, the average diameters, standard deviations (SD), maximum, and minimum fiber diameters of each sample. From these data, it can be confirmed that PHBH/ethanol–*centella* (15EC and 30EC) and PHBH/methanol–*centella* (15MC and 30MC) composite nanofibers showed the uniform fiber diameter. These also exhibited the same trend of

a decrease in fiber diameter by increasing the ratio of *centella* solutions (EC and MC) in spinning PHBH solution. The fiber diameter, with high concentrations of *centella* solution in PHBH/30EC (10%) and PHBH/30MC (10%), diminished to 349 ± 108 nm and 332 ± 62 nm, respectively. This phenomenon may be due to the decrease in the viscosity of polymer solutions by the addition of ethanol or methanol into HFIP. The viscosity of the mixture solution reduced when the considerable amounts of *centella* solution added into the polymer matrix [5,14]. Interestingly, the high concentration of *centella* in PHBH/30EC (10%) (Figure 3-6) resulted in fibers merging.

Such a bonded structure was also appeared in PHBH/30EP (7%). The bonded structure in high concentration solutions of EC and EP might be due to ethanol as the solvent and mixed with HFIP. By contrast, PHBH/30EP (7%) was accompanied by an increase in fiber diameter by loading a high concentration of 30EP. The fiber diameter was increased from 539 ± 99 nm PHBH/30EP (1%) to 739 ± 197 nm PHBH/30EP (7%). Similar behavior was obtained from cellulose acetate nanofibers with a high concentration of honey bee propolis prepared by ethanol solution [33]. Kim et al. [20] reported that the propolis concentration increased the fiber diameter and provided the linking of Polyurethane fibers due to its adhesive properties and demonstrated the optimum utilization of the bonding element for reinforcement of nonwoven fabric. However, different results of fiber diameter were obtained from PHBH composite nanofibers containing acetone-propolis (PHBH/10AP), which are 520 ± 83 nm, 527 ± 161 nm, and 529 ± 109 nm in the cases of 1, 5, and 10% (v/v) of 10AP, respectively. This is probably because the evaporation of acetone was faster than ethanol during the electrospinning process and obtained the brittle nanofibers.

For PHBH/ethanol–hinokitiol (EH) composite nanofibers, the surface morphology of PHBH/30EH (1%) was smooth, homogeneous without beads. The average diameter was 562 ± 87 nm, with a majority of fibers in the range of 438 nm to 745 nm. However, it was not very easy to

obtain uniform nanofibers with high ratios of hinokitiol solutions (EH), more than 1%. As shown in Figure 3-6 of PHBH/30EH (5%) and (7%), these resulted in aligned fibers with small grains like beads.

The final surface morphologies of PHBH composite nanofibers were influenced by the kind of used natural products and concentration ratios of natural product solutions to PHBH solutions. This result clearly indicates that the fiber diameters and their distributions can be controlled by concentration ratios of natural products in solutions. Thus, PHBH composite nanofibers with natural product solutions of PHBH/30EC (10%), PHBH/30MC (10%), PHBH/30EP (7%) and PHBH/30EH (1%) were chosen for further investigation by FT-IR, WAXD, mechanical properties, antibacterial test, and release characteristic because these samples had fiber diameter between 300–1000 nm, surface morphology without beads, and high concentration of natural products.

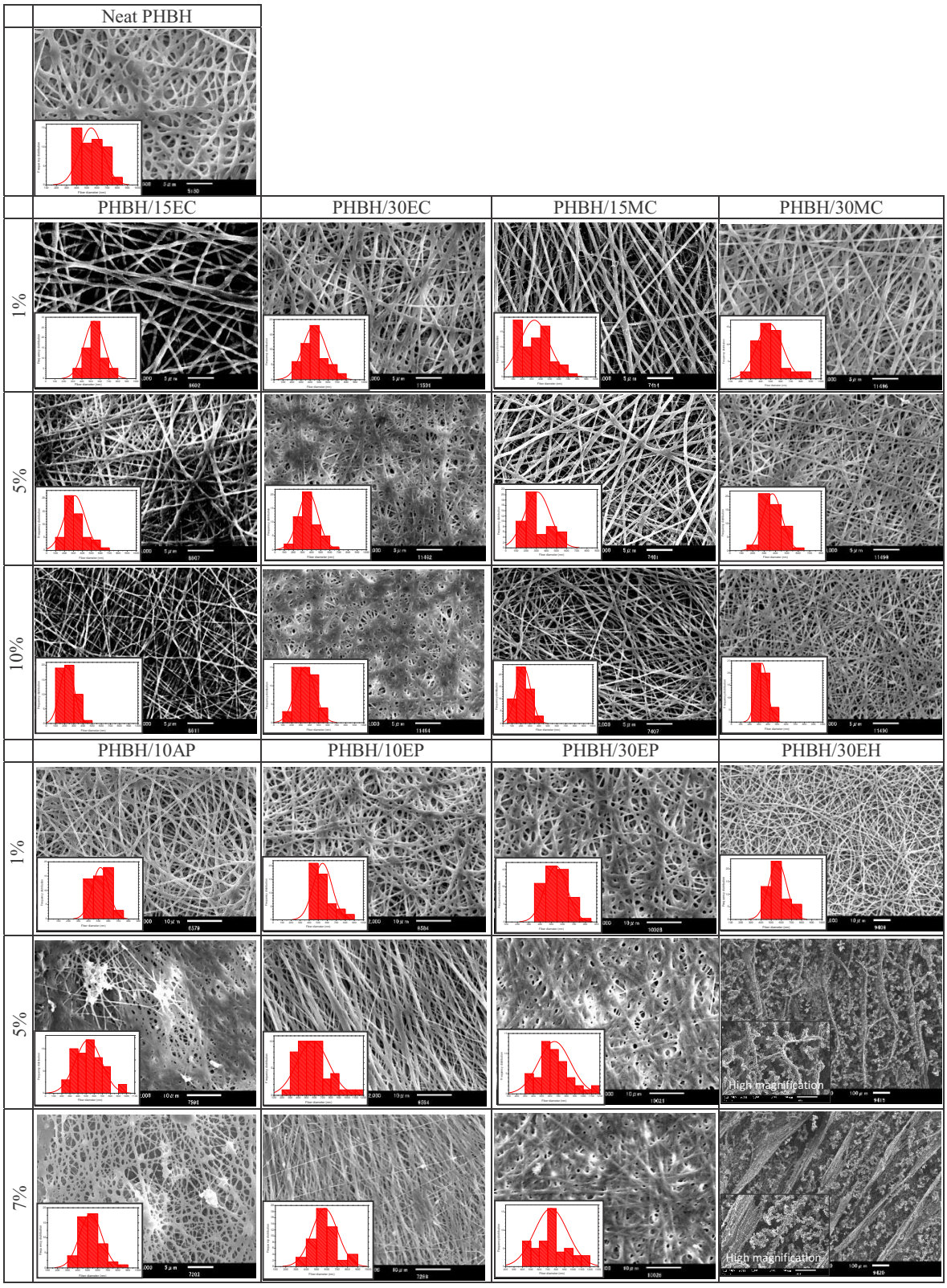

Figure 3-6. SEM images and diameter distributions of the electrospun neat PHBH 2 wt% and PHBH composite nanofibers containing different natural product solutions. PHBH/15EC, PHBH/30EC, PHBH/15MC, and PHBH/30MC with different concentration ratios of ethanol–*centella* (EC) and methanol–*centella* (MC) (1, 5, and 10%). PHBH/10AP, PHBH/10EP, PHBH/30EP, and PHBH/30EH with concentration ratios of 1, 5, and 7% of acetone–propolis (AP), ethanol–propolis (EP), and ethanol–hinokitiol (EH).

Table 3-2. Preparation of PHBH with natural products solution, electrospinning condition, and fiber diameter of samples.

No.	Polymer	Solvent-natural product-ratio to solvent-ratio to PHBH	Code	Electrospinning condition		Fibers diameter		
				Applied voltage (kV)	Flow rate (mm/min)	Ave. Ø (nm) ± SD	Max.	Min.
1	Neat PHBH	-	-	20	0.3	543	785	367
2	PHBH	Ethanol-*Centella* (EC) 15%	PHBH/15EC (1%)	15.5	0.13	524 ± 111	760	230
			PHBH/15EC (5%)	15.5	0.13	314 ± 116	631	157
			PHBH/15EC (10%)	15.5	0.13	226 ± 77	413	107
3	PHBH	Ethanol-*Centella* (EC) 30%	PHBH/30EC (1%)	15.5	0.15 - 0.2	447 ± 128	789	255
			PHBH/30EC (5%)	15.5	0.15 - 0.2	362 ± 107	690	131
			PHBH/30EC (10%)	15.5	0.15 - 0.2	349 ± 108	593	153
4	PHBH	Methanol-*Centella* (MC) 15%	PHBH/15MC (1%)	15.5	0.15	319 ± 107	630	152
			PHBH/15MC (5%)	15.5	0.15	310 ± 126	588	135
			PHBH/15MC (10%)	15.5	0.15	227 ± 81	413	101
5	PHBH	Methanol-*Centella* (MC) 30%	PHBH/30MC (1%)	15.5	0.15 - 0.2	487 ± 127	820	238
			PHBH/30MC (5%)	15.5	0.15 - 0.2	371 ± 83	571	194
			PHBH/30MC (10%)	15.5	0.15 - 0.2	332 ± 62	456	236
6	PHBH	Acetone-Propolis (AP) 10%	PHBH/10AP (1%)	20	0.1	520 ± 83	717	374
			PHBH/10AP (5%)	20	0.1	527 ± 161	978	286
			PHBH/10AP (7%)	20	0.1	529 ± 109	890	328
7	PHBH	Ethanol-Propolis (EP) 10%	PHBH/10EP (1%)	20	0.1	548 ± 104	850	422
			PHBH/10EP (5%)	20	0.1	576 ± 193	1192	289
			PHBH/10EP (7%)	20	0.1	579 ± 126	884	338
8	PHBH	Ethanol-Propolis (EP) 30%	PHBH/30EP (1%)	20	0.15 - 0.2	539 ± 99	752	393
			PHBH/30EP (5%)	20	0.15 - 0.2	653 ± 194	1180	300
			PHBH/30EP (7%)	20	0.15 - 0.2	739 ± 197	1185	408
9	PHBH	Ethanol-Hinokitiol (EH) 30%	PHBH/30EH (1%)	20	0.15 - 0.2	562 ± 87	745	438
			PHBH/30EH (5%)	20	0.15 - 0.2	-	-	-
			PHBH/30EH (7%)	20	0.15 - 0.2	-	-	-

3.3.2. FT-IR spectral analysis

The functional groups of natural antibacterial products contained in PHBH composite nanofibers were analyzed by using ATR (FT-IR). The FT-IR spectra of PHBH/30EC (10%), PHBH/30MC (10%), PHBH/30EP (7%), and PHBH/30EH (1%) are shown in Figure 3-7. The FT-IR spectra of neat PHBH nanofiber and PHBH nanofibers with natural products showed similar

peaks. The characteristic peaks of PHBH at 2970, 2937, 2870, and 1719 cm^{-1} were attributed to the stretching vibrations of C–CH_3, CH_2, CH, and C=O, respectively [4].

FT-IR graphs of *centella* powder from ethanol and methanol solutions after filtering and drying exhibit some bands centered at 3320 or 3300 cm^{-1} corresponding to O–H stretching vibration of carboxylic acid, whereas, 1690 or 1638 cm^{-1} peaks characterizing C–O stretching vibration. The bands at 1459, 1380, and 1025 cm^{-1} shows the presence of alkenes with C–H in-plane bending, the stretching vibration of C–N for aromatic amide group, and C–O stretching, respectively (Figure 3-7A). These spectra of those compounds were confirmed in the research of *centella asiatica* by Manotham et al. [5], Sondari et al. [34], and Sugunabai et al. [35]. As showed in Figure 3-7A, methanol solvent yielded higher content of Asiatic acid than ethanol with the same concentration from raw *centella* (30%EC and 30%MC). In the case of PHBH/30MC (10%) composite nanofibers, the decline of the band at 3340 cm^{-1} suggested the formation of the intermolecular hydrogen bond between *centella* and PHBH polymer.

The FT-IR spectra of propolis powder and PHBH/30EP (7%) nanofibers were exhibited in Figure 3-7B. In the case of propolis powder, the band at 3340 cm^{-1} was assigned to stretching vibration of the O–H group in the phenolic compound and the band at 2920–2870 cm^{-1} was attributed to C–H aliphatic stretching vibration (stretching vibration of CH_2 and CH_3) [36]. The bands at 1706 cm^{-1}, 1650–1602 cm^{-1}, and 1190 cm^{-1} were attributed to the C=O group, aromatic ring deformations C=C stretching vibration, and C–O stretching vibration, respectively. In PHBH/30EP (7%) composite nanofibers, some peaks appeared at between 1651 and 1610 cm^{-1}, and 1510 cm^{-1}, confirming the presence of propolis in PHBH nanofiber mats. These bands were assigned to stretching of C=C aromatic ring bands in flavonoids [17,36].

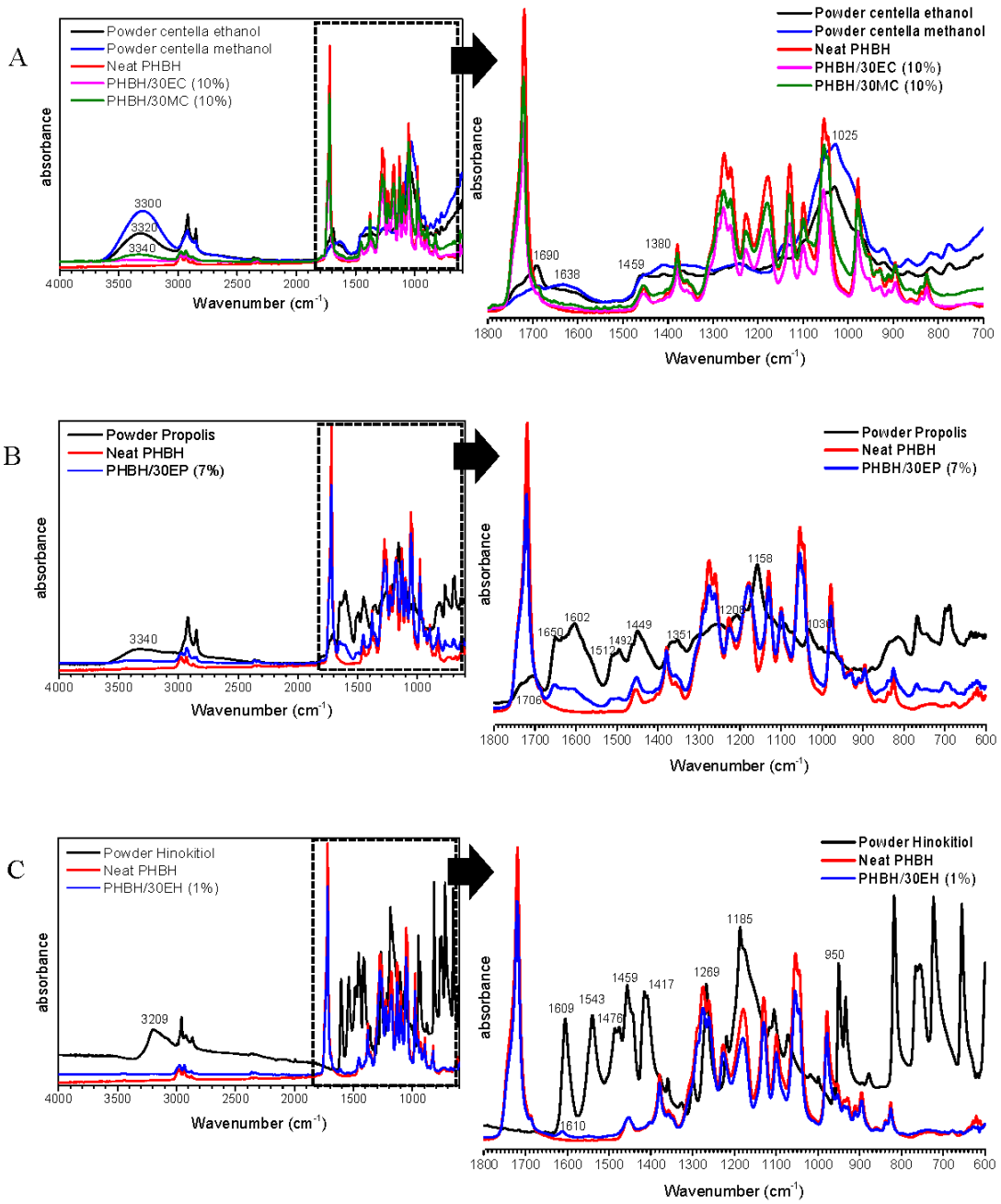

Figure 3-7. FT-IR spectra of neat PHBH and PHBH composite nanofibers with (**A**) EC and MC, (**B**) EP, (**C**) EH.

The characteristic absorption peaks of hinokitiol powder were observed at 3200, 1609, 1543, 1476, 1459, 1417, 1269, 1185, and 950 cm^{-1}. These bands represented O–H stretching, C=C and C=O stretching, C=C stretching (in-phase), ring CH bending, C–O–H group, and ring CH bending,

respectively [37]. Dyrskov et al. [23] reported that the absorbance bands in the hinokitol spectrum ascribed to C=O stretching in the tropolone carbon ring (1609 and 1543 cm^{-1}) and the C–O–H group (1189 cm^{-1}). The weak peak confirmed the presence of hinokitiol in PHBH composite nanofibers appeared at 1610 cm^{-1} that is related to the tropolone carbon ring. In general, the decrease of peak intensity by loading natural product might reveal that natural product is homogeneously distributed through the polymer matrix [20]. The nanofibrous samples with higher contents of natural antibacterial substances showed the peaks of carboxylic acid, aromatic ring, and tropolone carbon ring from *centella*, propolis, and hinokitiol, respectively.

3.3.3. Crystalline structure by wide-angle X-ray diffraction (WAXD)

The WAXD measurement was performed in order to confirm the influence of loading *centella*, propolis, and hinokitiol on the crystallinity of PHBH. All reflections of WAXD and intensity profile and 2D patterns are displayed in Figure 3-8 and Figure 3-9, respectively. The neat PHBH nanofibers exhibit diffraction peaks at $2\theta = 6.1°$, 7.7°, 9°, 10°, 11.7°, 12.4°, and 13.8° which were assigned to the (020), (110), (101), (121), (040), and (002) of the orthorhombic unit cell of PHB crystal, respectively [38]. The intensity of diffraction peaks of neat PHBH nanofibers slightly increased by loading *centella* and propolis in PHBH/30EC (10%) and PHBH/30EP (7%) composite nanofibers. Moreover, the calculated crystallinity of neat PHBH (47.0%) was slightly lower than that of PHBH/30EC (55.0%), PHBH/30MC (49.2%), and PHBH/30EP (54.5%) in Table 3-3. It was previously reported that the crystallinity of PHB nanofibers increased by adding the natural phenolic compound caffeic acid [30]. Kim et al. [39] supposed that intermolecular interaction through a hydrogen bonding of plant polyphenol with polycaprolactone probably increased by slight increment of crystallinity in polycaprolactone. Whereas, the crystallinity of PHBH/30EH (1%) composite nanofibers was declined to 44.1% compared to neat PHBH. These

results indicate that an intermolecular interaction between PHBH polymer and *centella* or propolis in nanofibers mat exists.

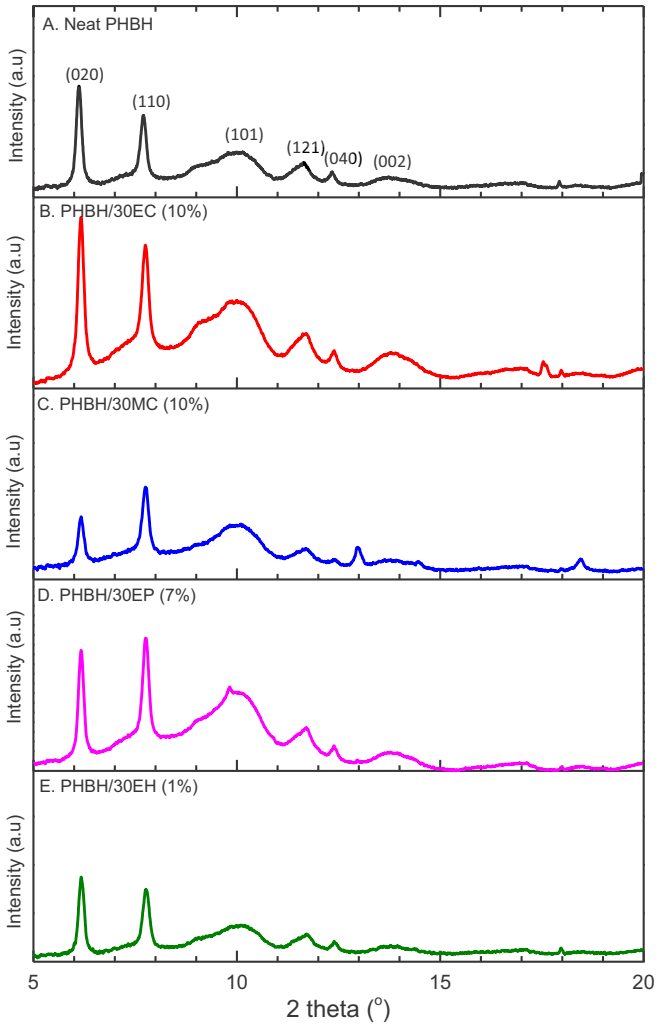

Figure 3-8. Wide-angle X-ray diffraction (WAXD) intensity profiles of (A) neat PHBH and PHBH composite nanofibers with natural products: (B) EC, (C) MC, (D) EP, (E) EH.

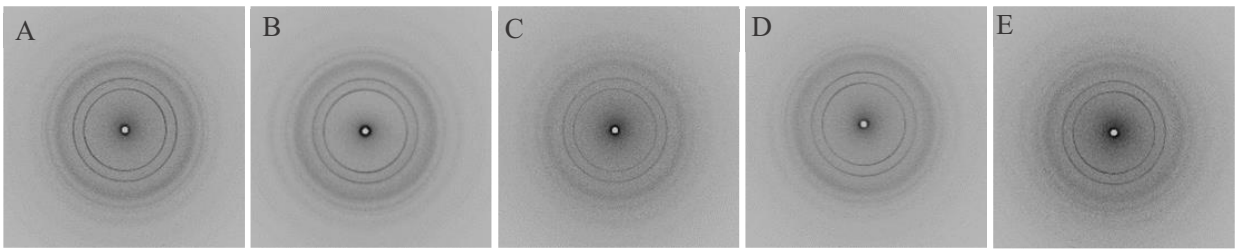

Figure 3-9. WAXD patterns by Laue camera of (A) neat PHBH and PHBH composite nanofibers with natural products: (B) EC, (C) MC, (D) EP, (E) EH.

3.3.4. Mechanical characteristic of composite nanofibers

The tensile test was conducted on neat PHBH and PHBH composite nanofibers with the natural antibacterial products in order to evaluate the influences of natural product loading. The tensile strength, elongation at break, and Young's modulus of neat PHBH, PHBH/30EC (10%), PHBH/30MC (10%), PHBH/30EP (7%), and PHBH/30EH (1%) are shown in Table 3-3. Figure 3-10 illustrates the representative stress-strain curves of PHBH composite nanofiber samples. The tensile strength of neat PHBH was 8.0 MPa with high elongation up to 61.5%. Interestingly, the loading of *centella* (EC 10%) and propolis (EP 7%) in PHBH demonstrated the same trend with the tensile strength rose to 17.8 and 16.4 MPa but it reduced elongation down to 15.6 and 9.3%, respectively. PHBH/30MC (10%) composite nanofibers exhibited no significant differences in tensile strength and Young's modulus compared to neat PHBH. PHBH/30EH (1%) resulted in a decline in both tensile strength and elongation compared to neat PHBH.

PHBH composite nanofibers with *centella* (EC) and propolis (EP) using ethanol as solvent displayed higher tensile strength in comparison to neat PHBH, PHBH/MC, and PHBH/EH. These phenomena may be due to the surface morphology and polymer structure in PHBH composite nanofibers. The surface morphology of PHBH/30EC (10%) and PHBH/30EP (7%) showed bonded-structure between fibers, whereas PHBH/30MC (10%) and PHBH/30EH (1%) surface revealed randomly oriented fibers. Kim et al. [20] reported the similar behaviors of merged structure, the adhesive properties of propolis might be useful to increase the mechanical strength of polyurethane fibers. The mechanical properties of nonwoven nanofibers also depended on the surface interaction among the fibers, average fiber diameter, fiber defects (bead formation) during electrospinning [10,11].

Additionally, the enhancement of physical properties in PHBH/30EC (10%) and PHBH/30EP (7%) might be related to the rise of the crystallinity of PHBH polymer in PHBH composite nanofibers (Table 3-3). It probably due to the interaction of EC and EP to PHBH polymer as explained by FT-IR and X-ray analysis.

Table 3-3. Mechanical properties and crystallinity of neat PHBH and PHBH composite nanofibers with natural products.

Sample	Tensile strength (MPa)	Elongation at break (%)	Young's modulus (MPa)	Crystallinity (%)
Neat PHBH	8.0 ± 0.7	61.5 ± 0.7	291.5 ± 41.8	47
PHBH/30EC (10%)	17.8 ± 4.7*	15.6 ± 4.6*	420.4 ± 146.1	55
PHBH/30MC (10%)	9.0± 1.5	10.0 ± 3.8	291.7 ± 118.9	49.2
PHBH/30EP (7%)	16.4 ± 1.8*	9.3 ± 3.3	545.6 ± 162.8*	54.5
PHBH/30EH (1%)	2.1 ± 0.7*	8.3 ± 1.8	78 ± 33.8*	44.1

*, $p < 0.05$ considered statistically significant between PHBH composite nanofibers in each group against neat PHBH nanofibers ($n = 10$) (except crystallinity, $n = 2$).

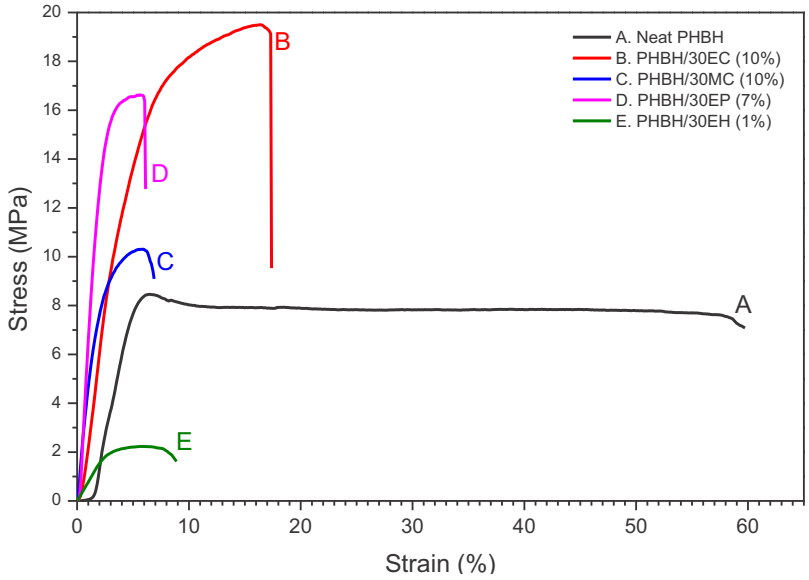

Figure 3-10. Representative stress-strain curves of (A) neat PHBH and PHBH composite nanofibers with (B) EC, (C) MC, (D) EP, and (E) EH.

3.3.5. *In vitro* antibacterial activity

The antibacterial activity of neat PHBH nanofibers, PHBH nanofibers with *centella*, propolis, and hinokitol against *S. aureus* and *E. coli* was evaluated using inhibition zone method [20,33,40,41]. The antimicrobial effect of samples was evaluated at 37 °C (*S. aureus*) and 30 °C (*E. coli*) for 24 h. Table 3-4 presents the diameters of the inhibition zone for PHBH nanofibers with natural products. The effects of natural antibacterial products via the agar diffusion test are clearly shown in Figure 3-11. PHBH/30EC (10%) was no effect against *S. aureus* and *E. coli* whereas, *centella* in PHBH/30MC (10%) demonstrated low antibacterial activity against *S. aureus* with an inhibitory zone of 7.7 mm and no effect against *E. coli*. The diameter of the inhibition zone of PHBH/30EP (7%) was 18.3 mm for *S. aureus* and 17.3 mm for *E. coli.* However, PHBH/30EH (1%) nanofibers have extensive inhibition zone against *S. aureus* (25.7 mm) and *E. coli* (29.7 mm), respectively. The zones of inhibition for PHBH/30EP (7%) against *S. aureus* were slightly broader than that against *E. coli*. Zeighampour et al. [21] explained that hydroalchoholic extract of propolis showed better antibacterial activities against gram-negative bacteria than gram-positive bacteria due to the different cell wall chemical structures of bacteria. However, the opposite results for PHBH/30EH (1%) might be due to the different modes of action and the bactericidal effects of natural products.

Regarding these results, the antimicrobial effects of PHBH nanofibers with propolis and hinokitiol were better than *centella*. However, the profound effect antibacterial activity of *centella* (EC or MC) might be due to the low chemical content in PHBH nanofiber as analyzed by FT-IR, which PHBH/30EC (10%) showed no precise detection of Asiatic acid. For further work, raising the *centella* concentrations in ethanol or methanol solutions might be as the solutions

to increase the antibacterial activity. Overall, propolis and hinokitiol loaded into PHBH composite nanofibers inhibited the growth of *S. aureus* and *E. coli* powerfully.

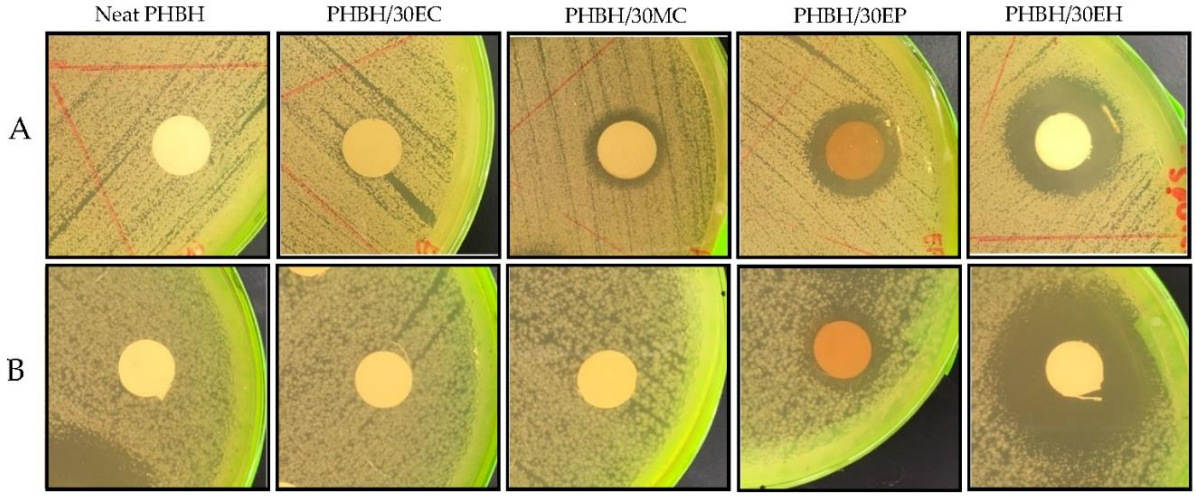

Figure 3-11. Representative inhibition zones of neat PHBH and PHBH composite nanofibers with *centella* (30EC) and (30MC), propolis (30EP), and hinokitiol (30EH) on gram-positive bacteria (*S. aureus*) (A) and gram-negative bacteria (*E. coli*) (B).

Table 3-4. Zone of inhibition for PHBH nanofibers with natural products against *S. aureus* and *E. coli*.

Sample	Inhibition zone (mm)		Natural product Contain (%)
	S. aureus	*E. coli*	
Neat PHBH	0	0	-
PHBH/30EC (10%)	0	0	13
PHBH/30MC (10%)	7.7 ± 6.7	0	30
PHBH/30EP (7%)	18.3 ± 1.5*	17.3 ± 5.1*	26
PHBH/30EH (1%)	25.7 ± 4.0*	29.7 ± 1.5*	6.7

*, $p < 0.05$ considered statistically significant, PHBH composite nanofibers in each group were compared with PHBH nanofibers ($n = 3$).

3.3.6. Release behavior of natural antibacterial product

The release profiles of *centella*, propolis, and hinokitiol from PHBH nanofibers were plotted as a function of time in PBS at pH 7.4, 37°C. The release curves of PHBH/30EC (10%), PHBH/30MC (10%), PHBH/30EP (7%), and PHBH/EH (1%) nanofibers demonstrated different release behaviors in each sample as shown in Figure 3-12. *Centella* from PHBH/30EC started to

release within the 10 min and completely released in 20 min. In the case of PHBH/30MC, Figure 3-12B, the similar behaviors were also observed with complete release in 20 min. The maximum releases of *centella* from PHBH/30EC and PHBH/30MC were 13.9 and 31.5%, respectively. Propolis was firstly released from PHBH/30EP nanofiber at 10 min after incubation and gradually released to 9.6% after 2880 min (48 h). The release of propolis from PHBH/30EP sustained longer with low release amount than other. The fast release of hinokitiol from PHBH/30EH was noticeable in the first 5 min and gradually increased up to 20 min with a maximum release of 46.1%. Afterward, the release of hinokitiol gradually declined over 240 min. This decline might be due to the degradation of hinokitiol in PBS solution by light, heat, or ethanol.

The release behavior supposes due to the relation between the release capacity and the characteristics of PHBH, which is a hydrophobic polymer. Ignatova et al. [43] reported that the release of caffeic acid phenethyl ester (CAPE) in the material was influenced by hydrophilic–hydrophobic features of the fibrous mats. In addition, CAPE was faster release from the PVP (hydrophilic) matrix rather than from the PHB (hydrophobic) matrix. The release of ciprofloxacin hydrochloride (CpHCl) from electrospun alginate was 24% of the total loaded drug due to the cross-linking process that obtained hydrophobic matrix and affected the release behaviors [42].

PHBH/30EC (10%) and PHBH/30EP (7%) have similar release behaviors, when only small amounts of natural products were released to PBS. It can be considered due to the high crystallinity of PHBH composite nanofibers that affected release characteristics. In comparison, PHBH/30EH (1%) with low crystallinity showed fast and high release amounts. Study of drug release of ampicillin incorporated poly(methyl methacrylate)–nylon6 core/shell nanofibers proved that the increase of released drug, most probably due to decreased crystallinity in the polymer matrix [44].

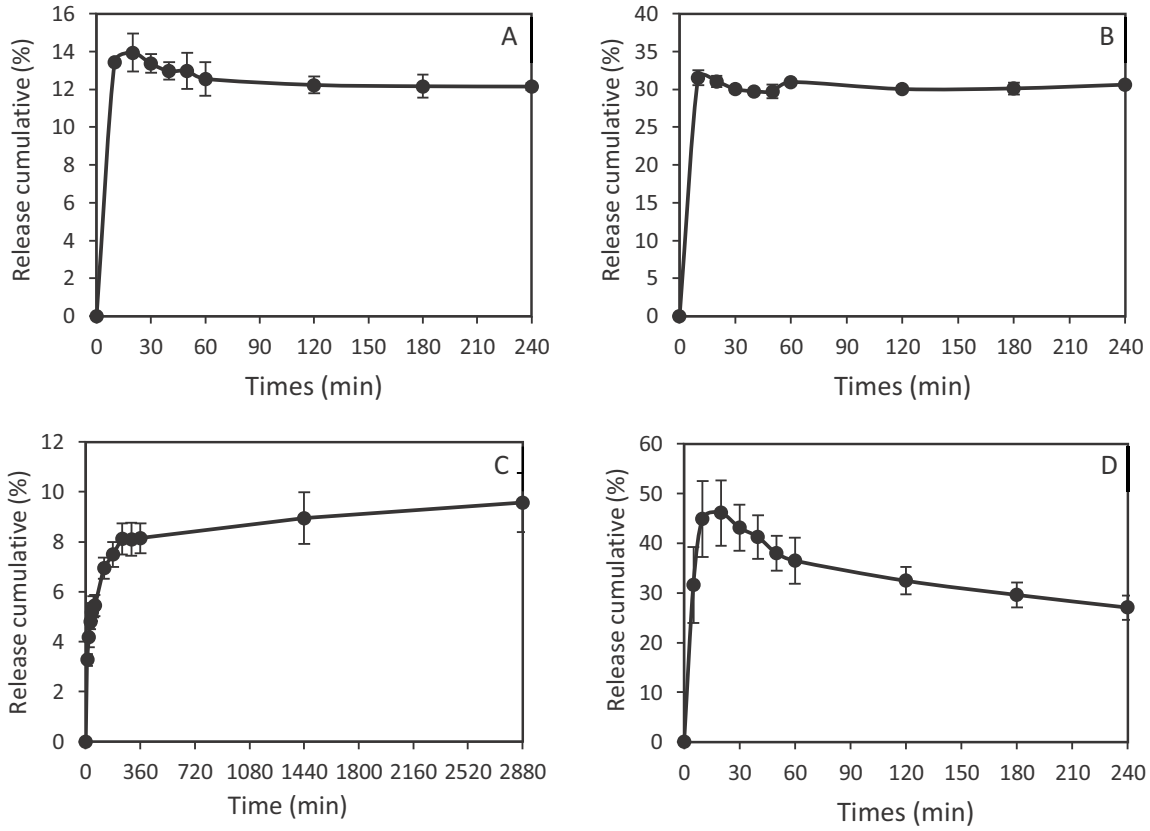

Figure 3-12. Cumulative release profiles of natural antibacterial products in PHBH composite nanofibers (A) PHBH/30EC (10%), (B) PHBH/30MC (10%), (C) PHBH/30EP (7%), and (D) PHBH/30EH (1%).

3.4. Conclusions

The natural antibacterial products was of *centella*, propolis, and hinokitiol loaded into PHBH composite nanofibers were successfully fabricated by the electrospinning process. The fiber diameter and surface morphology of PHBH composite nanofibers with antibacterial reagents can be controlled by different kinds of natural antibacterial products, solvent systems for dissolution, and component concentrations in the PHBH-HFIP polymer solutions. FT-IR confirmed the presence of carboxylic acid and aromatic amide groups in PHBH/*centella*, aromatic ring bands due to flavonoid in PHBH/propolis, and tropolone carbon ring in PHBH/hinokitiol. The loading of *centella* and propolis led to an increase in the crystallinity of the PHBH polymer. Furthermore,

the loading of *centella* and propolis improved the tensile strength, compared to neat PHBH nanofibers. Hinokitiol and propolis were proved to be potent antibiotics by large inhibition zones against both *E. coli* and *S. aureus*. The release of *centella* and hinokitiol from PHBH nanofibers was fast and finished in 20 min with a maximum release of 13.9% (PHBH/30EC), 31% (PHBH/30MC), and 46% (PHBH/30EH). The release of propolis was continued to 48 h, and maximal release was 9.5%. These results in this study indicated that natural antibacterial products loaded into PHBH composite nanofibers improve the mechanical properties PHBH/30EP and PHBH/30EC. The results also proved that the antibacterial effects in composite nanofibers against the gram-negative and gram-positive bacteria (PHBH/30EP and PHBH/30EH), which are important characteristics as wound healing materials. Interestingly, PHBH/30EC (10%) showcased good mechanical properties and PHBH/30MC (10%) exhibited good morphology in nanofiber form, however, it may necessary to increase the concentration of *centella* in *centella* solution (ethanol or methanol) if it is to be used as antibacterial reagents. PHBH/30EH (1%) might be used as drug delivery with the rapid release but possesses low mechanical properties. PHBH/30EP (7%) could be used in wound healing with needed mechanical properties and slow release for long-time effects.

3.5. References

[1] Sh Asran, A.; Razghandi, K.; Aggarwal, N.; Michler, G.H.; Groth, T. Nanofibers from blends of polyvinyl alcohol and polyhydroxy butyrate as potential scaffold material for tissue engineering of skin. *Biomacromolecules* **2011**, *11*, 3413–3421.

[2] Asawahame, C.; Sutjarittangtham, K.; Eitssayeam, S.; Tragoolpua, Y.; Sirithunyalung, B.; Sirithunyalug, J. Antibacterial activity and inhibition of adherence of Streptococcus mutans by propolis electrospun fibers. *AAPS Pharm. Sci. Tech.* **2015**, *16*, 182-191.

[3] Lee, H.S.; Lee, S.Y.; Park, S.H.; Lee, J.H.; Ahn, S.K.; Choi, Y.M.; Choi, D.J.; Chang, J.H. Antimicrobial medical sutures with caffeic acid phenethyl ester and their *in vitro*/*in vivo* biological assessment. *Med. Chem. Commun.* **2013**, *4*, 777-782.

[4] Rebia, R.A.; Rozet, S.; Tamada, Y.; Tanaka, T. Biodegradable PHBH/PVA blend nanofibers: Fabrication, characterization, *in vitro* degradation, and *in vitro* biocompatibility. *Polym. Degrad. Stab.* **2018**, *154*, 124-136.

[5] Manotham, S.; Pengpat, K.; Eitssayeam, S.; Rujijanagul, G.; Sweatmam, D.R.; Tunkasiri, T. Fabrication of Polycaprolactone/*Centella asiatica* Extract Biopolymer Nanofiber by Electrospinning. *Appl. Mech. Mater.* **2015**, *804*, 151-154.

[6] Philip, S.; Keshavarz, T.; Roy, I. Polyhydroxyalkanoates: biodegradable polymers with a range of applications. *J. Chem. Technol. Biotechnol* **2007**, *82*, 233-247.

[7] Ignatova, M. G.; Manolova, N. E.; Rashkov, L. B.; Markova, N.D.; Toshkova, R.A.; Georgieva, A.K.; Nikolova, E.B. Poly(3-hydroxybutyrate)/caffeic acid electrospun fibrous material coated with polyelectrolyte complex and their antibacterial activity and *in vitro* antitumor effect against HeLa cells. *Mat. Sci. Eng. C-Mater.* **2016**, *65*, 379-392.

[8] Bulman, S.EL.; Goswami, P.; Tronci, G.; Russell, S.J.; Carr, C. Investigation into the potential use of poly(vinyl alcohol)/methylglyoxal fibres as antibacterial wound dressing components. *J. Biomater. Appl.* **2015**, *8*, 1198-1200.

[9] Gun, J.; Zhang, M. Polyblend nanofibers for biomedical applications: perspectives and challenges. *Cell Press* **2010**, *28*, 189-197.

[10] Scaffaro, R.; Lopresti, F. Processing, structure, property relationships and release kinetics of electrospun PLA/Carvacrol membranes. *Eur. Polym. J.* **2018**, *100*, 165–171.

[11] Mutlu, G.; Calamak, S.; Ulubayram, K.; Guven, E. Curcumin-loaded electrospun PHBV nanofibers as potential wound-dressing material. *J. Drug. Deliv. Sci. Tec.* **2018**, *43*, 185-193.

[12] Andreau, V.; Mendoza, G.; Arruebo, M.; Irusta, S. Review: Smart dressings based on nanostructured fibers containing natural original antimicrobial, anti-inflammatory, and regenerative compounds. *Material* **2015**, *8*, 5154-5193.

[13] Kwon, M.C.; Choi, W.Y.; Seo, Y.C.; Kim, J.S.; Yoon, C.S.; Lim, H.W.; Kim, H.S.; Ahn, Jh.; Lee, H.Y. Enhancement of the skin-protective activities of *Centella asiatica* L. Urban by a nano-encapsulation process. *J. Biotechnol.* **2012**, *157*, 100-106.

[14] Yao, C.H.; Yeh, J.Y.; Chen, Y.S.; Li, M.H.; Huang, C.H. Wound-healing effect of electrospun gelatin nanofibres containing *Centella asiatica* extract in a rat model. *J. Tissue. Eng. Regen. Med.* **2017**, *11*, 905–915.

[15] Azis, H.A.; Taher, M.; Ahmed, A.S.; Sulaiman, W.M.A.W.; Susanti, D.; Chowdhury, S.R.; Zakaria, Z.A. *In vitro* and *In vivo* wound healing studies of methanolic fraction of *Centella asiatica* extract. *S. Afr. J. Bot.* **2017**, *108*, 163-174.

[16] Sikareepaisan, P.; Suksamrarn, A.; Supaphol, P. Electrospun gelatin fiber mats containing a herbal-*Centella asiatica*-extract and release characteristic of asiatocoside. *Nanotechnology* **2008**, *19*, 015102.

[17] Lima, G.G.; Souza, R.O.; Bozzi, A.D.; Poplawska, M.A.; Devine, D.M.; Nugent, M.J.D. Extraction Method Plays Critical Role in Antibacterial Activity of Propolis-Loaded Hydrogels. *J. Pharm. Sci.* **2016**, *105*, 1-10.

[18] Adomavičiūtė, E.; Stanys, S.; Žilius, M.; Juškaitė, V.; Pavilonis, A.; Briedis, V. Formation and biopharmaceutical characterization of electrospun PVP mats with propolis and silver nanoparticles for fast releasing wound dressing. *Biomed. Res. Int.* **2016**, DOI: 10.1002/app.45794.

[19] Wang, J.; Vermerris, W. Antimicrobial nanomaterials derived from natural products-A review. *Material* **2016**, *9*, 255-274.

[20] Kim, J.I.; Pant, H.R.; Sim, H.J.; Lee, K.M.; Kim, C.S. Electrospun propolis/polyurethane composite nanofibers for biomedical applications. *Mat. Sci. Eng. C-Mater.* **2014**, *44*, 52–57.

[21] Zeighampour, F.; Alihosseini, F.; Morshed, M.; Rahimi, A.A. Comparison of prolonged antibacterial activity and release profile of propolis-incorporated PVA nanofibrous mat, microfibrous mat, and film. *J. Appl. Polym. Sci.* **2018**, *135*, 45794.

[22] Paul, S.; Emmanuel, T.; Matchawe, C.; Alembert, T.T.; Elisabeth, Z.M.; Sophie, L.; Luce, V.E.; Maurice, T.F.; Joel, Y.G.A.; Alex, A.D.T.; Joseph, M.T. Pentacyclic triterpenes and crude extracts with antimicrobial activity from Cameroonian brown propolis samples. *J. Appl. Pharm. Sci.* **2014**, *4*, 1-9.

[23] Dyrskov, L.; Strobel, B.W.; Svensmark, B.; Hansen, H.C.B. *β*-Thujaplicin: New Quantitative CZE Method and Adsorption to Goethite. *J. Agric. Food Chem.* **2004**, *52*, 1452−1457.

[24] Shih, Y-H.; Lin, D-J.; Chang, K-W.; Hsia, S-M.; Ko, S-Y.; Lee, S-Y.; Hsue, S-S.; Wang, T-H.; Chen, Y-L.; Shieh, T-M. Evaluation physical characteristics and comparison antimicrobial

and anti-inflammation potentials of dental root canal sealers containing hinokitiol *in vitro*. *PloS One* **2014**, *9*, e94941. doi:10.1371/journal.pone.0094941.

[25] Hosoda, N.; Tsujimoto, T.; Uyama, H. Green composite of poly (3-hydroxybutyrate-*co*-3-hydroxyhexanoate) reinforced with porous cellulose. *ACS Sustain. Chem. Eng.* **2014**, *2*, 248-253.

[26] Bugnicourt, E.; Cinelli, P.; Lazzeri, A.; Alvare, V. Polyhydroxyalkanoate (PHA): review of synthesis, characteristics, processing and potential applications in packaging, *eXPRESS Polym. Lett.* **2014**, *8*, 791-808.

[27] Iwata, T.; Tsuge, T.; Taguchi, S.; Abe, H.; Tanaka, T. Bio-polyesters. In *Bio-based polymers*, 1st ed.; Kimura, Y.; CMC Publishing Co., Ltd.: Tokyo, Japan, 2013, pp. 71-85. ISBN978-4-7813-0271-3.

[28] Lu, X.; Wang, L.; Yang, Z.; Lu, H. Strategies of polyhydroxyalkanoates modification for the medical application in neural regeneration/nerve tissue engineering. *Adv. Biosci. Biotechnol.* **2013**, *4*, 731-740.

[29] Lee, S.Y. Bacterial polyhydroxyalkanoates, *Biotechnol. Bioeng.* **1996**, *49*, 1-14.

[30] Ignatova, M.; Manolova, N.; Rashkov, I.; Markova, N. Quaternized chitosan/κ-carrageenan/caffeic acid-coated poly(3-hydroxybutyrate) fibrous materials: Preparation, antibacterial and antioxidant activity. *Int. J. Pharm.* **2016**, *513*, 528-537.

[31] Sharaf, S.; El-Naggar, M.E. Eco-friendly technology for preparation, characterization and promotion of honey bee propolis extract loaded cellulose acetate nanofibers in medical domains. *Cellulose* **2018**, *25*, 5195–5204.

[32] Sondari, D.; Harmami, S.B.; Ghozali, M.; Randy, A.; Amanda-S, A.; Irawan, Y. Determination of the active asiaticoside content in *centella asiatica* as anti-cellulite agent. *Indones. J. Cancer Chemoprevent.* **2011**, *2*, 222-227.

[33] Sugunabai, J.; Jeyaraj, M.; Karpagam, T. Analysis of functional compounds and antioxidant activity of *centella asiatica*. *World J. Pharm. Pharm. Sci.* **2015**, *4*, 1982-1993.

[34] Oliveira, R.N.; Mancini, M.C.; Oliveira, F.C.S; Passos, T.M.; Quilty, B.; Thiré, R.M.S.; McGuinness, G.B. FTIR analysis and quantification of phenols and flavonoids of five commercially available plants extracts used in wound healing. *Revista materia* **2016**, *21*, 767-779.

[35] Ikegami, Y. The infrared spectra of troponoid compounds. VI. The infrared and Raman spectra of tropolone, 3- and 4-isopropyltropolones. *Bull. Chem. Soc. Jpn.* **1963**, *36*, 1118-1125.

[36] Ying, T.H.; Ishii, D.; Mahara, A.; Murakami, S.; Yamaoka, T.; Sudesh, K.; Samian, R.; Fujita, M.; Maeda, M.; Iwata, T. Scaffolds from electrospun polyhydroxyalkanoate copolymers: fabrication, characterization, bioabsorption and tissue response. *Biomaterials* **2008**, *29*, 1307-1317.

[37] Kim, Y-J.; Park, M.R.; Kim, M.S.; Kwon, O.H. Polyphenol-loaded polycaprolactone nanofibers for effective growth inhibition of human cancer cells. *Mater. Chem. Phys.* **2012**, *133*, 674-680.

[38] Moradkhannejhad, L.; Abdouss, M.; Nikfarjam, N.; Mazinani, S.; Heydari, V.; Electrospinning of zein/propolis nanofibers; antimicrobial properties and morphology investigation. *J. Mater. Sci.: Mater. Med.* **2018**, *29*, 165-175.

[39] Klančnik, A.; Piskernik, S.; Jeršek, B.; Možina, S.S. Evaluation of diffusion and dilution methods to determine the antibacterial activity of plant extracts. *J. Microbiol. Methods.* **2010**, *81*, 121-126.

[40] Sohrabi, A.; Shaibani, P.M.; Etayash, H.; Kaur, K.; Thundat, T. Sustained drug release and antibacterial activity of ampicillin incorporated poly(methyl methacrylate)-nylon6 core/shell nanofibers. *Polymer* **2013**, *54*, 2699-2705.

[41] Ignatova, M.; Manolova, N.; Rashkov, I.; Markova, N.D. Antibacterial and antioxidant electrospun materials from Poly(3-hydroxybutyrate) and polyvinylpyrrolidone containing caffeic acid phenethyl ester- “in” and “on” strategies for enhanced solubility. *Int. J. Pharm.* **2018**, *545*, 342-356.

Chapter 4

Fabrication and evaluation of PHBH monofilaments by heat treatment in various solvents

Chapter 4

4.1. Introduction

The use of biodegradable polymers is the possibility to reduce the amount of plastic waste that cannot easily decompose in nature and causing severe problems such as environmental pollution. Biodegradable polymers are completely decomposed into water and carbon dioxide by the action of microorganisms present in the soil and do not accumulate in the environment. One of the interesting biodegradable polymers is poly(3-hydroxybutyrate) (PHB), a homopolymer from polyhydroxyalkanoates (PHAs) family that produced from sugar, lipids, fatty acids, alkanes, alkenes, alkanoic acids, and palm oil through bacterial fermentation [1-3]. It is a thermoplastic polyester that can be produced by many types of microorganisms to store carbon as an intracellular carbon and energy storage compound [4].

As a thermoplastic, PHB has the potential for a fast production by melt spinning. However, rapid thermal degradation, low crystallization rate due to a low density of crystallization nuclei, and brittleness of PHB rendered it difficult to process [5]. Copolymerization with hydroxyalkanoic acid monomers such as 3-hydroxyhexanoates (3HHx), was attempted to reduce the obstacle of PHB. The use of the copolymer can decrease the glass transition temperature (T_g) and melting temperature (T_m), allowing the process at lower temperatures. Copolymer with 3-hydroxyhexanoates also resulted in soft and flexible material and increased mechanical properties.

Besides, the fabrication method of PHB and its copolymer can influence improvement in mechanical properties. Previous research reported that manufacture of PHB fibers by high-speed melt spinning, spin-drawing, and annealing resulted in a tensile strength of 330 MPa [6]. In the fabrication of PHB by one-step-drawing after isothermal crystallization for 72 h increased the tensile strength to 740 MPa [7]. Tanaka et al. [8] also reported that Poly(3-hydroxybutyrate-*co*-3-

hydroxyvalerate) (PHBV) fiber with a high tensile strength of 1.1 GPa was produced by directly rapid cooling in ice water after melt spinning process, followed by one-step-drawing after isothermal crystallization near the glass transition and annealing. This method explained that during cooling in ice water after spinning refers to the production of amorphous fibers. The isothermal crystallization in the ice bath for a certain period below the grass transition temperature allowed the formation of small crystal nuclei. Then, one-step-drawing and annealing performed highly orientation of molecular chain and fixation of the extended polymer chains, respectively [7-9].

Several organic solvents were used as a medium to deliver propolis subtract into monofilaments. The use of organic solvents in the treatment of synthetic fibers is related to the dyeing process or drug delivery. However, when organic solvents apply to synthetic fibers, it have a considerable effect on the characteristic of polymers. The synthetic fibers such as polyethylene terephthalate (PET) [6,10] and polypropylene [11] treated in various solvents exhibited the variation due to interaction between solvent and polymer such as longitudinal shrinkage, mechanical properties, and inner structure. It is known that some solvents are capable to swell fibers, especially in synthetic fibers and resulting in the relaxation of built-in strains such as shrinkage [6].

Our interest focused on the dimensional stability of biodegradable PHBH treated with the various organic solvents. The information on the interaction of biodegradable fibers, temperature effect, and several solvents are not much available. In this study, the effect of length and diameter as well as morphology of fibers after treatment with various organic solvents and temperature will be discussed.

4.2. Materials and methods

4.2.1. Materials

PHBH (X131A) containing 5.5 mol% of 3HH (M_w = 5.37x10^5 g/mol%) was provided from Kaneka Corp. Acetone, ethanol, hexane, and propanol were purchased from Wako Pure Chemical Industries, Ltd.

4.2.2. Fabrication of PHBH monofilament

The PHBH pellets were dried in vacuum at room temperature for 24 – 72 h prior to spinning process. Fabrication of PHBH fibers followed Tanaka et al. method [8]. PHBH was extruded by using a laboratory-size melt extrusion apparatus (Imoto Machinery Co. Ltd., Japan) at 190°C, Figure 4-1 (a). A 1.0 mm diameter of single nozzle was used as the extrusion port. The fiber was melted at an extrusion rotational speed of 4.0 rpm and rolled up in an ice water bath with a rotational speed of 30 rpm (bobbin diameter : 113 mm) to obtain the amorphous fibers.

(a (b

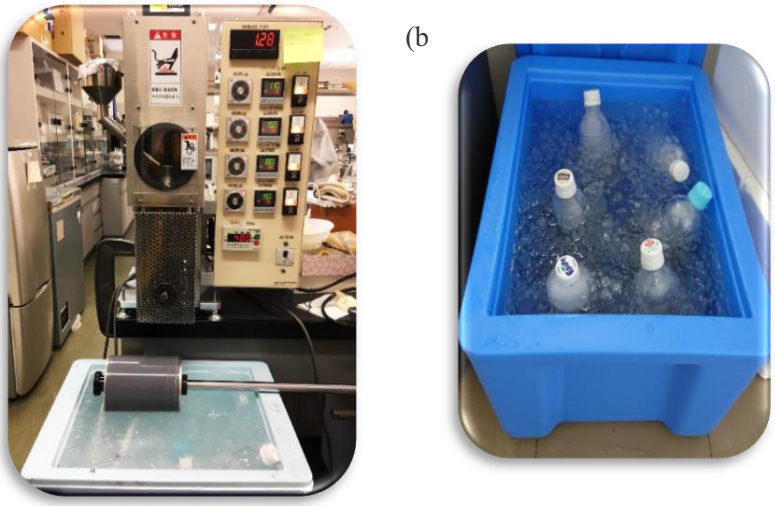

Figure 4-1. (a) A laboratory-size melt extrusion apparatus. (b) Isothermal crystallization process of PHBH monofilaments in the ice bath for 24, 48, and 72 h.

The isothermal crystallization (denoted as IC) was carried out in an ice water bath near the glass transition temperature for 24, 48, and 72 h. Then, the one-step-drawing method was used to

draw fibers without crystallization (0 h) and with isothermal crystallization (24, 48, 72 h) from initial length fiber of 30 mm to maximum by a stretching machine at room temperature. The fiber was stretched 9 times (270 mm) and immediately annealed at 60°C for 30 min under constant stress to increase the crystallinity of PHBH fibers. Scheme of PHBH fibers preparation by one-step-drawing and annealing is shown in Figure 4-2.

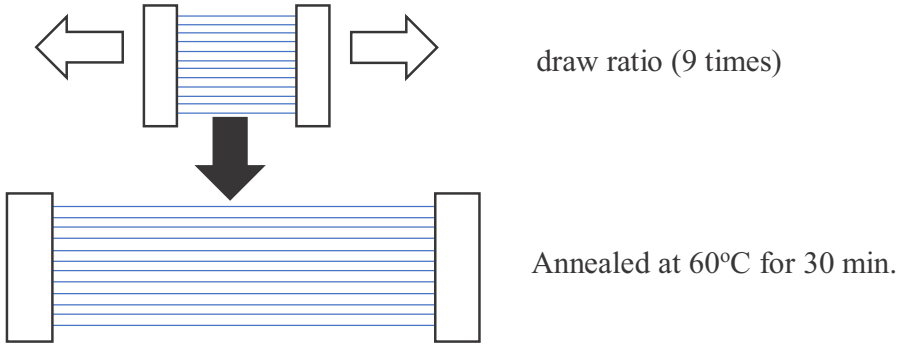

Figure 4-2. Scheme of PHBH fibers preparation by one-step-drawing and annealing.

4.2.3. Heat treatment of PHBH IC monofilaments

IC 0, 24, 48, and 72 h monofilaments were used for the next experiment. Heat treatment at several temperatures in water and several organic solvents such as ethanol, acetone, hexane, and propanol was used to evaluate the characteristic of monofilaments. Each solvent was filled in the tube with 10 cm in length of fibers, and closed. Each sample was placed in a water bath at different temperatures. The temperature was set up from 40 - 120°C. Table 4-1 shows heat treatment condition by the different heat treatment temperature and various solvents.

After 30 min of heat treatment, the tubes and fibers were taken out, and the fibers were kept at room temperature for 24 h to evaporate the solvent. The evaluation of fibers before and after heat treatment was carried out for SEM and its physical change.

Table 4-1. Different heat treatment temperatures and each solvent conditions

Solvent	Boiling point of solvent (℃)	Heat treatment temperature (℃)			
Water	100	60	80	90	100
Acetone	56	40	50		
Ethanol	78	60	80		
Hexane	68	40	60		
Propanol	97	40	60	80	
None (air)		80	100	120	

4.2.4. Characterization of PHBH IC monofilaments

4.2.4.1. Fiber length measurement

IC monofilaments after heat treatment with acetone-propolis (AP) solution for 0, 5, 10, and 15 circle times were dried overnight and measured its length. The average value of length was calculated from six filaments. The shrinkage as the change of fibers length was calculated according to the equation:

$$S = \frac{(\text{initial length} - \text{final length})}{\text{initial length}} \times 100\ \%$$

4.2.4.2.Fiber diameter measurement

The monofilament diameter on the upper, middle and lower side was measured by using a digital microscope (Keyence VHX-500FSP). The average value of diameter was calculated from six filaments. The expansion as the change in diameter was calculated according to the equation:

$$E = \frac{(\text{final diameter} - \text{initial diameter})}{\text{initial diameter}} \times 100\ \%$$

4.2.4.3. Scanning electron microscope (SEM)

The cross-section and surface of the PHBH fiber prepared by one-step-drawing and annealed before and after heat treatment were observed using a scanning electron microscope (SEM) (JEOL

JSM-7600F). The acceleration voltage was 10 kV with various magnifications. The samples were coated with platinum (Pt) in a sputtering device for 60 sec at 30 mA using a fine auto coating (JEOL JFC-1600).

4.3. Results and discussions

4.3.1. Shrinkage in length of PHBH IC monofilaments by heat treatment

IC fibers were treated in several solvents at different temperature conditions for 30 min. Fibers were then dried at room temperature for 24 h and measured its length. Figure 4-3 shows change in ratio shrinkage of fiber length by several organic solvents, water, and air at different temperatures. The samples tend to increase their shrinkage ratio as the heat treatment increased. Overall, PHBH fibers with IC for 24, 48, and 72 h exhibited a higher shrinkage ratio compared to those without isothermal crystallization (0 h). It considered that the fine-void in fibers obtained during the IC and drawing process affected the shrinkage behavior.

Mainly, IC 24 h monofilaments treated with acetone shrunk 30% at 40°C and went up to 40% at 50°C, Figure 4-3 (A). In the case of ethanol, the increasing of temperature at 60°C to 80°C resulted in an enhancement in shrinkage ratio of approximately 14%, Figure 4-3 (B). The shrinkage of fibers after treated with hexane and propanol were about 5 and 10% at 40°C and gradually increased to 11 and 20% at 60°C, respectively (Figure 4-3 (C, D)). Besides, IC monofilaments treated with water and air at 80°C to 100°C obtained a similar trend in shrinkage, Figure 4-3 (E, F). The comparison of the shrinkage ratio of IC 24 h and IC 72 h was slightly different in all various solvents. The factor that increases the shrinkage ratio of fibers might be due to isothermal crystallization that allowed the formation of fine-voids along the monofilaments and formation of small crystal nuclei and oriented fibers. The confined chains in oriented fiber will recover to the

original shape (molecular chain relaxation) by heat treatment. In the treatment of drawn PET fibers by heat treatment, the chain folding by reorientation was detected by IR spectroscopy after heat [11]. Aou et al. [26] reported that the presence of deformed amorphous chains was the thermodynamic driving force for shrinkage.

The ratio shrinkage of fiber in various solvents, water, and air at high temperature is summarized in Figure 4-4. Regarding these results at the highest temperature of each organic solvent, hexane displayed the lowest shrinkage at any heat treatment temperature. On the other hand, acetone demonstrated the highest shrinkage at 50°C. These results might be due to the different polarity of the solvent that affects PHBH IC monofilaments.

(A)

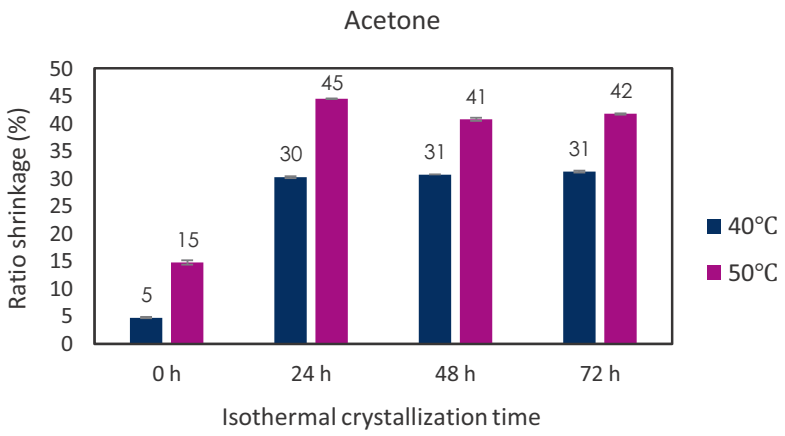

(B)

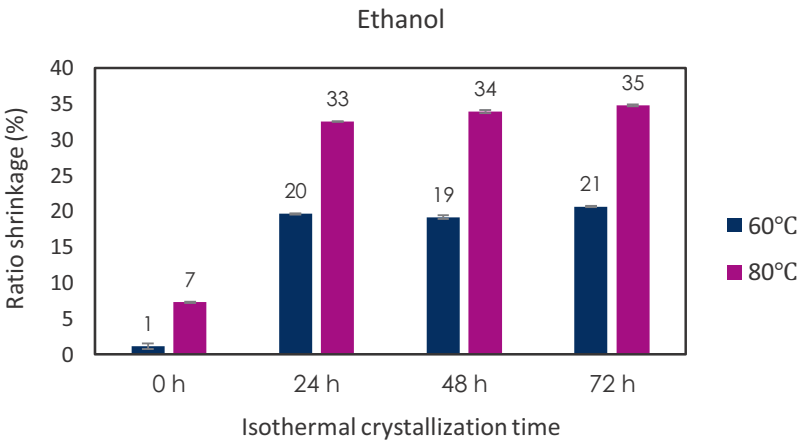

Figure 4-3. Cont.

(C)

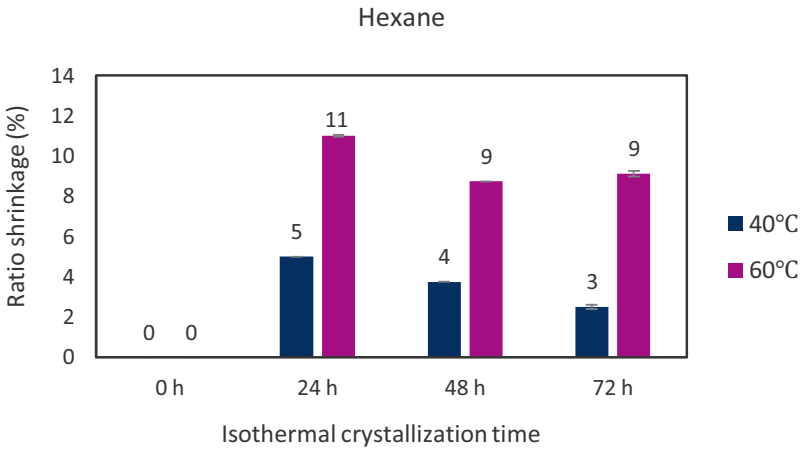

(D)

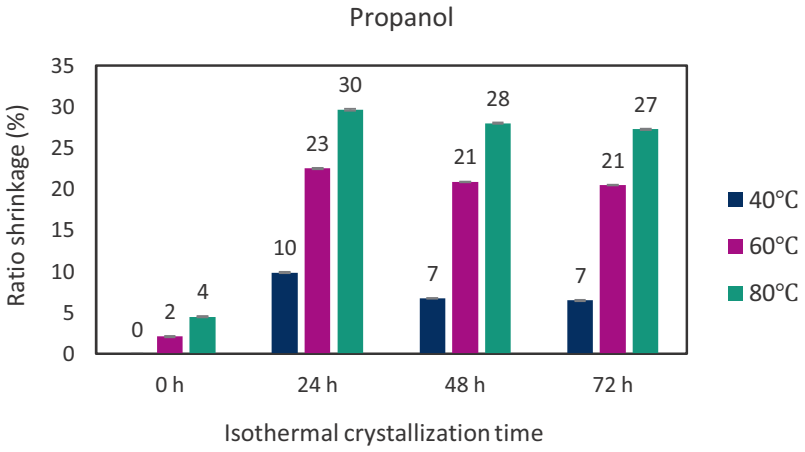

(E)

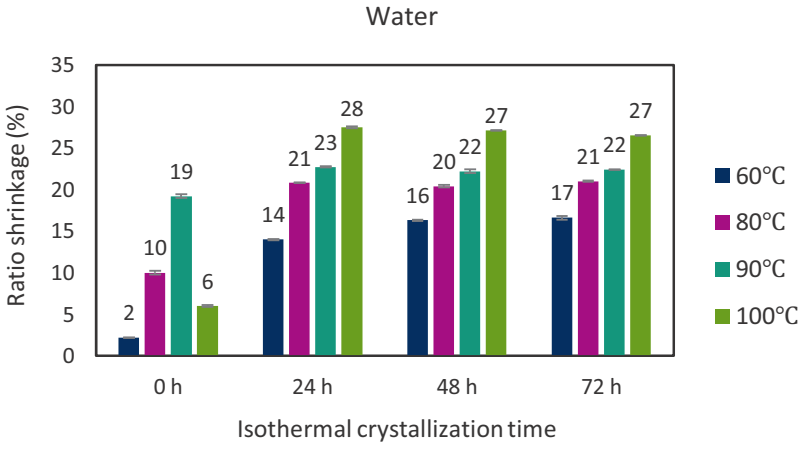

Figure 4-3. Cont.

(F)

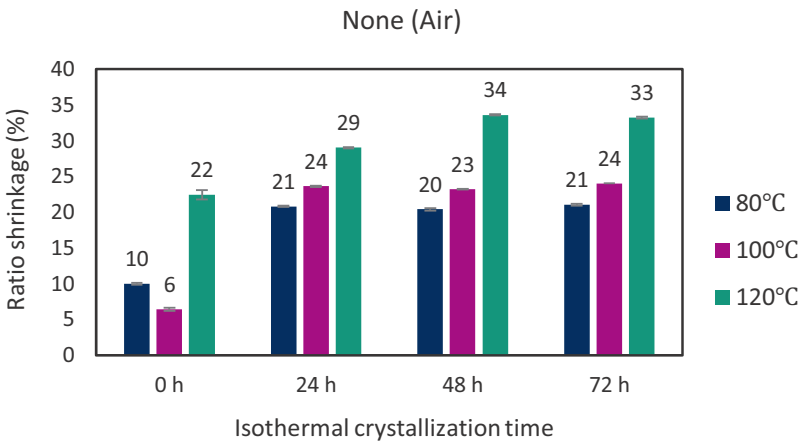

Figure 4-3. Ratio shrinkage of length fiber by heat treatment in acetone (A), ethanol (B), hexane (C), propanol (D), water (E), air (F) at various temperature against Isothermal crystallization time.

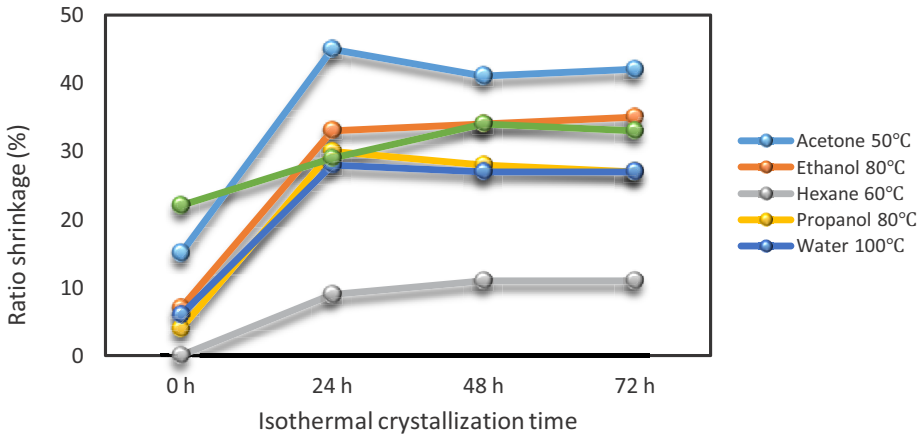

Figure 4-4. Ratio shrinkage of PHBH monofilaments at maximum heat treatment temperature in each solvent.

4.3.2. Expansion in diameter of PHBH monofilament by heat treatment

The physical change in IC monofilament diameters by heat treatment with various solvent is shown in Figure 4-5. In the PHBH fibers without IC (0 h) after heat treatment in various solvent, water, and air exhibited no difference in the change in diameter. Further, one-step-drawing after isothermal crystallization for 24, 48, and 72 h showed the expansion in fiber diameters. In the IC 24 h monofilaments after heat treatment, acetone as a solvent showed similar change in diameter

by applying temperature at 40 and 50°C, Figure 4-5 (A). The diameter of IC 24 h resulted in wider than IC 48 and 72 h fibers. In the case of ethanol, IC 24, 48, and 72 h after heat treatment at 60°C to 80°C showed increasing the fiber diameter. However, diameter of IC 72 h at 80°C decreased, Figure 4-5 (B). Hexane as a solvent for heat-treatment in IC fibers resulted dissimilar in fibers diameter between IC 24, 48, and 72 h, Figure 4-5 (C). Furthermore, propanol, water, and air (Figure 4-5 (D-F)) exhibited the increasing in IC 24, 48, and 72 h fibers diameter by applying heat treatment at 80°C. Regarding the different heat treatment temperatures and the same solvent, it confirmed that the fibers diameter changes due to the difference of IC fibers such as IC 24, 48, and 72 h. Thus, it has been clarified that the maximum value of expansion occurred in fibers with the condition of isothermal crystallization (IC) for 48 h except in acetone.

Figure 4-6 displays the comparison of diameter change in PHBH fibers at the maximum heat treatment temperature in each solvent, water, and air. The ratio expansion of fiber diameters of IC 24 h in acetone (50°C), ethanol (80°C), hexane (60°C), propanol (80°C), water (100°C), and air (120°C) were 11, 16, 2, 30, 11, and 22%, respectively. The low swollen of fibers in hexane is due to low diffusion rate of the solvent into the filaments [6]. Furthermore, the diameter of IC 48 and 72 h fibers in acetone (50°C) and IC 72 h fibers in ethanol (80°C) resulted in diameter shrinkage. It supposed due to the different polarity of each solvent that affect PHBH IC monofilaments. Besides, Venkatesh et al. [6] explained that the interaction depends between the presence of a particularly active group in the solvents and the aromatic group in polymers. It considered that PHBH IC fibers after heat treatment condition in several organic solvents, water, and air except acetone proved the shrinkage in fiber length and expansion in the diameter. However, the case of acetone showed the reduction in fiber diameter with the increase of IC time.

(A)

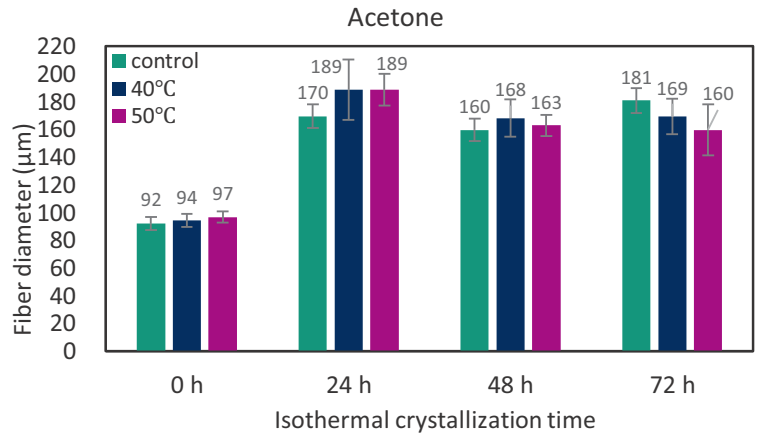

(B)

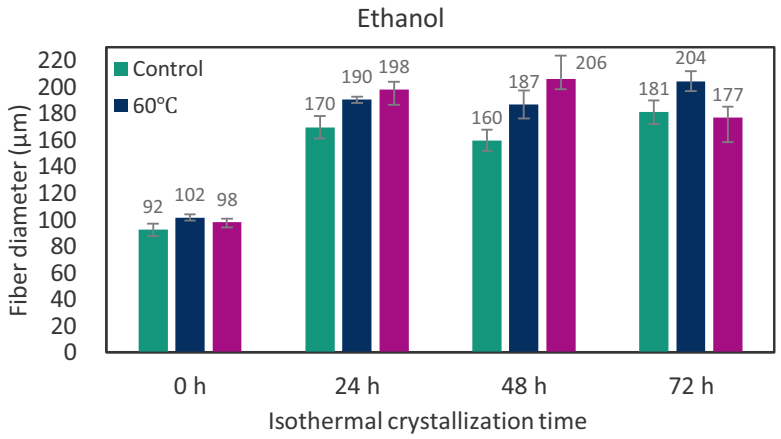

(C)

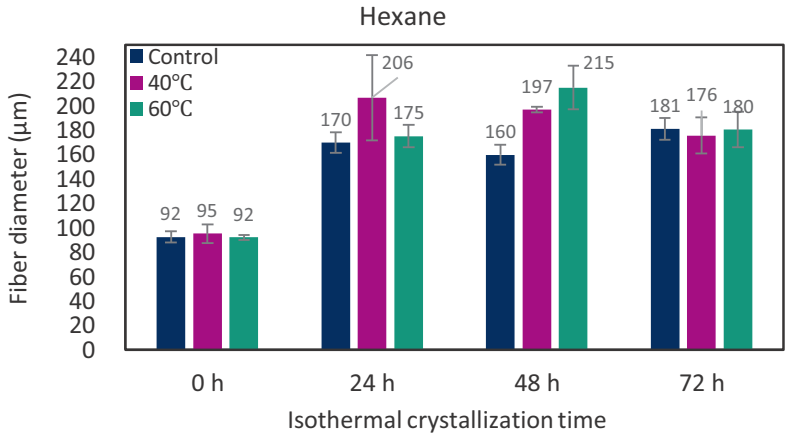

Figure 4-5. Cont.

(D)

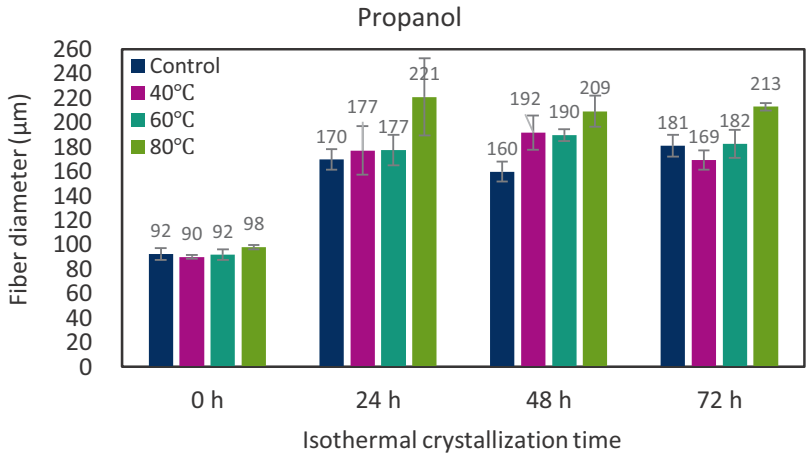

(E)

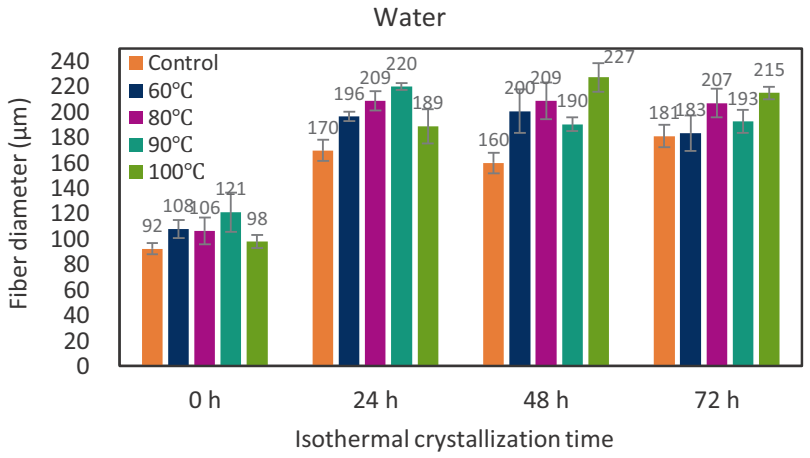

(F)

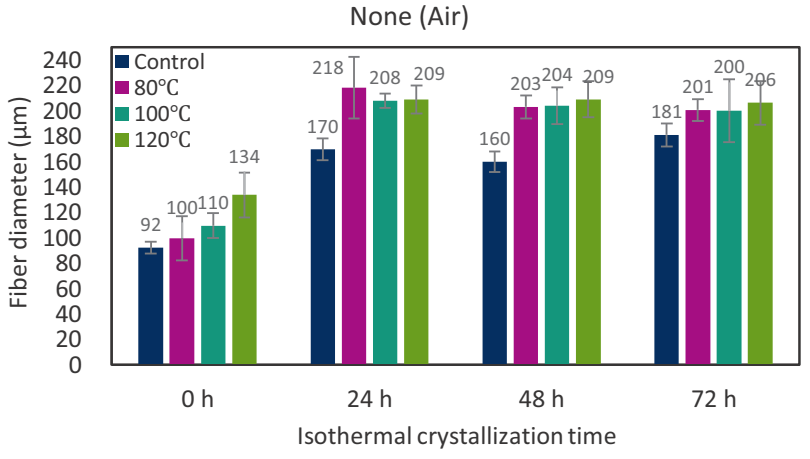

Figure 4-5. Diameter of PHBH fibers after heat treatment in acetone (A), ethanol(B), hexane(C), propanol(D), water(E), air (F) at various temperature agaist isothermal crystallization time.

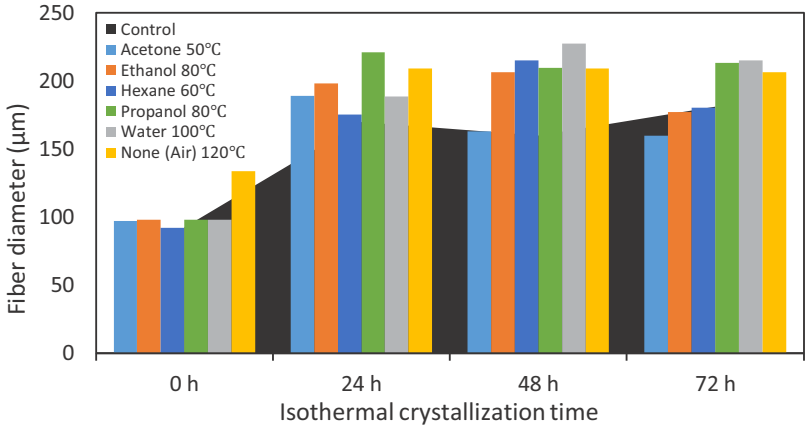

Figure 4-6. Comparison of diameter change in PHBH fibers at maximum heat treatment temperature in each solvent.

4.3.3. Cross-section of PHBH monofilaments by heat treatment

Melt-spinning followed by one-step-drawing without or after IC obtained a smooth surface PHBH monofilament with a diameter of 140 – 200 μm. Figure 4-7 shows the cross-section of the PHBH filaments after one-step-drawing without IC (0 h) and with IC for 24, 48, and 72 h by SEM image. These results show that fine-voids morphology was obtained by applying the isothermal crystallization method. IC 72 h displayed smaller void size compared to 24 and 48 h. The formation with small fine-voids in IC 72 h fibers might suppose due to increasing the number of small nuclei in the amorphous state during IC time and became closer cohesive elongated voids [9]. Figure 4-8 shows the cross-section of PHBH monofilaments at high heat treatment temperature in acetone (50°C), ethanol (80°C), hexane (60°C), propanol (80°C), water (100°C), and air (120°C)

In general, heat treatment at different temperatures in various solvents, water, and air showed a change in the void structure. The PHBH IC fibers treated in acetone exhibited the shrink in void structure and morphology fiber at 40 and 50°C. This change in acetone occurred in all fibers with the difference of isothermal crystallization time. In the case of ethanol at 60 and 80°C resulted in

the same morphology in cross-section of IC 24 and 48 h fibers. However, IC 72 h fibers that treated with ethanol had difficulty to cut and maintain the cross-section shape because fiber became soft. It confirmed that the use of hexane and propanol performed slight larger in the void of IC 24 h at any temperature conditions. Besides, PHBH IC fibers treated with water in the setup temperature from 60°C to 100°C showed no significant difference in the cross-section. This trend was similar to IC fiber with treated in the air at a temperature from 80°C to 120°C.

Overall, IC 48 and 72 h monofilaments showed a clearly unevenness with fine voids in the cross-section of PHBH fibers after heat treatment compared to IC 24 h. This is due to isothermal crystallization 24 h, which has large voids and may be able to maintain voids shape stability. Furthermore, the deformation in diameter fiber after heat treatment (expansion) was difficult to occur. The change of cross-section of fibers with treated in various solvents at high temperatures presumed due to the different polarity of the solvents affects PHBH fibers.

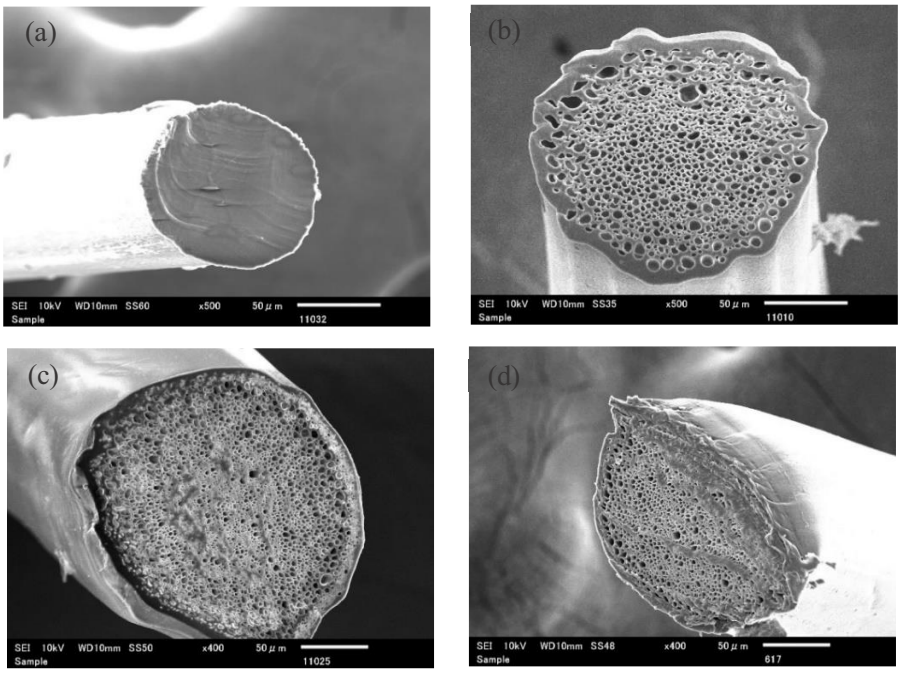

Figure 4-7. Cross-section of PHBH IC fibers without isothermal crystallization as control 0 h (a) and with isothermal crystallization for 24 h (b), 48 h (c), and 72 h (d).

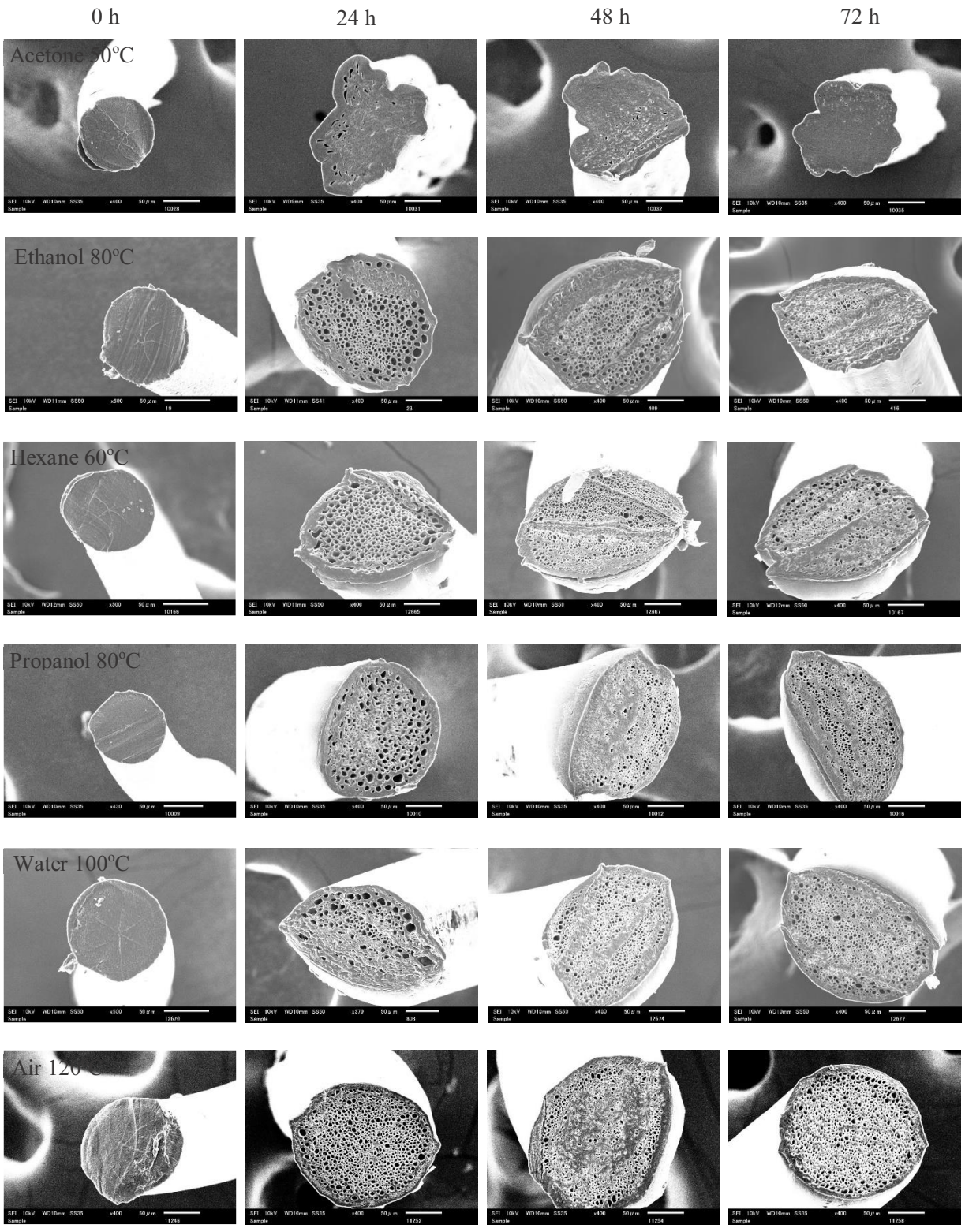

Figure 4-8. Cross-section of PHBH IC fibers (without and with isothermal crystallization 0, 24, 48, 72 h) at the maximum heat treatment temperature in each solvent.

4.4. Conclusions

The effect of heat treatment by several organic solvents, water, and air on physical change and cross-section morphology of PHBH fibers have been studied. The change in shrinkage and diameter fibers is found to be highly dependent on the temperature of each organic solvents and isothermal crystallization time. IC 24, 48, and 72 h monofilaments exhibited higher shrinkage in length and expansion in diameter compared to without IC (0 h) fiber. The trend of shrinkage and expansion ratio in IC monofilaments increased with increasing the heat treatment temperatures. Hexane displayed the lowest shrinkage and expansion at any heat treatment temperature. On the other hand, acetone demonstrated the highest shrinkage in diameter at 50°C and air resulted the highest expantion in diameter at 120°C. Heat treatment at different temperatures in various solvents, water, and air showed a change in the void structure. The clearly change of void structure in cross-section PHBH IC monofilaments was found in fibers after heat treatment in acetone. It might depend on the polarity of each solvent.

4.5. References

[1] Iwata, T.; Tsuge, T.; Taguchi, S.; Abe, H.; Tanaka, T. Bio-polyesters. In *Bio-based polymers*, 1st ed.; Kimura, Y.; CMC Publishing Co., Ltd.: Tokyo, Japan, 2013, pp. 71-85. ISBN978-4-7813-0271-3.

[2] Philip, S.; Keshavarz, T.; Roy, I. Polyhydroxyalkanoates: biodegradable polymers with a range of applications. *J. Chem. Technol. Biotechnol.* **2007**, *82*, 233-247.

[3] Bugnicourt, E.; Cinelli, P.; Lazzeri, A.; Alvare, V. Polyhydroxyalkanoate (PHA): review of synthesis, characteristics, processing and potential applications in packaging, *eXPRESS Polym. Lett.* **2014**, *8*, 791-808.

[4] Schmack, G.; Jehnichen, D.; Vogel, R.; Tandler, B. Biodegradable Fibers of Poly(3-hydroxybutyrate) Produced by High-Speed Melt Spinning and Spin Drawing. *J. Polym. Sci. Part B: Polym. Phy.* **2000**, *38*, 2841.

[5] Barham, P.J.; Keller, A. The relationship between microstructure and mode of fracture in polyhydroxybutyrate. *J. Polym. Sci. Part B: Polym. Phy.* **1986**, *24*, 69.

[6] Venkatesh, G. M.; Khan, A.H.; Bose, P.J.; Madan, G.L. Shrinkage and mechanical properties of Poly(ethylene terephthalate) filaments treated with various organic solvent. *J. Appl. Polym. Sci.* **1980**, *25*, 1601-1618.

[7] Tanaka, T.; Yabe, T.; Teramachi, S.; Iwata, T. Mechanical properties and enzymatic degradation of poly[(*R*)-3-hydroxybutyrate] fibers stretched after isothermal crystallization near T_g. *Polym. Degrad. Stab.* **2007**, *92*, 1016-1024.

[8] Tanaka, T.; Fujita, M.; Takeuchi, A.; Suzuki, Y.; Uesugi, K.; Ito, K.; Fujisawa, T.; Doi, Y.; Iwata, T. Formation of highly order structure in poly[(*R*)-3-hydroxybutyrate-*co*-(*R*)-3-hydroxyvalerate] high-strength fibers. *Macromolecules* **2006**, *39*, 2940 – 2946.

[9] Tanaka, T.; Uesugi, K.; Takeuchi, A.; Suzuki, Y.; Iwata, T. Analysis of inner structure in high-strength biodegradable fibers by X-ray microtomography using synchrotron radiation. *Polymer* **2007**, *48*, 6145-6151.

[10] Popoola, A.V.; Adetuyi, A.O.; Oyeleke, G.O. Shrinkage of polyester fibre in selected chlorinated solvents and effects on dimensional stability of the fabric. *J. Appl. Chem.* **2013**, *5*, 66-70.

[11] Tanaka, N.; Nakajima A. Partial melting, recrystallization and thermal shrinkage of polypropylene fibers. *Bull. Inst. Chem. Res.* **1971**, *49*, 382-389.

[12] Wilson, M.P.W. Shrinkage and chain folding in drawn poly(ethylene terephthalate) fibers. *Polymer* **1974**, *15*, 277-282.

[13] Aou, K.; Kang, S.; Hsu, S.L. Morphological study on thermal shrinkage and dimensional stability associated with oriented poly(lactic acid). *Macromolecules* **2005**, *38*, 7730-7735.

Chapter 5

Characterization of PHBH IC monofilaments in propolis-contained solvents by dip-coating method

Chapter 5

5.1. Introduction

Poly[(*R*)-3-hydroxybutyrate] (PHB) is a homopolymer in PHA, which is a family of polyesters that can be produced through biomass fermentation by many types of microorganisms in order to store carbon as an intercellular energy source[1-3]. PHB is highly crystalline in the range of 55 – 80%, with melting temperature 180ºC and has stiff, rigid, and brittle characteristics as well as poor mechanical properties became major drawbacks to the most standard application [1-3]. Nevertheless, copolymerization with other monomer units such as 3-hydroxyvalerate (3HV), 3-hydroxyhexanoate (3HH), and 4-hydroxybutyrate (4HB) into this main chains greatly improves homopolymer property and more suitable for practical applications [1,4-7]. Previous research proved that developed PHB copolymer as poly(3-hydroxybutyrate-*co*-3-hydroxyhexanoates) PHBH obtained softer and flexible properties compared to PHB homopolymer suitable for practical applications.

As a thermoplastic, PHB and its copolymer have the potential for a fast production by melt spinning. However, rapid thermal degradation, low crystallization rate due to a low density of crystallization nuclei, and brittleness of these polymers rendered it difficult to process [8]. Previous research reported that the innovation could reduce the obstacle of fabrication PHBH fiber by melt-spinning and also effect to improvement in mechanical properties. High-speed melt spinning of PHBH at high take-up velocity obtained an increase in the tensile strength to 156 MPa [9]. The manufactured PHB fibers by high-speed melt spinning, spin-drawing, and annealing resulted in tensile strength of 330 MPa [10]. The fabrication of PHB fibers by one-step-drawing after isothermal crystallization increased the tensile strength to 740 MPa [6]. Tanaka et al. [5] also

reported that Poly(3-hydroxybutyrate-*co*-3-hydroxyvalerate) (PHBV) fiber with a high tensile strength was produced by directly rapid cooling in ice water after the melt spinning process, followed by one-step-drawing after isothermal crystallization near the glass transition and annealing. Theses explained that one-step-drawing after isothermal crystallization in the ice bath for a certain period below the glass transition temperature allowed the formation of small crystal nuclei and performed highly oriented fibers [5-7].

The perspective area of PHB and its copolymer as filaments is the development of medical devices such as surgical suture, textile products, fishing lines, etc [5,11]. Recently, PHBH and other copolymers of PHB have been attractive much intention for using in medical applications. These polymers have been developing as implanted medical devices for dental, craniomaxillofacial, orthopedic, hernioplasty, skin surgery, drug delivery, and surgical suture [12]. The most advantage of these polymers is their ability that can completely degrade by microorganisms under aerobic and anaerobic conditions without forming a toxic product [3,13]. Especially in the living systems including *in vivo* and *in vitro*, these polymers can degrade by an enzyme present in blood and animal tissue as *in vivo* condition. Besides, PHB and PHBV suture were reported to possess the strength for the healing of myofascial wound as well as suggested to be an absorbable suture [4].

A feasible way to improve the functionality of those fibers is the incorporation of the natural compound as an antimicrobial reagent. The natural compound can demonstrate various biological effects, including antibacterial, antifungal, and antioxidant activity. The advantage of using a natural antibacterial product such as plant extract, essential oil, aloe vera, honey, etc instead of synthetic antibacterial reagent (iodine and silver) due to prevent wound infection is to diminish the risk of sensitization and development of resistance [14]. Propolis is one of a natural product, the

resinous substance and is well-known contained flavonoids and related phenolic acid. Previous studies reported that raw propolis contained more than 300 compounds, among which polyphenols, terpenoids, steroids, sugars, and amino acids that have been using in medicine pharmaceuticals such as protection against the entry of microorganisms, fungi, and bacteria [15]. Thus, several studies proved that propolis has excellent potential for wound healing application.

From Chapter 4, the characteristic change of PHBH IC monofilaments by heat treatment in several organic solvents was evaluated. Nevertheless, some of the organic solvents were chosen as a medium for loading propolis to the void structure in IC monofilaments. This research was attempted to investigate the physical, mechanical properties, inner structure change in PHBH IC monofilamnets after dip-coating treatment with the natural antibacterial product (propolis) solution as well as the antibacterial test. To my knowledge, the information by dip-coating method on the interaction of biodegradable PHBH fibers and the effect of the organic solvent containing propolis as an antibacterial reagent is not much available and has not reported hitherto, especially to PHB copolymer with 3-hydroxyhexanoate (3HH) unit.

5.2.Materials and methods

5.2.1. Materials

PHBH (X131A) containing 5.5 mol% of 3HH (M_w = 5.37x10^5 g/mol%) was provided from Kaneka Corp., Osaka, Japan. Acetone and ethanol 99.5% were purchased from Wako Pure Chemical Industries, Ltd. Propolis as the natural antibacterial was purchased from Stakich, Inc., Troy, USA.

Staphylococcus aureus (NBRC 12732) for antibacterial activity test was purchased from the National Institute of Technology and Evaluation, Biological Resource Center (NBRC), Tokyo, Japan.

5.2.2. Fabrication of PHBH monofilament

Prior to the spinning process, the PHBH pellets were dried in vacuum at room temperature for 24 – 72 h. Fabrication of PHBH IC monofilaments followed Tanaka et al. method [5]. PHBH pellets were extruded by using a laboratory-size melt extrusion apparatus (Imoto Machinery Co. Ltd., Japan) at 190°C and directly rolled up in an ice water bath to obtain the amorphous fibers. The isothermal crystallization (denoted as IC) was carried out in an ice water bath near the glass transition temperature for 24, 48, and 72 h. Then, the one-step-drawing method was used to draw fibers without crystallization (0 h) and with isothermal crystallization (24, 48, 72 h) from initial length fiber of 30 mm to maximum by a stretching machine at room temperature. The fiber was stretched 9 times (270 mm) and immediately annealed at 60°C for 30 min under constant stress to increase the crystallinity of PHBH fibers.

5.2.3. Penetration of propolis solution into PHBH IC monofilaments by dip-coating

Ethanol and acetone were chosen as the solvent to prepare propolis solutions. The propolis solutions were stirred in ethanol or acetone to prepare the concentration of propolis of 10% (w/v) for 24 h at room temperature. All solutions were filtered to remove insoluble substances. The concentrations of propolis in ethanol-propolis (EP) and acetone-propolis (AP) were 8.95 and 5.43%, respectively. The concentration propolis was determined from the dry weight by evaporating solutions under vacuum. A five mL of each propolis solution was put in the tube with 3 replicates. Each sample of IC 0, 24, 48, and 72 h monofilaments was cut into 3 cm and filled in the tube with propolis solution. The tubes with IC monofilaments were stored in a dry thermo bath (EYELA MG-2100) at 50-80°C for 24 h. The penetration of EP and AP solutions into IC monofilament was tried by this method. The dip-coating with AP solution at 50°C was maintained for 0, 5, 10, and 15 circle times, Figure 5-1. One circle means the dipping in the solution for 1 h

and drying at room temperature for 30 min; thus, it applied for 5, 10, and 15 times. These samples dried at room temperature for 24 h to evaporate the solvent and futher analysis.

Figure 5-1. Dip-coating AP solution in PHBH monofilament at 50°C.

5.2.4. Characterization of PHBH IC monofilaments by dip-coating

5.2.4.1. Polarized microscope

The penetration of EP and AP solution was evaluated by using a polarized microscope (NIKON OPTIPHOT-POL) at various magnification. The rate of penetration into PHBH IC fibers in propolis-solvents were analyzed by observing the change of color under polarized microscope.

5.2.4.2. Scanning electron microscope (SEM)

The morphology of the cross-section and inner-longitudinal fibers was investigated by scanning electron microscopy (SEM - JSM-6010LA, JEOL) at an accelerating voltage of 10-15 kV at various magnifications with surface coated by platinum (Pt) in a sputtering device for 60 sec at 30 mA. The diameter and distribution of voids in fibers were measured using Image J software.

5.2.4.3. Physical change in length, diameter, and weight of fibers

Fiber length measurement

IC monofilaments after dip-coating in acetone-propolis (AP) for 0, 5, 10, and 15 circle times were dried overnight and measured its length. The average value of length was calculated from six filaments. The shrinkage as the change of length fibers was calculated according to the equation:

$$S = \frac{(\text{initial length} - \text{final length})}{\text{initial length}} \times 100\ \%$$

Fiber diameter measurement

The monofilament diameter on the upper, middle and lower side was measured by using a digital microscope (Keyence VHX-500FSP). The average value of diameter was calculated from six filaments. The expansion as the change in diameter was calculated according to the equation:

$$E = \frac{(\text{final diameter} - \text{initial diameter})}{\text{initial diameter}} \times 100\ \%$$

Fiber weight measurement

The monofilaments weight was measured by using a digital measuring after dried in vacuum at room temperature for 24 h. The average value of diameter was calculated from six filaments. The change of weight (W) in filaments was calculated according to the equation:

$$W = \frac{(\text{final weight} - \text{initial weight})}{\text{initial weight}} \times 100\ \%$$

5.2.4.4. Mechanical properties

The mechanical properties of IC monofilaments after dip-coating at 50°C in AP solution for 0, 5, 10, and 15 circle times were investigated by using a tensile testing machine (EZ-S SHIMADZU) with 50N load cell at room temperature. Ten specimens from each sample were prepared from 0, 5, 10, and 15 circle times with initial length 10 mm and width around 0.2 mm, Figure 5-2. Two grips stapled the ends of each sample with an initial distance of 10 mm and a crosshead speed of 20 mm/min. Tensile strength, Young's modulus, and elongation at break were calculated based on the stress-strain curve of each sample.

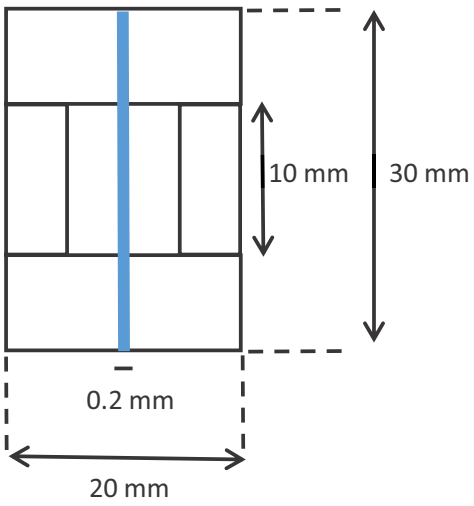

Figure 5-2. A paper template used to prepare tensile specimens of the fibers.

5.2.4.5. X-ray (XRD)

Wide-angle X-ray diffraction (WAXD) and small-angle X-ray scattering (SAXS) were used for crystalline structure analysis of IC monofilaments after dip-coating for 0, 5, 10, and 15 circle times. The two-dimensional (2D) patterns of IC monofilaments were recorded by X-ray diffraction equipment (SPring-8, Japan) with a wavelength of 0.07085 nm (WAXD) and 0.1 nm (SAXS) at 2θ scanning angle between 5°– 30°. The distance from the sample to the detector (PILATUS 3 x 2M) was 326.5 mm (WAXD), and 222 mm (SAXS) with the exposure time was 2.0 sec. The X-ray diffraction of fibers was investigated by the MDPI application.

Linear WAXD profile from the equatorial scans in 2D WAXD pattern samples was obtained to estimate the degree of crystallinity and orientation of crystallites in fibers. The crystalline degree was determined from WAXD diffraction intensity according to Vonk's method [5,16]. Crystalline orientation (f_c) was evaluated from the half-width (β_c) of the azimuthal direction of the (020) reflection based on the following equation: $f_c = (180^o - \beta_c) / 180^o$ [5]. For SAXS measurements, a long period was measured according to Bragg's Law equation ($L = \lambda/(2 \sin \theta)$). The lamellar

thicknesses of IC monofilaments was calculated from the relation between the long period (SAXS) and degree of crystallinity (WAXD).

2.5.4.6. Antibacterial test

S. aureus was used as a representative for gram-positive bacteria to examine the antibacterial activity against propolis. The diffusion test was used as a method to evaluate which has been well established by previous reports [17-18]. The bacterial culture was spread on the Luria Bertani (LB) agar surface by using a sterile cotton bat. IC 72 h monofilaments after dip-coating in AP solution for 10 circle times were placed on the surface of the Petri dishes then they were incubated at 37ºC (*S. aureus*) for 24 h. The distance of inhibition zone (mm) from IC fibers were measured.

5.3. Results and discussions

5.3.1. Morphology of PHBH IC monofilaments

Melt-spinning followed by one-step-drawing after isothermal crystallization (IC) obtained a smooth surface PHBH monofilament with a diameter of 140 – 200 μm. The smoothness of monofilament is thought to be advantageous because it provides uniform distribution and lowers infection risk [19]. Figure 5-3 shows the cross-section and porous distributions of IC 24, 48, and 72 h monofilaments. The fine-voids morphology was obtained by applying the isothermal crystallization method. The appearance of many fine-voids in one-step-drawing supposed to generate by contraction of polymer chain during IC and entry of water storage into PHBH fibers in an ice bath near T_g or thermal shrinkage of the polymer chain and outflow water during annealing at 60ºC [7]. Furthermore, the difference between IC 24 h to 48 h and 72 h fibers is the size of fine-voids in cross-section along a perpendicular to the direction of drawing.

Figure 5-3(B) shows the different distribution in fine-voids area of IC 24, 48, and 72 h fibers. Thus, the fine-voids in diameter, distribution, and thickness of the wall from cross-sections of IC fibers were measured by using Image J software and exhibited in Table 5-1. In general, a short time of IC 24 h displayed large voids morphology compared to 72 h. The diameter voids of IC 24, 48, and 72 h fibers were 4.14 μm, 2.94 μm, and 2.45 μm, respectively. The average void diameters reduced with increasing isothermal crystallization time. The formation with small fine-voids in IC 72 h fibers might suppose due to increasing the number of small nuclei in the amorphous state during IC time and became closer cohesive elongated voids [6,7].

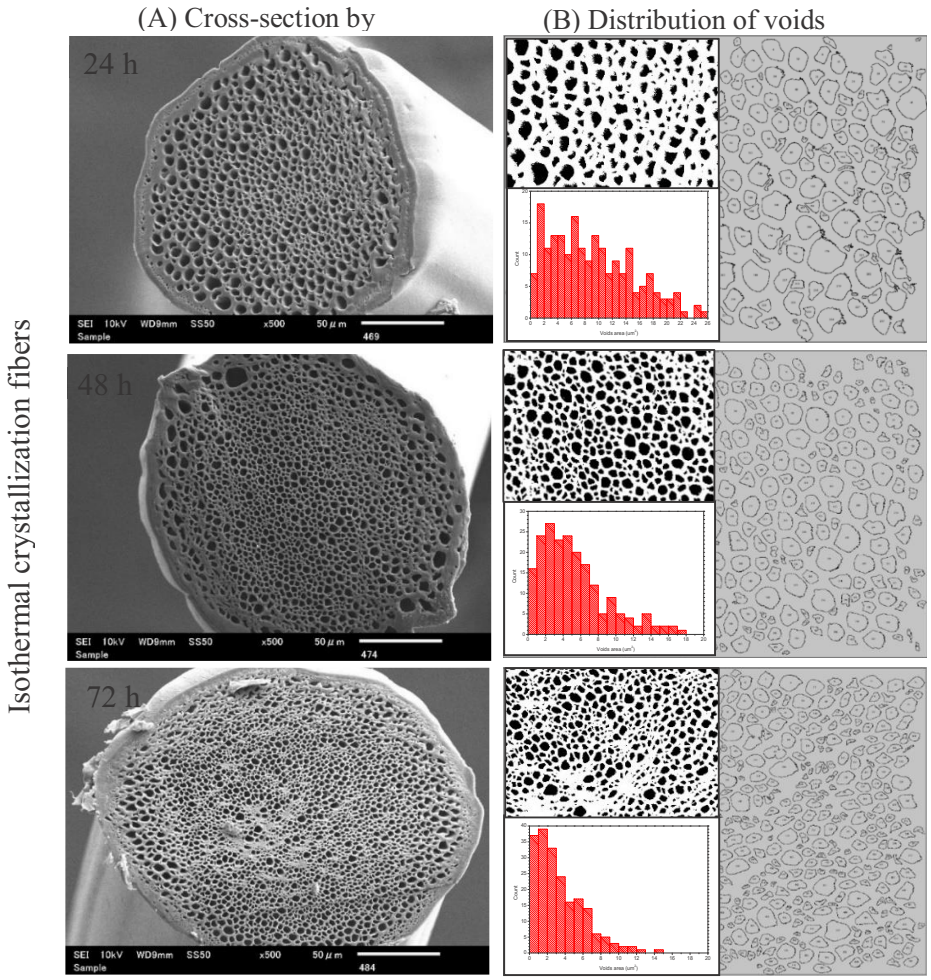

Figure 5-3. PHBH monofilaments one-step-drawing after isothermal crystallization (IC) 24, 48, and 72 h by SEM and porous distribution by Image J.

Table 5-1. Diameter, size area of voids, thickness wall between voids in isothermal crystallization 24, 48, and 72 h fibers.

Isothermal crystallization	**24 h**	**48 h**	**72 h**
Diameter (Ø) voids (μm)	4.1 ± 1.6	2.9 ± 1.1	2.5 ± 1.0
Size area of voids (μm^2)	9.0 ± 6.0	5.5 ± 3.8	3.5 ± 2.7
Thickness wall between voids (μm)	1.5 ± 0.6	1.2 ± 0.5	1.0 ± 0.4

5.3.2. Penetration rate of PHBH IC monofilaments by dip-coating in propolis solutions

The penetration rate of ethanol, acetone, EP, and AP solution into IC monofilaments at several temperatures for 5 and 24 h were evaluated by polarized microscopy. The polarized microscopy was used to record the penetration of these solutions into IC 24 h monofilaments. Polarized light microscope images of IC 24 h monofilaments after dip-coating in ethanol and EP solution at 60 to 80°C are shown in Figure 5-4. The penetration rate was faster with increasing the set-up temperature in ethanol. However, EP solution exhibited difficulty penetration to IC 24 h monofilaments after dip-coating for 5 or 24 h at 50-80°C. Even though the temperature was raised to 80°C and dip-coating for 24 h, there is difficulty to penetrate to fibers by ethanol. Thus, the polarized light microscope also observed slightly penetration to fibers and the transmitted light cannot be observed primarily into fibers, Figure 5-4 (B).

Furthermore, the penetration of acetone and AP solution was also observed in 5 and 24 h at 50°C, Figure 5-5. These images explained that acetone was able to completely penetrate into fiber for 5 h at 50°C (A). Thus, the AP solution resulted in a faster penetration into fiber compared to EP solutions. It might depend on the polarity of each solvent. For the next experiment, the AP solution was used for dip-coating to PHBH fibers at 50°C with several circle times of 5, 10, and 15.

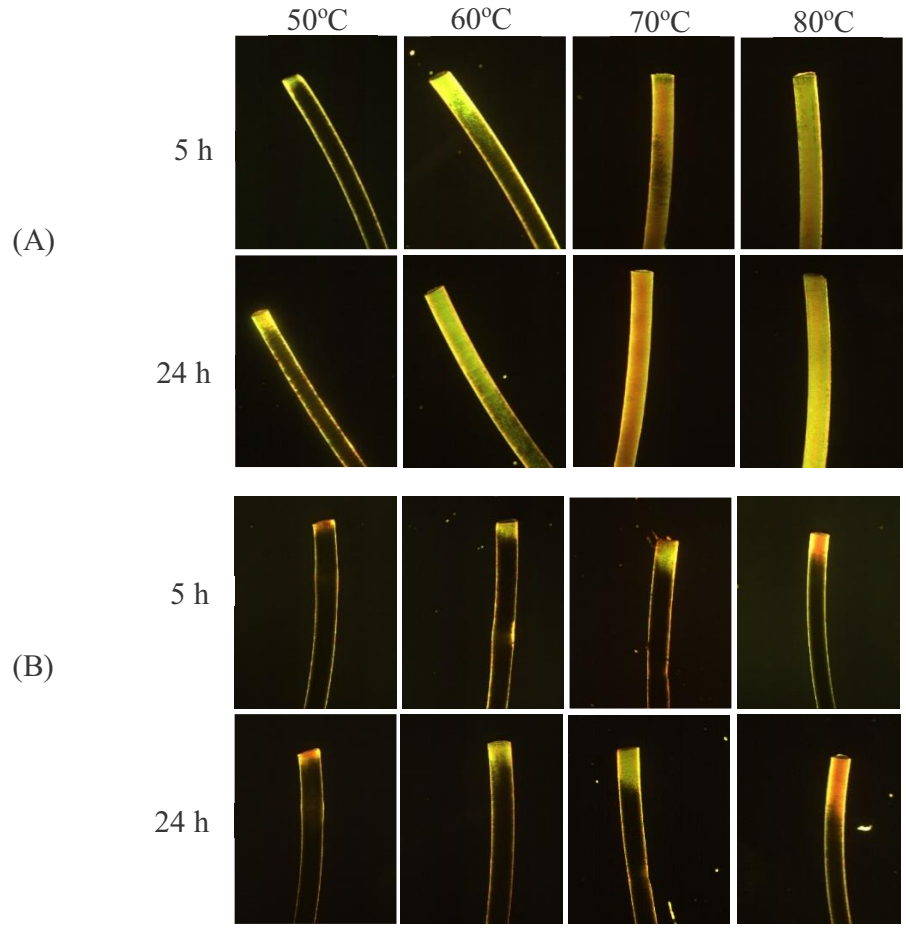

Figure 5-4. Polarized light microscopy image of IC 24 h monofilaments after dip-coating for 5 h and 24 h with ethanol (A) and EP solution (B) at 50 to 80°C.

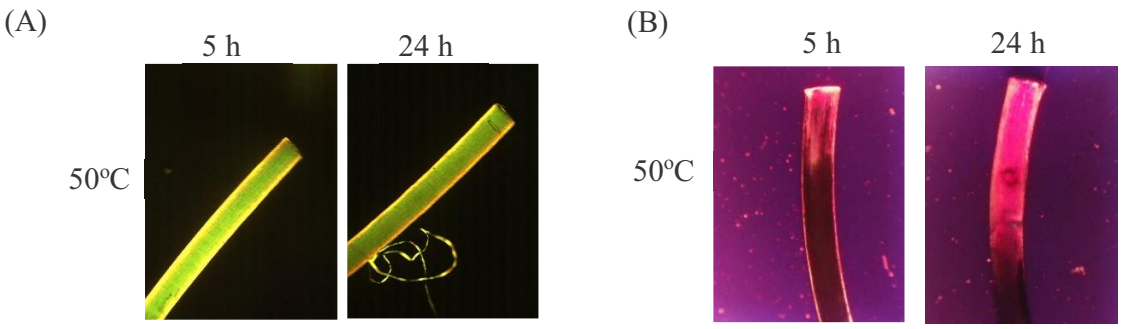

Figure 5-5. Polarized light microscopy image of IC 24 h monofilaments after dip-coating for 5 h and 24 h with acetone (A) and AP solution (B) at 50°C.

5.3.3. Penetration of PHBH IC monofilaments by dip-coating in AP solution

Acetone was chosen as a solvent to penetrate propolis into PHBH IC 24 and 72 h monofilaments at 50°C for 5, 10, and 15 circle times due to its good penetration. IC monofilaments were observed in the penetration in each circle time by SEM and polarized light microscope. Figure 5-6 displays the penetration, cross-section, and inner-longitudinal IC 24 and 72 h monofilaments after dip-coating with AP solution in different circle times. AP solution was started to penetrate into IC monofilaments in 5 circle times. Above 10 circle times, AP solution gradually penetrated through the IC fibers. The increase in dip-coating circle times showed the higher penetration of AP solution into fibers.

IC 72 h monofilament had faster penetration than IC 24 h in AP solution at 5 circle times. It considered as the difference in fine-voids morphology of fibers between isothermal crystallization 24 and 72 h. Fine-voids size of IC 72 h monofilaments was smaller than that of IC 24 h. It might supposed due to the different mobility of AP solution in narrow voids (capillary phenomena). The other possibility might be the thinner thickness of walls between fine-voids in IC 72 h fibers that connected to other voids can facilitate the penetration rate of AP solution, Table 5-1. Furthermore, some of the propolis substrates were covered on the cross-section and settled in the inner-longitudinal section of IC 24 and 72 h fibers, Figure 5-6. These confirmed that propolis substrate by dip-coating in AP solution at 50°C has the possibility to be loaded into fine-voids IC of 24 and 72 h fibers.

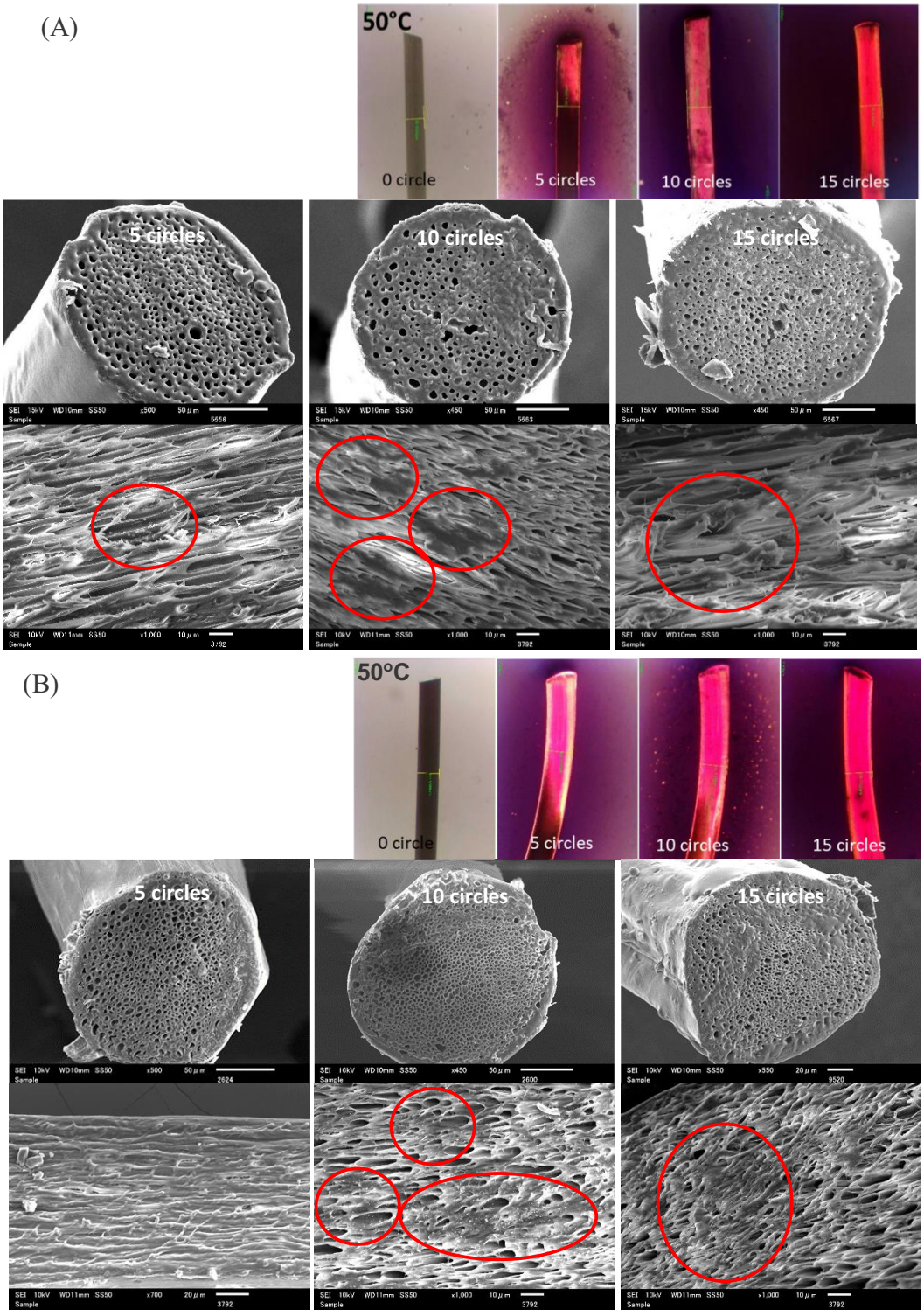

Figure 5-6. Penetration of AP solution into IC 24 h (A) and 72 h (B) monofilaments for 5, 10, and 15 circle times by polarized microscope. Cross-section and inner-longitudinal IC fibers after dip-coating AP solution for 5, 10, and 15 circle times by SEM.

5.3.4. Physical change in PHBH IC monofilaments by dip-coating in AP solution

The physical changes of IC 24 and 72 h fibers after dip-coating with AP solution for 0, 5, 10, and 15 circle times were evaluated in the length, diameter, and weight Figure 5-7. In general, IC 24 h and 72 h fibers showed the same behavior in physical change. The length of IC 24 and 72 h fibers after dip-coating for 5 circle times dramatically shrank 23 and 25% from the initial length, respectively. The total shrinkage of IC 24 and 72 h fibers after 15 circle times were 25 and 26%, respectively (Figure 5-7 (A)). The shrinkage occurs after the penetration AP solution supposed that the solvent was penetrated entirely into fiber and had good interaction with fibers. Venkatesh [10] reported that shrinkage in PET filament by several solvent-induced is primarily a relaxation phenomenon of orientation stresses presented during the melt-spinning and drawing processes. However, with propolis, the shrinkage of fiber was lower compared to acetone only for 30 min (Figure 4-3 (A)). It supposed that the propolis as the filler in the fine-void of monofilament affect to decrease the shrinkage in length of IC monofilaments.

The diameter of IC 24 and 72 h fibers expanded by dip-coating in AP solution. The expansion of IC 24 h fibers after dip-coating for 5, 10, and 15 circle times were 23, 26, and 27%, respectively. This behavior similar to IC 72 h fibers with total diameter expanded for 26% after 15 circle times, Figure 5-7(B). The physical changes in IC fibers after dip-coating in AP solution were suggested that shrinkage in length and wider in diameter of the fiber, Figure 5-8.

Figure 5-7(C) displays the change in weight of IC monofilaments after dip-coating for 5, 10, and 15 circle times. The weight of IC 24 and 72 h fibers after dip-coating for 5 circle times was increased by 13 and 12%, respectively. After 15 circle times, the total weight increased to 25 and 18% for IC 24 and 72 h fibers, respectively. Regarding these results, acetone as a solvent for penetrating propolis might have an interaction with PHBH IC fibers, such as an interaction with

fine-voids in IC fibers or the inner structure of the fiber, including amorphous and crystalline region.

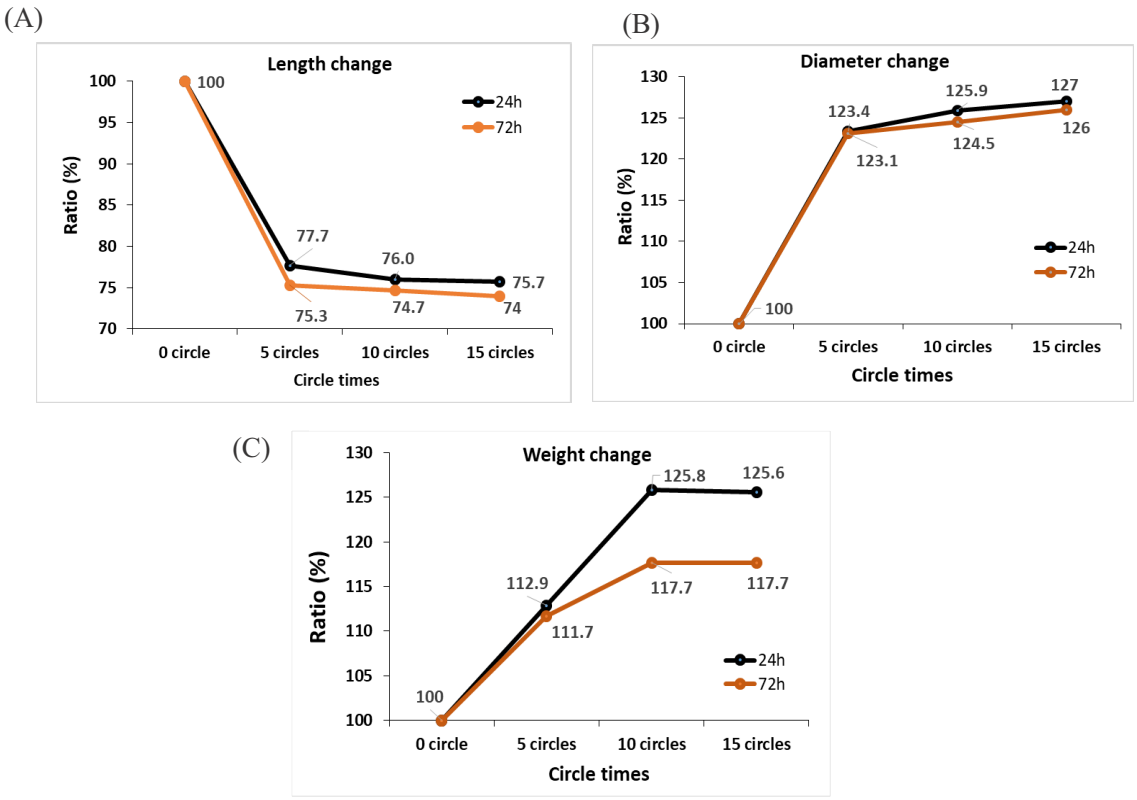

Figure 5-7. The physical change in IC 24 and 72 h monofilaments after dip-coating with AP solution for 0, 5, 10, 15 circle times. (A) length change, (B) diameter change, (C) weight change.

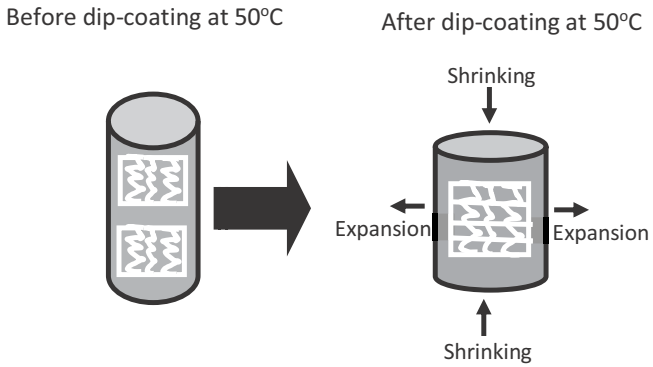

Figure 5-8. Model of physical change of PHBH IC fiber before and after dip-coating at 50°C in AP solution.

5.3.5. Mechanical properties of PHBH IC monofilaments by dip-coating in AP solution

Table 5-2 and Figure 5-9 show the mechanical properties of IC 24 and 72 h fibers untreated (0 h) and after dip-coating in AP solution at 50°C for 5, 10, and 15 circle times. Untreated fiber (0 h) for both IC 24 and 72 h fibers resulted in tensile strength of 72.0 and 94.6 MPa with elongation of 36.2 and 45.6 %, respectively. In the case of IC 24 h fibers, the decrease of tensile strength after 5 circle times was 30.0%, with a total reduction of 36.6% after 15 circle times. Thus, IC 72 h fibers after dip-coating for 5 and 15 circle times affected on the reduction of the tensile strength of 33.8% and 39.7%, respectively. The elongation of IC 24 h and 72 h fibers was increased from 36.2 and 45.6 % (0 circle time) to 100.8 and 101.0 % (5 circles time), respectively. Furthermore, Young's modulus of IC 24 h and 72 h monofilaments after dip-coating in AP solution was decreased. The other research of polyester fiber treated with chlorinated solvents explained that Young's modulus was decreased with increasing the elongation might be due to the reduction in stiffness of the phenyl residue on the terephthalate group [20].

Change in the mechanical properties of IC 24 h and 72 h fibers after dip-coating were occurred due to physical change in the length (shrinkage). The relaxation in length by dip-coating (shrinkage) can increase the extension of fibers due to the increase of mobility of molecular chain. In the case of PET yarn treated with nitrobenzene at 120°C as a solvent resulted in shrinkage 26% and an increase in elongation which were found highly dependent on time and temperature, as well as on tension applied on the yarn during the treatment [10]. Poopola et al. [20] also explained that an increase in extension of fibers can be linked to the stability conferred by the solvent treatments and the convolution occurring from chain folds in the treated fibers. The other reason might be due to the change in the inner structure of the PHBH polymer after treatment that showed a decline in

the crystallinity of PHBH polymer after dip-coating in AP solution for 15 circle times (Table 5-3). Moreover, it would be discussed in the X-ray analysis section.

Table 5-2. Mechanical properties of PHBH IC 24 h and 72 h monofilaments after dip-coating for 0, 5, 10, 15 circle times.

Isothermal Crystallization	Dip-coating (circle times)	Tensile strength (MPa)	Young's modulus (MPa)	Elongation at break (%)
24 h	0	72.0 ± 7.2	750.0 ± 103.4	36.2 ± 6.5
	5	50.3 ± 3.8	463.3 ± 61.5	100.8 ± 10.6
	10	49.4 ± 8.5	465.4 ± 73.4	89.1 ± 9.1
	15	46.0 ± 6.8	474.4 ± 100.2	85.8 ± 16.1
72 h	0	94.6 ± 21.1	945.7 ± 229.1	45.6 ± 11.5
	5	62.7 ± 8.3	464.3 ± 70.5	101.0 ± 13.9
	10	60.1 ± 11.7	503.2 ± 103.6	98.1 ± 11.6
	15	57.0 ± 8.2	560.8 ± 97.3	81.9 ± 42.4

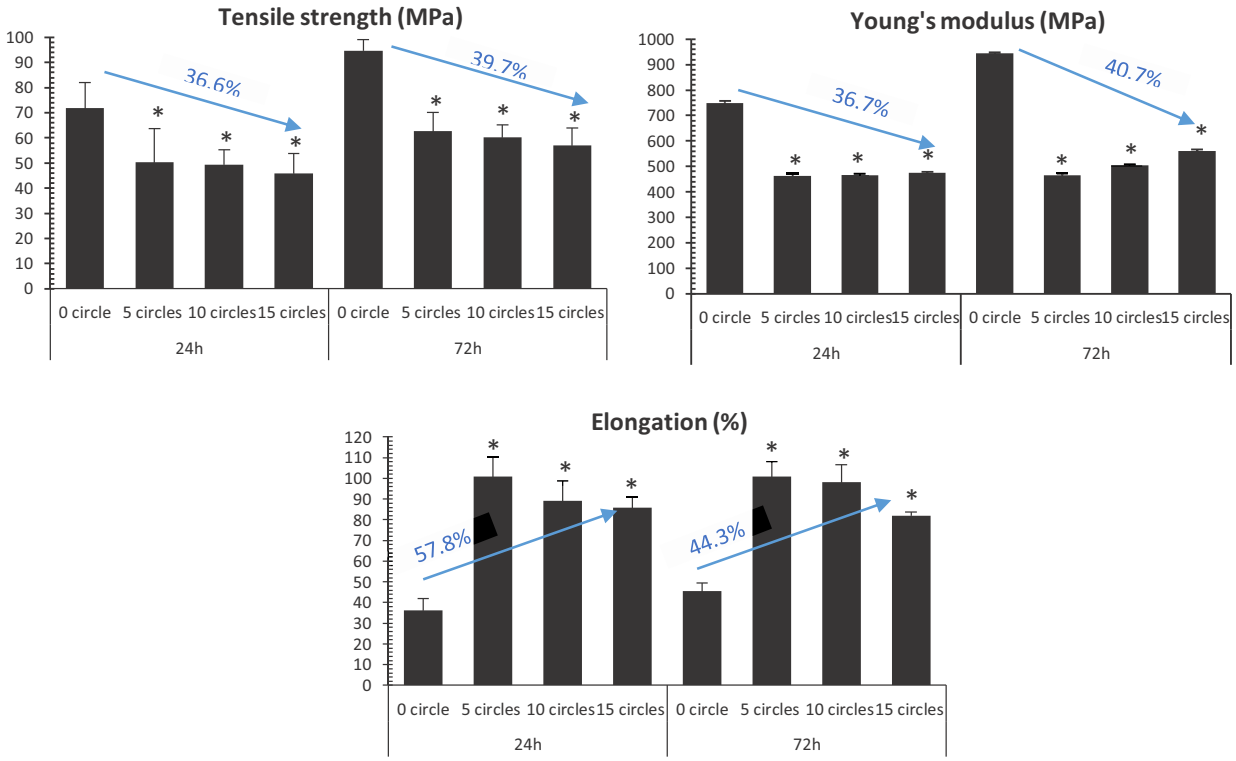

*, $p < 0.05$ considered statistically significant compared between IC 24 and 72 h untreated fibers (0 circle time) and after dip-coating for 5, 10, 15 circle times in each group.

Figure 5-9. Mechanical properties of IC 24 and 72 h monofilaments after dip-coating in AP solution for 0, 5, 10, 15 circle times.

5.3.6. X-ray analysis of PHBH IC monofilaments by dip-coating in AP solution

The inner structure of IC 24 and 72 h fibers after dip-coating were analyzed by wide-angle X-ray scatterings and small-angle X-ray scatterings (WAXD and SAXS). It has been reported that PHB and its copolymer generally crystallize in 2_1 helix conformation (α-form) and a planar zig-zag conformation (β-form) that can be observed in the highly drawn fiber as PHB crystal form [6,16,21]. WAXD patterns of IC 24 and 72 h monofilaments before (0 circle) and after by dip-coating for 5, 10, and 15 circle times are shown in Figure 5-10 (A). The WAXD pattern of IC 24 and 72 h fibers without dip-coating (0 circle) showed the α-form reflection of (020), (110), (021), (101), and (111), respectively. These patterns also showed a broad spot (β-form) on the equator as well as highly oriented fiber with α-form. The degree of crystallinity in IC 24 and 72 h fibers before dip-coating has been determined to be approximately 61 and 62.5 %, Table 5-3. The high oriented of IC fibers was performed from isothermal crystallization near the glass transition temperature that allowed growing many small crystal nuclei and one-step-drawing led to increasing the orientation and crystallization of the molecular chains in the limited amorphous region between small crystal nuclei [6].

In the case of IC fibers after dip-coating in AP solution at 50°C for several times, these patterns showed the disappearance of β-form and the change into arc reflection in α-form. These results considered that β-form might transform into random molecular chains by relaxation, illustrated the chains in the amorphous phase, Figure 5-10(B). Thus, arc reflection in the WAXD patterns might indicate the decrease of the crystalline orientation and polymer chains in α-form, Table 5-3. The degree of crystallinity of IC 24 and 72 h was slightly decreased (5 and 10 circle times) and declined to 54.7 and 58.5% after 15 circle times. Along with that, the tensile strength of IC 24 and 72 h fibers after dip-coating in AP solution was reduced compared to untreated. It

supposed that due to a decrease in crystalline orientation and the number of the tie chain between the stacked lamellar crystals.

Table 5-3. X-ray analysis of IC 24 and 72 h monofilaments after dip-coating in AP solution for 0, 5, 10, and 15 circle times.

Isothermal crystallization	Circle times	Crystallinity (%)	Crystalline orientation	Crystalline size (b-axis) (nm)	Long period (nm)	Lamellar thickness (nm)
24 h	0	61.0	0.95	0.14	7.5	4.6
	5	59.2	0.89	0.15	8.4	5.1
	10	60.3	0.91	0.19	8.5	5.2
	15	54.7	0.91	0.20	8.3	5.0
72 h	0	62.5	0.94	0.14	7.4	4.5
	5	60.9	0.90	0.17	8.4	5.1
	10	60.5	0.91	0.17	8.5	5.2
	15	58.5	0.90	0.17	8.3	5.0

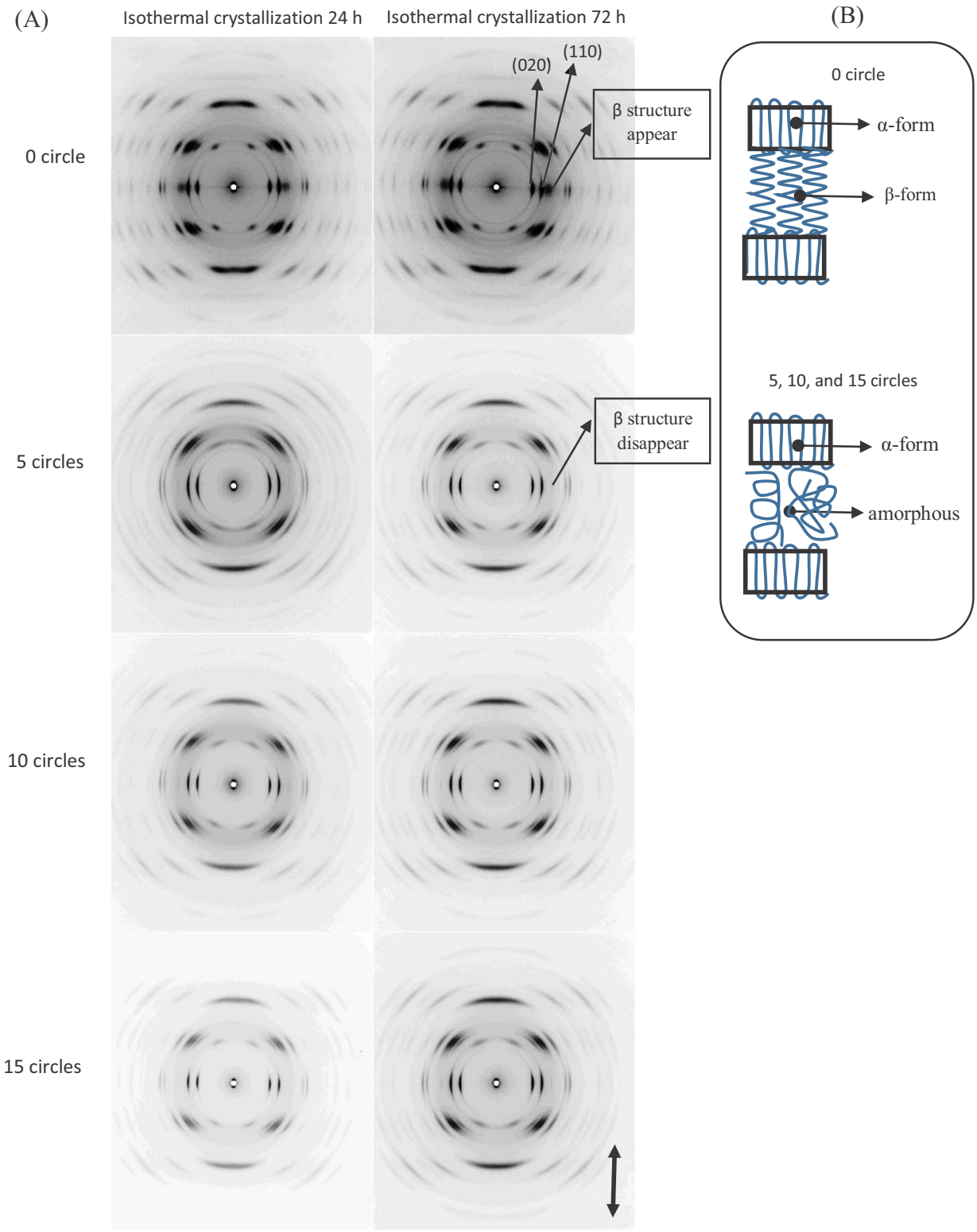

Figure 5-10. (A) WAXD patterns of IC 24 and 72 h monofilaments after dip-coating in AP solution for 0, 5, 10, and 15 circle times. (B) Molecular models of IC fibers before and after dip-coating in AP solution at 50°C.

Figure 5-11 (A) and (B) show the linear SAXS profiles and SAXS patterns of IC 24 and 72 h fibers before and after dip-coating in AP solution for 0, 5, 10, and 15 circle times. IC 24 and 72 h fibers without dip-coating displayed noticeable streak scattering along the equator and weak two-spot reflection along the meridian. The clear streak scattering along the equator suggests that many voids exist in IC monofilaments [8]. The lamellar thickness of IC 24 and 72 h monofilaments were calculated from the long-periods obtained from SAXS and crystallinity obtained from WAXD, Table 5-3. The lamellar thickness of IC 24 and 72 h fibers are 4.6 and 4.5 nm, respectively. Moreover, after dip-coating at 50°C for 5, 10, and 15 circle times led to approximately 5 nm in the thickness of lamellar crystal. In the case of IC 24 and 72 h fibers untreated (0 circle), the intensity of the meridional reflection was lower compare to fibers after dip-coating treatment. It supposed that the density between α-form and β-form crystals might be almost similar. Tanaka et al. [8] explained that the density between α-form and β-form crystals in drawn IC fibers are nearly identical, and the molecular chain in drawn fibers after isothermal crystallization (IC) has a highly oriented with various thicknesses of α-form lamellar crystals. In general, tensile strength increases with increasing lamella thickness [18]. However, in this research, IC fibers after dip-coating resulted in a decrease in tensile strength and obtained large lamellar thickness. It supposed to molecular chain change (relaxation and from β-form into amorphous) due to heating temperature or effect of solvent by dip-coating.

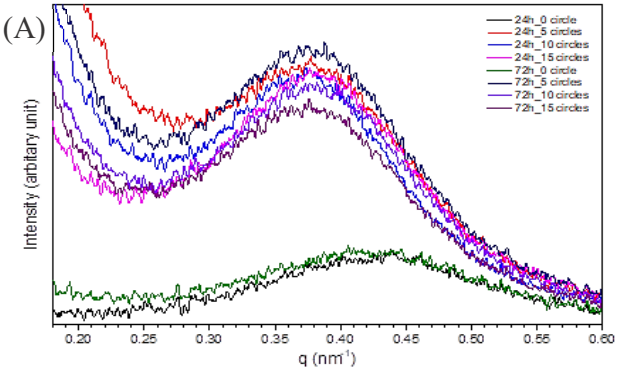

Figure 5-11. Cont.

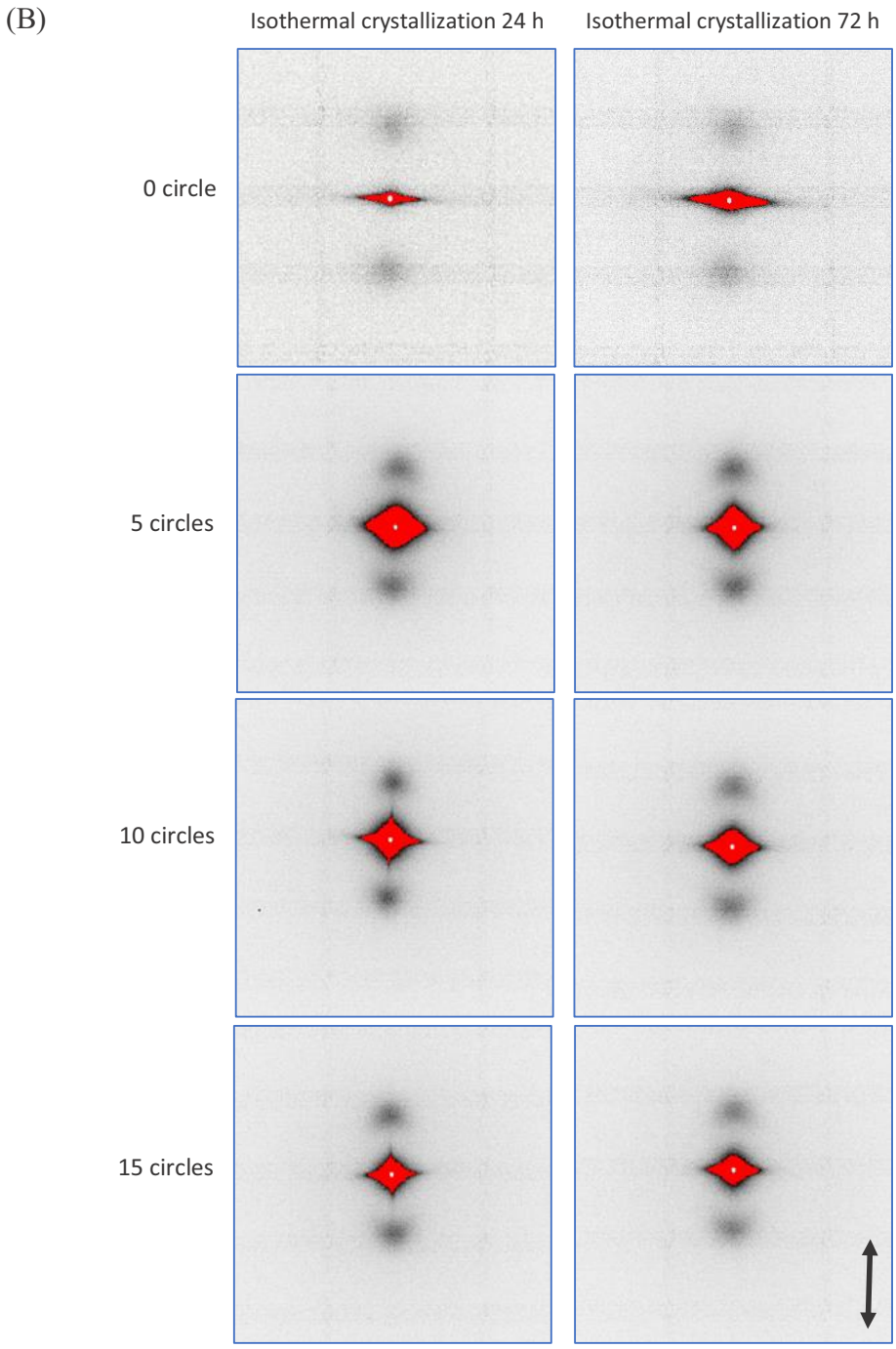

Figure 5-11. (A) Linear SAXS profiles obtained from the meridional scans in 2D SAXS patterns, the scattering vector q is definded by $q = (4\pi/\lambda) \sin \theta$. (B) SAXS patterns of IC 24 and 72 h monofilaments after dip-coating in AP solution for 0, 5, 10, and 15 circle times.

5.3.7. Antibacterial test

IC 72 h monofilaments after dip-coating in AP solution for 10 circle times was used as a representative in all fiber samples for antibacterial test against the gram-positive bacteria *S. auerus*. The antibacterial test was investigated by using inhibition zone method. The antibacterial effect of IC 72 h fiber was evaluated at 37ºC for 24 h. The effect of propolis loaded in IC 72 h fibers via the agar diffusion test is shown in Figure 5-12. IC 72 h fiber with propolis was observed low antibacterial activity against *S. aureus* with inhibition zone approximately 2.5 ± 2.5 mm. The low antibacterial activity might be due to the low propolis concentration contained in the IC fibers. For further work, increasing the propolis concentration in acetone or using the pure extract of derivative propolis might become one of the solutions to increase the antibacterial activity.

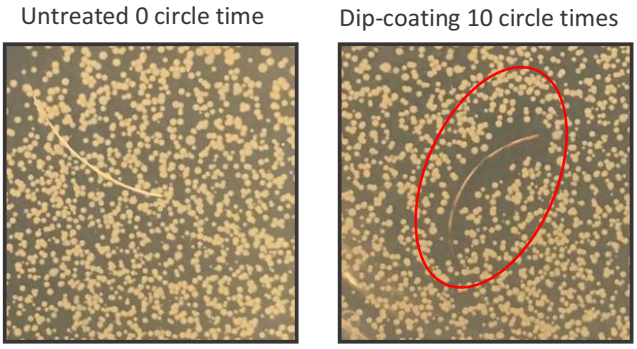

Figure 5-12. The representative of inhibition zone of IC 72 h fiber after dip-coating in AP solution for 0 and 10 circle times.

5.4. Conclusions

The loading of propolis as an antibacterial reagent by using acetone into IC fibers was evaluated by dip-coating with several temperatures and circle times. The penetration of AP solution into IC 24 and 72 h fibers was influenced by solvent and circle times. The use of acetone as a solvent to penetrate propolis exhibited higher penetration into monofilaments at a lower temperature compared to ethanol. Applying more than 5 circle times by dip-coating in AP solution

resulted in good penetration of propolis into the fibers. However, by dip-coating treatment at 50°C has influenced to physical, mechanical, and crystalline change in IC 24 and 72 h fibers. IC 24 and 72 h fibers shrank in length and expanded in diameter by applying the dip-coating treatment. IC 24 and 72 h fibers after dip-coating obtained a decrease in tensile strength and increased in elongation. From X-ray analysis, penetration of AP solution was also affected to the decrease in crystallinity after 15 circle times. Thus, dip-coating led to the increase in thickness of the lamella crystal. Overall, IC 24 h fibers after dip-coating for 5 circle times showed in lower penetration rate compared to 15 circle times. However, the decrease in mechanical properties was almost the same. Besides, IC 72 h fibers after dip-coating for 5 circler time resulted in faster penetration with the similar behavior change in physical and mechanical properties. In conclusion, from all samples, IC 72 h monofilaments after dip-coating in AP solution at 50°C obtained better results than other variables. Based on those results, the characteristic change in PHBH IC monofilaments by heat treatment with various organic solvent and dip-coating with AP solution can apply for the next research in the dyeing process or drug delivery as references.

5.5. References

[1] Iwata, T.; Tsuge, T.; Taguchi, S.; Abe, H.; Tanaka, T. Bio-polyesters. In *Bio-based polymers*, 1st ed.; Kimura, Y.; CMC Publishing Co., Ltd.: Tokyo, Japan, 2013, pp. 71-85. ISBN978-4-7813-0271-3.

[2] Philip, S.; Keshavarz, T.; Roy, I. Polyhydroxyalkanoates: biodegradable polymers with a range of applications. *J. Chem. Technol. Biotechnol.* **2007**, *82*, 233-247.

[3] Bugnicourt, E.; Cinelli, P.; Lazzeri, A.; Alvare, V. Polyhydroxyalkanoate (PHA): review of synthesis, characteristics, processing and potential applications in packaging, *eXPRESS Polym. Lett.* **2014**, *8*, 791-808.

[4] Chen, X.; Yang, X.; Pan, J.; Wang, L.; Xu, K. Degradation behaviors of bioabsorbable P3/4HB monofilament suture *in vitro* and *in vivo*. *J. Biomed. Mater. Res. B. Appl. Biomater.* 2010, **92**(2), 447-455.

[5] Tanaka, T.; Fujita, M.; Takeuchi, A.; Suzuki, Y.; Uesugi, K.; Ito, K.; Fujisawa, T.; Doi, Y.; Iwata, T. Formation of highly order structure in poly[(*R*)-3-hydroxybutyrate-*co*-(*R*)-3-hydroxyvalerate] high-strength fibers. *Macromolecules* **2006**, *39*, 2940 – 2946.

[6] Tanaka, T.; Yabe, T.; Teramachi, S.; Iwata, T. Mechanical properties and enzymatic degradation of poly[(*R*)-3-hydroxybutyrate] fibers stretched after isothermal crystallization near T_g. *Polym. Degrad. Stab.* **2007**, *92*, 1016-1024.

[7] Tanaka, T.; Uesugi, K.; Takeuchi, A.; Suzuki, Y.; Iwata, T. Analysis of inner structure in high-strength biodegradable fibers by X-ray microtomography using synchrotron radiation. *Polymer* **2007**, *48*, 6145-6151.

[8] Barham, P.J.; Keller, A. The relationship between microstructure and mode of fracture in polyhydroxybutyrate. *J. Polym. Sci. Part B. Polym. Phys.* **1986**, *24*, 69.

[9] Qin, Q., Takarada, W., Kikutani, T. Fiber Structure development of PHBH through stress-induced crystallization in high-speed Mmelt spinning process. *J. Fiber Sci. Technol.,* **2017**, *73*, 49-60.

[10] Venkatesh, G. M.; Khan, A.H.; Bose, P.J.; Madan, G.L. Shrinkage and mechanical properties of Poly(ethylene terephthalate) filaments treated with various organic solvent. *J. Appl. Polym. Sci.* **1980**, *25*, 1601-1618.

[11] Bonartsev, A.P., Myshkina, V.L., Nikolaeva, D.A., Furina, E.K., Makhina, T.A., Livshits, V.A., Boskhomdzhiev, A.P., Ivanov, E.A., Iordanskii, A.L., Bonartseva, G.A. Biosynthesis, biodegradation, and application of poly(3-hydroxybutyrate) and its copolymers - Natural polyesters produced by diazotrophic bacteria. *A. Méndez Vilas (Ed.) FORMATEX*, **2007**, 295-306.

[12] Bonartsev, A.P.; Myshkina, V.L.; Nikolaeva, D.A.; Kirpichnikov, M.P. Poly(3-hydroxybutyrate) and poly(3-hydroxybutyrate)-based biopolymer systems. *Biochemistry (Moscow) Suppl. Ser. B: Biomed. Chem.* **2011**, *5*, 10–21.

[13] Lee, S.Y. Bacterial polyhydroxyalkanoates. *Biotechnol. Bioeng*. **1996**, 49, 1-14.

[14] Andreau, V.; Mendoza, G.; Arruebo, M.; Irusta, S. Review: Smart dressings based on nanostructured fibers containing natural original antimicrobial, anti-inflammatory, and regenerative compounds. *Material* **2015**, *8*, 5154-5193.

[15] Wagh, V.D. Propolis: a wonder bees product and its pharmacological potentials. *Adv. Pharmacol. Sci.* 2013, Article ID 308249.

[16] Zhang, J.; Kasuya, K.; Hikima, T.; Takata, M.; Takemura, A.; Iwata, T. Mechanical properties, structure analysis and enzymatic degradation of uniaxially cold-drawn films of poly[(*R*)-3-hydroxybutyrate-*co*-(*R*)-4-hydroxybutyrate]. *Polym. Degrad. Stab.* **2011**, 96, 2130-2138.

[17] Rebia, R.A., Sadon, N.S.b., Tanaka, T. Natural Antibacterial Reagents (*Centella*, Propolis, and Hinokitiol) Loaded into Poly[(*R*)-3hydroxybutyrate-*co*-(*R*)-3-hydroxyhexanoate] Composite Nanofibers for Biomedical Applications. *Nanomaterials* **2019**, *9*, 1665.

[18] Phan, D.-N., Dorjjugder, N., Khan, M.Q., Saito, Y., Taguchi, G., Lee, H., Mukai, Y., Kim, I.-S. Synthesis and attachment of silver and copper nanoparticles on cellulose nanofibers and comparative antibacterial study. *Cellulose* **2019**, *26*, 6629–6640.

[19] Silva, M.C.; Silva, H.N.; Holanda, S.A.; Silva, A.R.O.; Fook, M.V.L. Biodegradable polymeric wires: monofilament and multifilament. *Mater. Res. Innov.* **2019**, https://doi.org/10.1080/14328917.2019.1622256.

[20] Popoola, A.V.; Adetuyi, A.O.; Oyeleke, G.O. Effect of chlorinated solvents on some mechanical properties of polyester fibre. *J. Appl. Chem.* **2014**, *7*, 54-57.

[21] Lee, J-C.; Yasui, A.; Jeong, Y.; Sakurai, S.; Yamane, H. Higher-order structural analysis of bacterial poly[(*R*)-3-hydroxybutyrate-*co*-(*R*)-3-hydroxyhexanoate] highly oriented films. *Polymer* **2008**, *49*, 2362-2367.

Chapter 6

Conclusions

Chapter 6

6. Conclusions

This thesis focused on is multi-fabrication of biodegradable PHBH for nanofibers and monofilament by electrospinning and melt-spinning, respectively. PHBH nanofibers were blended with another polymer and natural antibacterial. To penetrate antibacterial solution to PHBH monofilament, various solvents were used as well as to evaluate the fibers performance.

In chapter 2, poly(3-hydroxybutyrate-*co*-3-hydroxyhexanoate) (PHBH) / poly(vinyl alcohol) (PVA) blend nanofibers were successfully prepared and fabricated by electrospinning in HFIP and mixed solvent (HFIP/water). The addition of PVA into PHBH affected in the dimentional stability of nanofibers against water. This system also improved the degradation rate after four weeks. In contrast, pure PHBH nanofiber promoted the NIH3T3 cell attachment and proliferation compared to blend nanofiber PHBH/PVA of 50/50. Although the blend system of PHBH/PVA was difficult to grow up and adhered fibroblast cells, however, it may be necessary to use other cells, such as keratinocytes for evaluating the biocompatibility. Overall, the surface characteristics of blend nanofiber affected in degradation and cell attachment and proliferation.

In chapter 3, PHBH nanofiber was incorporated with several natural antibacterial reagents (*centella*, propolis, and hinokitiol) by electrospinning. In general, surface morphology and fiber diameters nanofibers were influenced by different kinds of natural antibacterial products, the type of solvent for dissolution of the natural antibacterial products, solution concentration of natural antibacterial products in the PHBH-HFIP polymer solution. A loading of propolis to PHBH composite nanofibers showed good mechanical properties, increased in crystallinity of PHBH, proved the antibacterial effect, and long release period. The use of hinokitiol in PHBH composite nanofibers proved effective zone inhibition (*S. Aureus* and *E. coli*) and a rapid release period. Thus,

it might be used in drug delivery with a fast period time of release and low mechanical properties. In the case of *centella* incorporated in PHBH composite, it may be necessary to increase the concentration of *centella* in *centella* solution (ethanol or methanol) if it is used as an antibacterial reagent.

In chapter 4, biodegradable PHBH was fabricated as monofilament by the melt-spinning process followed by one-step-drawing after isothermal crystallinity near T_g. Ethanol, acetone, hexane, propanol, and water were used to evaluate the physical and morphological changes of PHBH monofilaments by heat treatment at several temperatures. The result showed that various solvent and heat treatment temperature were found to affect the shrinkage in length and the expansion in diameter of PHBH fibers.

In chapter 5, ethanol and acetone were used to load propolis as an antibacterial reagent to PHBH monofilament. Whereas, dip-coating treatment was applied for PHBH IC fiber to penetrate the propolis solution. These results showed that acetone-propolis (AP) solution can penetrate into the PHBH IC fibers at higher rate. Characterization of PHBH monofilament after dip-coating treatment showed the change in physical, mechanical properties, and inner structure of PHBH monofilaments. For all samples, 72 h isothermal crystallization PHBH monofilaments after dip-coating in AP solution at 50^{o}C showed better results than others.

List of publications

1. **Rina Afiani Rebia,** Sélène Rozet, Yasushi Tamada, Toshihisa Tanaka*.
   Biodegradable PHBH/PVA blend nanofibers: Fabrication, characterization, *in vitro* degradation, and *in vitro* biocompatibility.
   Polymer Degradation and Stability, 2018, 154, 124-136.
   https://doi.org/10.1016/j.polymdegradstab.2018.05.018

2. **Rina Afiani Rebia**, Nurul Shaheera binti Sadon, Toshihisa Tanaka*.
   Natural antibacterial reagents (*Centella*, Propolis, and Hinokitiol) loaded into poly[(*R*)-3-hydroxybutyrate-*co*-(*R*)-3-hydroxyhexanoate] composite nanofibers for biomedical applications.
   Nanomaterials. Special Issue: Electrospun Nanomaterials: Applications in food, environmental remediation, and bioengineering, 2019, 9, 1665.
   https://doi:10.3390/nano9121665

3. Duy-Nam Phan, **Rina Afiani Rebia**, Yusuke Saito, Davood Kharaghani, Muzamil Khatri, Toshihisa Tanaka, Hoik Lee, Ick Soo Kim*.
   Zinc oxide nanoparticles attached to polyacrylonitrile nanofibers with hinokitiol as gluing agent for synergistic antibacterial activities and effective dye removal.
   Journal of Industrial and Engineering Chemistry, Joutnal Pre-proof (accepted 8 February 2020). https://doi.org/10.1016/j.jiec.2020.02.008

4. **Rina Afiani Rebia,** Shizukuishi Kaho, and Toshihisa Tanaka*.
   Characteristic changes in PHBH isothermal crystallization monofilaments by the effect of heat treatment and dip-coating in several solvents.
   European Polymer Journal, 22 January 2020 [Submitted, under review].

Patents

1. Toshihisa Tanaka, Rina Afiani Rebia.
   Nanofiber and Its Production Methods (ナノ繊維及びその製造方法).
   Japan patents application 特願 2016-111493, 3 June 2016.

2. Toshihisa Tanaka, Nurul Shaheera binti Sadon, Rina Afiani Rebia, Takanori Hatano.
   A nanofiber and a manufacturing method for the same (ナノ繊維及びその製造方法).
   Japan patents application 特願 2018-89078, 7 May 2018.

Scientific presentations

Oral presentations:

1. Rina Afiani Rebia, Nurul Shaheera binti Sadon, Toshihisa Tanaka.
   Effect of natural antibacterial products on P(3HB-*co*-3HH) nanofiber composites, The 16th Pacific Polymer Conference, 8 – 12 December 2020, Convention Centre – SUNTEC Singapore. (PPC16-A-0135).

2. Rina Afiani Rebia, Nurul Shaheera binti Sadon, Toshihisa Tanaka.
   Characterization of P(3HB-*co*-3HH) nanofiber composite loaded by natural antibacterial reagent, 68th Symposium on Macromolecules, 25 – 27 September 2019, Bunkyo Campus, Fukui University, Japan. (2T10)

3. Rina Afiani Rebia, Sélène Rozet, Yasushi Tamada, Toshihisa Tanaka.
   Characteristic of biodegradable polyester PHBH and water-soluble poly(vinyl alcohol) blend nanofiber, 255th ACS National Meeting, 18 – 22 March 2018, New Orleans Marriott Canal Street, New Orleans, Louisiana, USA.

4. Rina Afiani Rebia, Toshihisa Tanaka.
   P(3HB-*co*-3HH)/Polyvinyl alcohol blend nanofibers: characterization and *in vitro* degradation and bio-compatibility. 2017 Annual Meeting of the Society of Fiber Science and Technology, 7 – 9 June 2017, Tokyo, Japan. (2B02)

5. Rina Afiani Rebia, Toshihisa Tanaka.
   Preparation of poly[(*R*)-3-hydroxybutyrate-*co*-(*R*)-3-hydroxyhexanoate] / poly(vinyl alcohol) blend nanofibers, The 11th SPSJ International Polymer Conference (IPC2016), 13 – 16 December 2016, Fukuoka, Japan. (16C09)

Poster Presentation:

1. Rina Afiani Rebia, Toshihisa Tanaka.
   Characteristic properties of P(3HB-*co*-3HH) fiber by penetration of natural antibacterial reagent solution, 68th Symposium on Macromolecules, 25 – 27 September 2019, Bunkyo Campus, Fukui University, Japan. (1Pe085)

2. Rina Afiani Rebia, Toshihisa Tanaka.
   Additive of natural product into biodegradable polymer P(3HB-*co*-3HH) fiber, 6th International Conference on Multifunctional, Hybrid and Nanomaterials, 11 – 13 March 2019, The Meliá Sitges Hotel Congress Centre, Sitges, Spain.

3. Rina Afiani Rebia, Nurul Shaheera binti Sadon, Toshihisa Tanaka.
   Biodegradable polymer P(3HB-*co*-3HH) nanofibers with natural product as antibacterial reagent, The 10th International Conference of Modification, Degradation and Stabilization of Polymers (MoDeSt2018), 2 – 5 September 2018, Yayoi Campus, The University of Tokyo, Tokyo, Japan. (P-5-18)

4. Rina Afiani Rebia, Nurul Shaheera binti Sadon, Toshihisa Tanaka.
   Morphology of P(3HB-*co*-3HH) fiber and nanofiber with propolis as an antibacterial agent, Textile Summit 2018, 20 – 22 September 2018, Shinshu University, Ueda, Nagano, Japan. (P19)

5. Nurul Shaheera binti Sadon, Rina Afiani Rebia, Toshihisa Tanaka.
   Preparation of PHBH nanofibers with *Centella asiatica* and emu oil as antibacterial agent, Textile Summit 2018, 20 – 22 September 2018, Shinshu University, Ueda, Nagano, Japan. (P2)

6. Rina Afiani Rebia, Nurul Shaheera binti Sadon, Toshihisa Tanaka.
   Fabrication of P(3HB-*co*-3HH) fiber and nanofiber with antimicrobial properties, 67th The Society of Polymer Science (SPSJ) Annual Meeting, 23 – 25 May 2018, Nagoya Congress Center, Japan. (3Pa111)

7. Rina Afiani Rebia, Toshihisa Tanaka.
   Poly[(*R*)-3-hydroxybutyrate-*co*-(*R*)-3-hydroxyhexanoate] / polyvinyl alcohol blend Nanofibers: fabrication, characterization and *in vitro* enzymatic biodegradation, Research Day and Textile Summit 2017, 18 – 22 March 2017, NC State University, North Carolina, USA.

8. Rina Afiani Rebia, Toshihisa Tanaka.
   Preparation of poly[(*R*)-3-hydroxybutyrate-*co*-(*R*)-3-hydroxyhexanoate] / polyvinyl alcohol Blend Nanofibers. 2016 Annual Meeting of the Society of Fiber Science and Technology, 8 – 9 June 2016, Tokyo, Japan. (1P223)

Acknowledgments

All praises and thanks are to Allah SWT, the Lord of the worlds, the most beneficent, the most merciful for helping me accomplish this work.

The present thesis is submitted to the Interdisciplinary Graduate School of Science and Technology, Shinshu University, for the degree of Ph.D. (Engineering). It is my pleasure to express my gratitude to all those who have directly and indirectly contribute to this work.

I sincerely appreciate a Grant-in-Aid for the Shinshu University Advanced Leading Graduate Program provided by the Ministry of Education, Culture, Sports, Science, and Technology of Japan for financial support.

I would like to express my deepest gratitude to my supervisor, Prof. Toshihisa Tanaka, for guidance and supporting me with a lot of pertinent advices through my master and doctoral course in Shinshu University.

I would like to thank to Prof. Miura for his support and kindness. I would like also to express my gratitude to Professors and staffs in the Leading Program for supporting me during my study in Shinshu University.

I would like to express my gratitude to the reviewers, Prof. Masayuki Takatera, Prof. Hiroaki Ishizawa, Prof. Yasushi Tamada, Prof. Tadahisa Iwata, and Prof. Myrtha Karina Sancoyorini for their kind supports and their invaluable comments and insights. Their advice, insightful comments, and suggestions provided significant support on this work.

I deserve my special thanks to Prof. Sri Nugroho Marsoem, Faculty of Forestry, Gadjah Mada University, for the opportunity and his support.

Many thanks to the members of Tanaka Laboratory from 2015 – 2020 and Leading Program students for their great support, warm, and memorable friendship.

Finally, I would like to appreciate and thanks especially for my mother and all beloved family for their endless love, blessing, and mental support during my study here. Big love.

My husband, Zam, always be patient and support me in every condition during my studies here. Who always known me well, encourage me to be myself, remind me to Allah, and blessing me in every prayer. I love you.

Rina Afiani Rebia
Shinshu University
March, 2020